

**An investigation of temporal variability of
CO₂ fluxes in a boreal coniferous forest and
a bog in central Siberia
: from local to regional scale**

Dissertation
zur Erlangung des akademischen Grades Doctor rerum naturalium
der Fakultät für die Graduiertenschule Forst- und Agrarwissenschaften
Forstwissenschaften
der George-August-Universität Göttingen

vorgelegt von

Sung-Bin Park

geboren am 26. Dezember 1982 in Seoul, Südkorea

Göttingen, 2019

1. Gutachter: Alexander KNOHL, Prof. Dr. Georg-August-Universität Göttingen, Göttingen
2. Gutachter: Martin HEIMANN, Prof. Dr. Max-Planck Institut für Biogeochemie, Jena and Division of Atmospheric Sciences, Department of Physics, University of Helsinki, Helsinki, Finland
3. Prüfer: Dirk HÖLSCHR, Prof. Dr. George-August-Universität Göttingen, Göttingen
4. Prüfer: Christoph GERBIG, Dr.habil. Max-Planck Institut für Biogeochemie, Jena

Date of oral examination: July 4, 2019

Abstract

Boreal forests and peatlands are the major types of vegetation in northern Eurasia. These ecosystems store large amount of carbon in their vegetation and soil, thus are essential ecosystems to understand the global carbon cycle. Compared to the other boreal regions, tower-based CO₂ measurements in the Eurasian boreal ecosystems of central Siberia are very sparse. The objective of my thesis is to investigate temporal variability of CO₂ fluxes at a boreal coniferous forest and a bog in Zotino, Russia. In Chapters 3 and 4, I present data on site-level CO₂ flux measurements using the eddy covariance (EC) method. In Chapter 5, the site-level CO₂ flux measurements were utilized to evaluate the reliability of regional CO₂ flux estimates obtained from the modified Bowen Ratio (MBR) method.

Chapter 3 investigates the diffuse radiation fertilization effect during the Siberian wildfire period from 2012-2013 using a data-driven model trained with CO₂ fluxes and meteorological measurements. Key findings are: 1) Approximately 54-58% of variability in forest net ecosystem productivity (NEP) was controlled by photosynthetically active radiation (PAR), vapour pressure deficit (VPD), and diffuse fraction (f_{dif}) of PAR during the growing season, 2) Incoming PAR decreased significantly at very high levels of f_{dif} and high aerosol loading, 3) The diffuse radiation fertilization effect induced by clouds and aerosols increased NEP but this effect was less than a 10% increase, mainly due to sparse canopy structure and low leaf area index.

Chapter 4 investigates the similarity and differences in abiotic controls of CO₂ fluxes during the winter-spring transition period at a coniferous forest and bog. Key findings are: 1) Air temperature regulated CO₂ flux variability in the forest, whereas surface peat temperature was the primary driver of CO₂ flux variability in the bog, 2) Rapid net CO₂ uptakes occurred when both air and soil temperatures exceed 5 °C, 3) Sporadic warm spells can lead to an earlier start of CO₂ uptake, 4) Spring frost reduced the net ecosystem productivity in both ecosystems, however vegetation productivity increased again after frost.

Chapter 5 presents the variability of regional CO₂ fluxes from the profile measurements, combined using the MBR method. This study shows that diurnal cycles of profile measurements were useful for understanding the surface boundary layer structure. Since night-time mixing mostly did not extend beyond the top of the tall tower (304 m), night-time CO₂ flux estimates can be reliably used without direct EC flux measurement.

Despite the uncertainties in both daytime and night-time CO₂ fluxes, magnitudes and patterns of diurnal cycles of regional CO₂ flux estimates generally followed the EC CO₂ flux measurements.

Overall, this thesis shows that boreal ecosystems respond to changing environmental conditions in non-linear and complex ways. The results would be useful to evaluate CO₂ fluxes from both process-based biosphere models and inverse models. In order to characterize an annual carbon budget in Zotino, further efforts such as methane flux measurement at bog, flux footprint analysis, evaluation of the snow season CO₂ flux, and uncertainty estimation in flux partitioning of the long-term net ecosystem exchange of CO₂, would be necessary.

Zusammenfassung

Boreale Wälder und Moore sind die dominanten Vegetationstypen im nördlichen Eurasien. Der Boden und die Vegetation in diesen Ökosystemen speichern große Mengen Kohlenstoff, weshalb diese Ökosysteme eine große Rolle für das Verständnis des globalen Kohlenstoffkreislaufs spielen. Im Vergleich zu anderen borealen Regionen werden in den eurasischen borealen Ökosystemen in Zentralsibirien sehr wenige turmgestützte Messungen von Kohlendioxid (CO₂) durchgeführt. Ziel meiner Dissertation ist die Untersuchung der zeitlichen Variabilität von CO₂-Flüssen in einem borealen Nadelwald und einem Moor in Zentralsibirien.

In Kapitel 3 und 4 werden Daten präsentiert, die an beiden Standorten mit Hilfe der Eddy-Kovarianz(EC)-Methode gewonnen wurden. In Kapitel 5 werden die mittels EC ermittelten CO₂-Flüsse verwendet, um die Zuverlässigkeit regionaler CO₂-Flüsse zu evaluieren, welche durch die modifizierte Bowen-Ratio-Methode bestimmt wurden.

Kapitel 3 behandelt den Fertilisationseffekt diffuser Strahlung während der sibirischen Waldbrandperiode zwischen 2012 und 2013, welcher mittels eines datengetriebenen Modells anhand von CO₂-Flüssen und meteorologischen Messungen untersucht wurde. Dabei stellt sich heraus, dass 1) etwa 54-58% der Variabilität des Nettoökosystemaustauschs (NEP) während der Wachstumsperiode durch die vorhandene photosynthetisch aktive Strahlung (PAR), das Dampfdruckdefizit (VPD) und den diffusen Strahlungsanteil (f_{dif}) gesteuert wird, 2) die PAR bei sehr hohem f_{dif} und hohem Aerosolgehalt der Luft signifikant abnimmt und dass 3) der Fertilisationseffekt diffuser Strahlung durch Wolken und Aerosole zu einem erhöhtem NEP führt, diese Erhöhung aber kleiner als 10% ist, was hauptsächlich der offenen Kronenstruktur und einem geringen Blattflächenindex geschuldet ist.

Kapitel 4 behandelt die Gemeinsamkeiten und Unterschiede zwischen den CO₂-Flüssen im Nadelwald und im Moor hinsichtlich der abiotischen Einflüsse während der Übergangszeit zwischen Winter und Frühjahr. Dabei stellt sich heraus, dass 1) im Wald die Albedo einen statistisch signifikanten Einfluss auf die CO₂-Flüsse hat, während im Moor die Temperatur der obersten Torfschicht der wichtigste Einflussfaktor ist und dass 2) beide Ökosysteme sich während der Schneeschmelze bereits dann in eine Nettosenke für CO₂ verwandeln, wenn der Boden noch gefroren ist. Darüber hinaus können 3) sporadische warme Perioden zu einem früheren Beginn der CO₂-Aufnahme führen. Außerdem zeigt sich,

dass 4) Frühjahrsfrost den NEP in beiden Ökosystemen verringert, die Produktivität der Vegetation nach dem Frost aber wieder ansteigt.

In Kapitel 5 wird die Variabilität regionaler CO₂-Flüsse präsentiert, welche aus einem in sechs Höhen gemessenen Vertikalprofil ermittelt wurden. Diese Untersuchung zeigt, dass der Tagesgang von Profilmessungen dabei helfen kann, die Struktur der oberflächennahen Grenzschicht zu verstehen. Da eine vertikale Durchmischung in der Nacht in den meisten Fällen nicht über die Höhe des Messturmes (304 m) hinaus erfolgte, können die nächtlichen CO₂-Flüsse auch ohne direkte EC-Messungen zuverlässig verwendet werden. Trotz der Unsicherheiten, mit denen die CO₂-Flüsse am Tag und in der Nacht behaftet sind, folgen die Größenordnung und der Tagesgang der regionalen CO₂-Flüsse im Allgemeinen den mittels EC ermittelten CO₂-Flüssen.

Insgesamt zeigt diese Dissertation, dass boreale Ökosysteme auf veränderliche Umgebungsbedingungen in nichtlinearer und komplexer Weise reagieren. Diese Ergebnisse können dabei helfen, von prozessbasierten Biosphärenmodellen und von inversen Modellen bestimmte CO₂-Flüsse zu evaluieren. Um ein jährliches Kohlenstoffbudget für Zotino aufzustellen, wären zusätzliche Untersuchungen (Messung der Methanflüsse im Moor, Identifikation der die Flussmessungen beeinflussenden Gebiete, d.h. Analyse des Footprints, sowie Unsicherheitbetrachtung zur Partitionierung des langfristigen Nettoökosystemaustauschs von CO₂) erforderlich.

Declaration

I hereby declare that I wrote this PhD thesis under the supervision of Prof. Alexander Knohl. Any sources of information and used literature have been acknowledged.

Jena, July, 2019

Sung-Bin Park

Acknowledgements

The ZOTTO project is funded by the Max Planck Society through the International Science and Technology Center (ISTC) partner project no. 2757 within the framework of the proposal “Observing and Understanding Biogeochemical Responses to Rapid Climate Changes in Eurasia”.

I appreciate to my thesis committee and PhD committee advisory (PAC): Prof. Alexander Knohl, Prof. Martin Heimann, Prof. Dirk Hölscher, Dr. Christoph Gerbig, Dr. Jost Lavric and Prof. Timo Vesala.

Thank you for Dr. Lavric and Prof. Heimann who gave me an opportunity to study PhD at the Max Planck Institute for Biogeochemistry.

Thanks to Prof. Knohl, I earned the STIBET finishing grant of the Graduate School Forest and Agricultural Science (GFA) from Jan-Mar, 2019 when I desperately needed it. Without his interests, supports, and guidance, I won't be able to earn my PhD degree. Thank you very much for his numerous efforts and constructive criticism on manuscript revisions for the good quality of research.

I don't know where to start my deep appreciation to Dr. Gerbig. Thanks to his speedy and clear comments, I was able to finish Chapter 5. He always attended my PAC meetings with supporting and constructive comments. He spent countless days, sitting next to me and worked on R scripts line-by-line when I stuck data handling.

Thanks to Prof. Heimann's good research network, I had a great opportunity to work with Prof. Vesala and his group. It was a great opportunity for me to work with the top micrometeorology group during my research stay in University of Helsinki. Thank you for Prof. Vesala, connecting me with Dr. Ivan Mamarella and Dr. Olli Peltola who were great contributors on my work during the Eddy covariance workshop 2015. During the research stay, Prof. Vesala was a private tour guide of Hyytiälä research station just for a visiting PhD student. Thank you for his interests on me while I was staying there. His clear and straightforward comments during PAC meeting helped me prioritizing tasks.

I appreciate Dr. Mirco Migliavacca's interests on my research, encouragements, and practical supports in applying statistical methods and general data analysis in Chapter 3 and Chapter 4. Thank you very much for his open and sharing minds, including his knowledge, R scripts, and experiences in writing a good manuscript. Thank you for his efforts to reach me via email, skype, and at his office as possible as he could. I was not his group member but I appreciate him offering me a good opportunity to learn about active discussions and supporting atmosphere through his group meeting.

Again thanks to Prof. Heimann, I had a great opportunity to work with Dr. Moffat who was one of the main contributors on Chapter 3. I believe Chapter 3 was more valued because of using her ANN models. I appreciate her efforts in active communications via phone, email, and at her home office whenever I needed it. Thanks for her invitation to Braunschweig, I was able to have key figures and good story line. She guided me what to show, what we need to highlight, how to present result, how to structure manuscript to convey clear messages. Her PhD thesis and Moffat et al. (2010) inspired me a lot while I was working on this study.

Thank you for Dr. Tea Thum's gave me practical suggestions for Chapter 4. I thank her efforts to read many versions of unpolished and poorly structured early versions of Chapter 4. Her comments were always on time and valuable to improve the structure of contents. Thank you for he cheering comments and seeing the values of data while I was frustrating on data analysis and writing manuscript.

Thank you for Frieland group, BSY technicians, and local staffs in ZOTTO, doing all the hard and challenging field & lab works for me. Without their efforts, station will not run properly: Olaf Kolle, Karl Kübler, Steffen Schmidt, Martin Hertel, Kerstin Hippler, Thomas Seifert, Thomas Tresselt, Uwe Schultz. Crew from the V.N. Sukachev Institute of Forest in Krasnoyarsk; Dr. Alexey Panov, Dr. Anatoly Provshkin, Alexander Zukanov, Nikita Sidenko, Roman Kolosov, Sergey Titov, and Anastasiya Timokhina. Thank you for Mihal Rütimann who came from University of Basel as a visiting student and her hard work in ZOTTO in September, 2014.

Thanks to members of the BSY department: Gionata, Fabio, Panos, Martina, Lena, Sabrina, Fanny, Min, Friedmann, Tonatiuh, Ditreich, Annu, Santiago, Michał, Julia, Saqr, and Christian.

Especially, my deep appreciation goes to Ulli who always supported me with her warm heart and cheerful encouragements. From the first day she picked me up at the Westbahnhof, she was like my German mom. I won't go through well this long journey without her wise, practical advices, generosity, and sympathy. Thank you for supporting me not just PhD student as one of our department but also showed her interests in me as a person and opened her hearts and eyes on my struggles. Her family, Alfred, Julius, Helena, and Benjamin always welcomed me with warm hearts and fed me with feast via countless of their family dinners. Thank you for their invitation during Christmas and Easter and cared me a lot not feeling lonely.

I can't miss Annette for sure. Thank you so much for her kindness, open minded, positive, and consideration on me as her friend. Annette, Sven, and her parents always remember my birthday and invited me many years of their family Christmas lunch with lots of gourmet and presents. I didn't have time to feel lonely during this time with surrounded by good family members.

Thank you for Maik, sharing his R scripts and suggested me easy and practical solutions for data handling. I am grateful to Frank-Thomas who was always willing to help me every time I was struggled in R.

Thank you for Jan who shared all his R scripts for post-processing and Chapter 5.

I appreciate to Martin Kuntz for writing a German abstract.

Thank you for Silvana and Iris who prepared graphical abstract.

Thank you for Thomas Seifert's persistent encouragements, his sincere prayers, car services every time when I need it.

Marcus was not just my Yoga teacher but helped me a lot for land cover maps using ArcGIS and helping me debugging R scripts as a peer.

Thanks to Thomas Wutzler his kindness and practical supports for using REddyProc.

Emily, Olya, Lailah, Gabi, Haeyoung, Seungjoo, Yeonjin, Silvia, Sven, Nora, Su, Huiying cheered me to complete thesis writing.

Thanks to Johannes's offering for nice meals and comforting driving service to the outside of Jena when I felt bored being in the same city all the time.

Half of my life in Jena was with John's family. I wish all the best wishes for his family, Catarina, Luca, and Luise.

Thank you is not enough to say my gratitude to my proofreading team who were happy to help me: Saqr, Somak, Jenia, John, Komi, Annu, Su, Kasun, Ingo. Especially, Jeff, Richard, Kendal, and Shane who helped me a lot especially until the day I submitted my thesis. I appreciate their encouragements and extra work for speedy proofreading and constructive suggestions.

Without Andrew's support, my first paper won't be published with very encouraging comments. His comments were very though and accurate based on the good understanding of my work. I appreciate his speedy, constructive comments and encouragements. Thank you so much for his efforts reading my 70% of rough and early versions of thesis contents.

I don't know how to express my gratefulness to Kendal. Thanks to my cheerful and funny flatmate, I could go through the most stressful time. Thank you for her warm heart and generous understanding on my situation, I won't be able to finish my thesis writing with a good spirit. Kendal and his catbird Finn made me always happy to be at home.

I am thankful to biometeorology department of Prof. Knohl. Thank you for their welcoming me when I visited in Göttingen: Yuanchao, Cliff, Rijan. Mattia and Jelka cordially offered me to stay overnight or few days whenever I needed it. Thanks to supportive group member, Rijan, Florian, Nina, Christian, and many others, I had a great wagon tour and ceremony in Gänseliesel.

Anna and John at the IMPRS office supported me lots of administrative work and settling down well in Germany. Steffi always supported me during PAC meetings and encouraged me to keep moving forward. Inga and Robert helped me a lot for administrative works related to GFA.

Jonghwa, Jihye, and Kyuhee helped me a lot whenever I had difficult situations due to German.

My deep appreciation, respect, and love go to all my parents, grandparents, family and my boyfriend Jonghwa Lee, who is always praying for me with full of hope in all circumstances. Thank God, who lead me not giving up this task.

Table of Contents

Abstract	i
Zusammenfassung	iii
Acknowledgements	vi
Table of Contents	xi
List of Figures	xiii
List of Tables	xviii
Chapter 1 Introduction	1
1.1 The Carbon Cycle	1
1.2 Terrestrial carbon cycle	4
1.3 Boreal ecosystems in central Siberia	5
1.4 Wildfires and snowmelt	7
1.5 Objectives and research questions	8
1.6 References	11
Chapter 2 Materials and methods	18
2.1 Study site	18
2.2 Ground-based CO₂ measurements	19
2.3 References	25
Chapter 3 Strong radiative effect induced by clouds and smoke on forest net ecosystem productivity in central Siberia	31
3.1 Introduction	32
3.2 Materials and methods	34
3.2.1 Study site	34
3.2.2 Measurement systems	35
3.2.2.1 Eddy covariance flux measurements.....	35
3.2.2.2 Auxiliary measurements	37
3.2.3 Data processing and quality control.....	38
3.2.4 Data selection	39
3.2.5 Artificial Neural Networks	40
3.3 Results	42
3.3.1 Meteorological conditions and NEP.....	42
3.3.2 Wildfire.....	44
3.3.3 Drivers of NEP	44
3.3.4 How do clouds and smoke affect the partitioning of PAR?.....	47
3.3.5 How relevant is the effect of smoke on NEP?	51
3.4. Discussion	53
3.4.1 Environmental drivers of NEP identified by the ANNs	53
3.4.2 Effects of clouds and smoke on radiation.....	54
3.4.3 Requirements of the diffuse radiation fertilization (DRF) effect	55
3.5. Conclusion	56
3.6. References	58

Chapter 4 Beginning of snowmelt and surface soil thaw determine spring CO₂ fluxes in boreal forest and bog in central Siberia	65
4.1 Introduction.....	66
4.2 Materials and methods	69
4.2.1 Study site	69
4.2.2 Measurement system	71
4.2.3 Post-processing and data quality control.....	75
4.2.3.1 Definition of metrics and analysis	76
4.2.3.2 Statistical analysis.....	77
4.3. Results	79
4.1 The abiotic controls of spring CO ₂ fluxes	79
4.2 CO ₂ fluxes and abiotic drivers during the transition period	82
4.3 Interannual variability in spring cumulative net ecosystem exchange of CO ₂	84
4.4 Spring air temperature and cumulative net ecosystem exchange of CO ₂	86
4.5 Impact of spring frost on photosynthetic related process.....	88
4.4 Discussion	91
4.4.1 Abiotic variables regulating springtime CO ₂ flux.....	91
4.4.2 Triggers of the start of CO ₂ uptake	92
4.4.3 Variability of spring CO ₂ fluxes after the start of CO ₂ uptake	94
4.4 Variability of spring cumulative net ecosystem exchange of CO ₂	95
4.4.4 Effect of spring frost on the photosynthesis-related processes	95
4.5 Conclusion	97
4.7 References.....	101
Chapter 5 Reliability of regional CO₂ flux estimates from tall tower profile measurements.....	106
5.1. Introduction.....	106
5.2 Material and methods	107
5.2.1 Measurements system	107
5.2.2 Data processing	108
5.2.3 Flux calculation	109
5.3. Results and discussion	111
5.3.1 The PBL structure from the tall tower profile data.....	111
5.3.2 Evaluation of regional NEE estimates	117
5.4 Conclusion	121
5.5 References.....	122
Chapter 6 Synopsis	125
6.1 Net ecosystem productivity reduction by clouds and fire aerosols at a sparse boreal coniferous forest	125
6.2 The impact of spring snowmelt on variability in CO₂ fluxes in boreal forest and bog.....	128
6.3 Understanding of the reliability of regional CO₂ flux estimates	129
6.4 Conclusion	131

List of Figures

- Figure 1.1 The global carbon cycle components. Yellow numbers are natural fluxes, reds are human activities, and white numbers indicate stored carbon in Gt C/year (1 Gt = 1 billion tonnes = 1 Petagram = 1×10^{15} g) (Courtesy: US DOE. Climate Placemat: Energy-Climate Nexus, US Department of Energy Office of Science. (p. 1)).....2
- Figure 1.2 Atmospheric CO₂ concentration measured at the Mauna Loa Atmospheric Baseline Observatory (19.5 °N 155.6 °W, 3397 m.a.s.l.) in Hawaii from 1958-2018. Retrieved July 2, 2018, from https://scripps.ucsd.edu/programs/keelingcurve/wp-content/plugins/sio-bluemoon/graphs/mlo_full_record.png.....3
- Figure 1.3 The global carbon budget averaged over the period of 1959-2017. The carbon emissions from fossil fuels, industry, and land use change are balanced by the atmosphere and carbon uptakes by land and ocean. Grey line denotes the mean global budget imbalance between the total emissions and the total sinks (atmosphere+land+ocean) (Courtesy: Global Carbon Project. (2017). Supplemental data of Global Carbon Budget 2017 (Version 1.0) [Data set]. Global Carbon Project. <https://doi.org/10.18160/gcp-2017>).....4
- Figure 2.1 The eddy covariance technique directly measures the exchanges of gases, energy, and momentum exchanges between the surface and the atmosphere. In surface layer, the air flow (big arrows) consists of numerous and various sizes of individual eddies and vortices (small arrows). Eddies move in both horizontal and vertical directions. Adopted from Burba and Anderson (2010), [Online image]. Retrieved on December 18, 2017, from https://upload.wikimedia.org/wikipedia/commons/6/65/Pyörrekovarianssi-tekniikan_kaaviokuva.jpg.....22
- Figure 3.1 Land cover (top) and geographical location (bottom) of the ZOTTO site. Land cover map derived from 30-meter Landsat-8 imagery. Round circle and triangle shapes indicate the forest eddy covariance flux tower and the tall tower sites.37
- Figure 3.2 Time series of daily observation at ZOTTO. (a) Air temperature (T_a , black), vapor pressure deficit (VPD, blue), (b) total precipitation (Pr_{cp}, black), soil moisture

at 0.32 m (SWC, blue), (c) total incident photosynthetic active radiation (PAR_t), (d) diffuse fraction (f_{dif} , black), clearness index (CI, blue), (e) net ecosystem productivity (NEP, red), and (f) AOD from June 19 to September 4, 2012 (left) and June 1 to September 4, 2013 (right). Only f_{dif} and CI are averaged in daylight hours ($R_{pot} > 20 \text{ Wm}^{-2}$). The horizontal grey dashed line of (f) is the mean background AOD value of 0.18 during June - August in Siberia (Remer et al., 2008).43

Figure 3.3 Results of the ANN benchmarked with all fourteen environmental drivers: (a) Measured (black) and modelled (red) daytime NEP response projected onto PAR_t . (b) Scatterplot of measured versus modelled daytime NEP. The linear regression fit (blue solid line) is close to the 1:1 line (grey dashed line). Positive NEP values indicate CO_2 uptake by forests whereas negative values indicate CO_2 released to the atmosphere. See Table 1 for details on the environmental drivers.....45

Figure 3.4 Performance (R^2) of the ANNs trained with 14 input drivers: (a) with a single (primary) driver at a time, (b) with PAR_t plus a secondary driver, and (c) with PAR_t and VPD plus a tertiary driver. The performance improvement (red) indicates the relevance of the secondary and tertiary drivers. The horizontal dotted line is the benchmark performance with all 14 drivers.46

Figure 3.5 Daytime NEP response (upper panel) and partial derivatives (lower panel) modelled with three drivers PAR_t (a), VPD (b), and f_{dif} (c). The modelled (red circles) and measured (black circles) NEP values are shown in gradient colours from light to dark denoting low to high PAR_t47

Figure 4.1 Land cover maps and geographical location of forest (ZF; red circle), bog flux towers (ZB; red rectangle), and tall tower (red triangle) at Zotino (black circle). 14 initial land cover types have been reclassified into 3 types. Forests include reforestation, regrowth, lichen with pines, bogs containing shrubs, flooded and wet body. Other classes include clear-cut/barren, burned, sand, and sparse vegetation. .70

Figure 4.2 Eddy covariance flux towers (a) at the Zotino Forest (ZF) site in growing season and (b) snow season and (c) Zotino Bog (ZB) site in growing season and (d) snow season. The measurement heights are 30.3 m and 9.9 m, respectively. Details of the instrumentation are shown in Table 4.2.72

Figure 4.3 Relative importance of six abiotic variables for CO₂ fluxes for the Zotino forest (ZF) with bootstrapped 95% confidence intervals. Bootstrap replicates (n) were set to 1000 and overall R² was 71.78%, which is the sum of the percentage of response variance. The variables are denoted in the importance: surface albedo (Alb), photosynthetically active radiation (PAR), surface soil temperature (T_{s04}), soil temperature at the depth of 0.16m (T_{s16}) and 0.64m (T_{s64}), and air temperature (T_a). Total 285 daily mean values from DOY 99-155 during 2013-2017 were used.80

Figure 4.4 Relative importance of five abiotic variables for CO₂ flux for the Zotino bog (ZB) with the bootstrapped 95% confidence intervals. Bootstrap replicates (n) were set to 1000 and R² was 80.64%, which is the sum of the percentage of response variance. The variables are denoted in the order of importance: peat temperature in the depths of 0.04m (T_{s04}), 0.32m (T_{s32}), 0.64m (T_{s64}), surface albedo (Alb), photosynthetically active radiation (PAR), respectively. Total 216 daily mean values from DOY 111-155 in 2013 and DOY 99-155 during 2014-2016 were used. Peat temperatures at the depth of 0.08m and 0.16m were excluded from the analysis due to the long-term gaps (>3 months) during springtime in 2014-2015.81

Figure 4.5 Time series of 3-day moving averaged meteorological variables and net ecosystem exchange of CO₂ (NEE) from DOY 91 to DOY 165 for the forest site (ZF) in 2016 and 2017. In (a) and (b), blue lines denote air temperature (T_a), red lines denote soil temperature at the depth of 0.04m (T_{s04}), and black lines denote surface albedo (Alb). In (c) and (d), black dots and red lines indicate daily sum of NEE (NEE_d) and moving averaged value (NEE_{3d}). The earliest and the latest start of CO₂ uptake were in 2016 and in 2017 during the study period. Vertical dotted lines in (a) and (b) indicate SCU_{Bsnow} (grey), SCU_{T5(5 °C)} (blue), and SCU_{Ts04(0 °C)} (red). Horizontal red dotted lines in (c) and (d) denote the start of CO₂ uptake (SCU). SCU_{T5(5 °C)} were DOY 115 in 2016 and DOY 132 in 2017. SCU_{Ts04(0 °C)} were DOY 140 in 2016 and DOY 134 in 2017. SCU_{Bsnow} were DOY 114 in 2016 and DOY 132 in 2017. SCU_{Fsnow} were DOY 139 in 2016 and DOY 134 in 2017. SCU were DOY 114 in 2016 and DOY 130 in 2017. Vertical dashed line in (c) and (d) corresponding to the start of CO₂ uptake (red). Negative NEE is a net CO₂ uptake, positive NEE is a net CO₂ release.83

Figure 4.6 Same as Fig. 4.5 but for ZB. Horizontal red dotted lines in (c) and (d) denote the start of CO₂ uptake (SCU). SCU_{T5(5 °C)} were DOY 142 in 2013 and DOY 116 in 2016. SCU_{Ts4(0 °C)} were both DOY 126 in 2013 and 2016. SCU_{Bsnow} were DOY 117 in 2013 and DOY 112 in 2016. SCU_{Fsnow} were DOY 126 in 2013 and DOY 127 in 2016. SCU were DOY 132 in 2013 and DOY 120 in 2016.84

Figure 4.7 Cumulative net ecosystem exchange of CO₂ (NEE_{cum}) at the Zotino forest (ZF) and Zotino bog (ZB) from DOY 99-151 during 2013-2017. The grey dashed zero-line denotes the transition from a cumulative CO₂ source (positive) to cumulative CO₂ sink (negative). Positive values indicate a cumulative ecosystem carbon loss, and negative values indicate a cumulative ecosystem carbon uptake.85

Figure 4.8 The relationships (a) between the frequency of frost days and air temperature in May and (b) between the frequency of late frost days and air temperature in May from 2013-2017 for the ZF and ZB sites. Black colours denote the ZF and the grey colours denote the ZB. Linear regressions for (a), frequency of frost days = $-1.8505 \cdot T_a$ in May + 24.3589, $R^2=0.8652$, $p=0.02191$ for ZF and $-1.0405 \cdot T_a$ in May + 22.2346, $R^2=0.5598$, $p=0.1458$ for ZB. Linear regressions for (b), Frequency of frost days = $1.635 \cdot T_a$ in May + 16.109, $R^2=0.4617$, $p=0.207$ for ZF and $-2.0312 \cdot T_a$ in May + 22.1708, $R^2=0.805$, $p=0.03894$ for ZB.89

Figure 4.9 Ecosystem light response curves on pre-frost days (black dot and line), frost days (blue dot and line), and post-frost days (red dot and line) for (a) the Zotinio forest (ZF) and Zotino bog (ZB). Half-hourly days in 2014 were chosen after the snowmelt (DOY 134 for ZF and DOY 133 for ZB, respective): DOY 133-136 for the pre-frost days, DOY 137-140 for the frost days, DOY 141-144 for the post-frost days, respectively. Model parameters are listed in Table 4.6.90

Figure 5.1 Diagram of flux calculations using profile measurements. The six measurement heights are shown in Table 5.1. Regional net ecosystem exchange (NEE) of CO₂ is the sum of storage flux (F_{stor}), turbulent flux (F_{Eddy}), and advection flux (F_{Adv}) terms. Note that F_{Adv} term is ignored in this study.111

Figure 5.2 Diurnal cycle of half-hourly averaged CO₂ concentrations [ppm] measured at six levels (301 m, 227 m, 157 m, 92 m, 52 m, and 4 m) for individual months and years (2012-2015).112

Figure 5.3 Two contrasting nights, showing unstable or well-mixed (black) and stable (dark grey) boundary layers. Profiles of half-hourly CO ₂ mixing ratios and potential temperatures on 2014-09-20 at 02:30:00 were chosen for the unstable night and on 2014-09-25 at 23:00:00 for the stable night, respectively. The time is given for the Krasnoyarsk time zone (KRAT=UTC+7h).	114
Figure 5.4 Diurnal cycle of the half-hourly averaged potential temperature for all height levels (301 m, 227 m, 157 m, 92 m, 52 m, and 4 m) for individual months from 2012-2015. (a) potential temperature using ambient air temperature (T _a), (b) corrected sonic air temperature (T _s).	115
Figure 5.5 Diurnal cycles of regional NEE (black dots with error bar and grey shaded area) using the best temperature data during summertime from 2012-2015. Error bar denotes errors of mean of half-hourly data. Overlaying dark green and orange line denote CO ₂ fluxes measured at the Zotino Forest (ZF) and the Zotino Bog (ZB) flux towers, respectively. Red dashed line is up-scaled CO ₂ fluxes using the weighted average of fractions of forests (60%) and bogs (40%) in the ZOTTO footprint (Timokhina et al. 2016).	119
Figure 5.6 Diurnal cycle of differences in half-hourly regional NEE using sonic air temperature (T _s) and ambient air temperature (T _a) with standard error of the mean for individual months and years from 2012-2015. Shaded area indicates the storage flux (F _{stor}). Error bar denotes errors of mean of half-hourly data.	120
Figure 6.1 A graphical abstract, presenting main findings in this thesis.	132

List of Tables

Table 3.1 List of environmental variables used for ANN trainings.	41
Table 3.2 Midday (11:00-15:00) normalized mean NEP during summer was estimated by considering the percentage decreases and increases in PAR_t and f_{dif} . VPD variation is fixed. All values are percentage changes in NEP relative to our measured midday mean NEP during summer. Zero is the measured NEP with no change in meteorology. We simulated 10 - 60 % decreases in PAR_t by increasing f_{dif} from 50 to 400 %. Corresponding PAR_t values for the relative changes decrease 10 – 60 % from 1400 to 600 $\mu\text{mol photon m}^{-2}\text{s}^{-1}$ at a rate of 100 $\mu\text{mol photon m}^{-2}\text{s}^{-1}$ (Fig. 6b). In the same manner, relative increases from 0.2 to 1 in f_{dif} range from 50 to 400 % in increments of 0.1. The first column indicates NEP considering the reduction of PAR_t , while the first row indicates NEP only considering the f_{dif} increase. Increasing AOD from 0.3 to 0.7, 1, 1.5, 2, and 3.5, the relative changes in PAR_t decrease by about 7, 11.5, 19.6, 27.8, and 52.4 %, respectively (Fig. 3.7a). Similarly, the relative increases in f_{dif} from 50 to 200 % with AOD are 41, 67.5, 104.5, 132, 158.3 %, respectively (Fig. 3.7b). The thick bold line indicates the line between negative and positive effects due to PAR_t and f_{dif} changes.	52
Table 4.1 Site characteristics of the flux measurement sites at Zotino.	73
Table 4.2 Instrument setup and sensor types of the flux towers at the Zotino flux sites...	74
Table 4.3 The percentages (%) of high quality flux data during spring season (April-June) at the Zotino forest (ZB) and Zotino bog (ZB) sites.....	75
Table 4.4 The day of year (DOY) of transition from NEE_{cum} source to NEE_{cum} sink, maximum NEE_{cum} ($(NEE_{cum})_{peak}$) with corresponding DOY, mean slopes ($\frac{\partial NEE_{cum}}{\partial DOY}$) before and after reaching peak of the NEE_{cum} for ZF and ZB during 2013-2017. The same data were used in Fig.4.3. Values in bold indicate the maximum, whereas values in bold and italic indicate the minimum.	86
Table 4.5 Mean air temperature (T_a) and cumulative net ecosystem exchange of CO_2 (NEE_{cum}) for April, May, and season-average values for the ZF and ZB flux sites, as well as year-average values during the study period (2013-2017). Both T_a and	

NEE_{cum} were calculated on DOY 99 (9 April) except the NEE_{cum} in 2013 for ZB, which starts on DOY 110 (20 April). Therefore, the mean value of the NEE_{cum} for ZB only presents a three-years average over the period of 2014-2016. Bold values indicate the maximum, whereas bold and italic values indicate the minimum.87

Table 4.6 Model parameters of the rectangular light response function for pre-frost, and post-frost days for the Zotino forest (ZF) and Zotino bog (ZB). Numbers in parentheses denote the standard errors of the mean parameters. R^2 is coefficient of determination and n is the number of half-hourly data. NEP₁₅₀₀ was computed with three parameters as saturating PAR of 1500 $\mu\text{mol photon m}^{-2} \text{s}^{-1}$. The standard deviations of NEP₁₅₀₀ were computed from the mean of the maximum and minimum of each parameter.....90

Table S 4.1 The ranking of variable importance of CO₂ flux estimated by the MARS model during spring (9 April-15 June) from 2013-2017 at the Zotino forest (ZF) site. Daily mean values of the nine variables were used as an initial data: Ta, T_{s04}, T_{s08}, T_{s16}, T_{s32}, T_{s64}, Alb, PAR, and vapour pressure deficit (VPD). Proportion of variance in daily CO₂ fluxes explained by model (R^2) was 84%.98

Table S 4.2 Same as Table S4.1 but for ZB. Data is used from 2013-2016. Proportion of variance in daily CO₂ fluxes explained by model (R^2) was 89%.98

Table S 4.3 The metrics for the start of CO₂ uptake using 5-day mean air temperature threshold (SCU_{T5(5°C)}), the start of surface soil or peat warming (SCU_{Ts4(0°C)}), the beginning of snowmelt (SCU_{Bsnow}), the final day of snowmelt (SCU_{Fsnow}), and the start of CO₂ uptake (SCU) at forest (ZF) and bog (ZB) during 2013-2017. Bold values indicate the maximum, whereas bold and italic values indicate the minimum.99

Table S 4.4 The frequency of frosts ($T_{\text{min}} < 0 \text{ }^\circ\text{C}$) and late frosts (after snowmelt) in April and May and spring (April and May) for the ZF and ZB flux sites from 2013-2017. Bold values indicate the maximum in spring, whereas bold and italic values indicate the minimum in spring. DOY in parentheses is the last day of frost. DOY in bracket indicates the end of frost days. 100

Table 5.1 Set up for meteorological measurements at the Zotino tall tower..... 108

Table 5.2 Data availability of available half-hourly net ecosystem exchange of CO₂ (NEE) and storage flux (F_{stor}) using the best temperature measurements during summertime (June-September) 2012-2015. The last row of each month indicates the temperature data used for flux calculations. T_a denotes the ambient air temperature measurement and T_s denotes the sonic air temperature measurements. “-“ denotes none of temperature measurements were available to calculate NEE.....116

Chapter 1 Introduction

1.1 The Carbon Cycle

Carbon (C) is one of the most abundant chemical elements on Earth. The C cycle is the biogeochemical pathway of C through the atmosphere, land and ocean of the earth system (Ciais et al., 2013; Heimann and Reichstein, 2008). The majority of C is stored in the land and ocean, while a minority moves through these pools, being released into and taken up from the atmosphere through different processes on different timescales (Fig. 1.1). Important driving factors, such as solar radiation, temperature, and precipitation, regulate C exchange and their interaction with other biogeochemical cycles are not fully understood. In addition, the non-linear and complex nature of the climate system makes global C cycling more difficult to understand (Heimann and Reichstein, 2008; Huntzinger et al., 2017; Raupach et al., 2014).

Carbon dioxide (CO₂) is one of the most important inorganic C compounds. Despite constituting only 0.04% (equivalent to 400 ppm) of the atmosphere, CO₂ is the most important anthropogenic greenhouse gas (GHG) along with other trace gases, such as methane (CH₄) and nitrous oxide (N₂O). GHGs absorb and release radiation, maintaining the surface mean temperature at approximately 15 °C, which is suitable for the life on the Earth (Liou, 2002).

However, excessive CO₂ emissions by human activities alter the natural C cycle. Human activities (e.g. fossil fuel burning, land-use and land cover changes, and deforestation) are the main source of CO₂ emissions (Fig. 1.1, Fig 1.3). Approximately 40% of anthropogenic CO₂ emissions remain in the atmosphere, while the remainder is taken up by land and ocean (Prentice et al. 2011). Excessive CO₂ emissions remain in the atmosphere for 5-200 years, intensifying the greenhouse effect (IPCC, 2014). Atmospheric CO₂ level was approximately 280 ppm before the industrial revolution in the 19th century (circa 1750), however it has exceeded 400 ppm in recent years (IPCC, 2014). In fact, the average global atmospheric CO₂ concentration was 402.8 ± 0.1 ppm in 2016 (Le Quéré et al., 2018). In the northern hemisphere, atmospheric CO₂ concentration reached 409.65 ppm on June 2018 (Fig. 1.2).

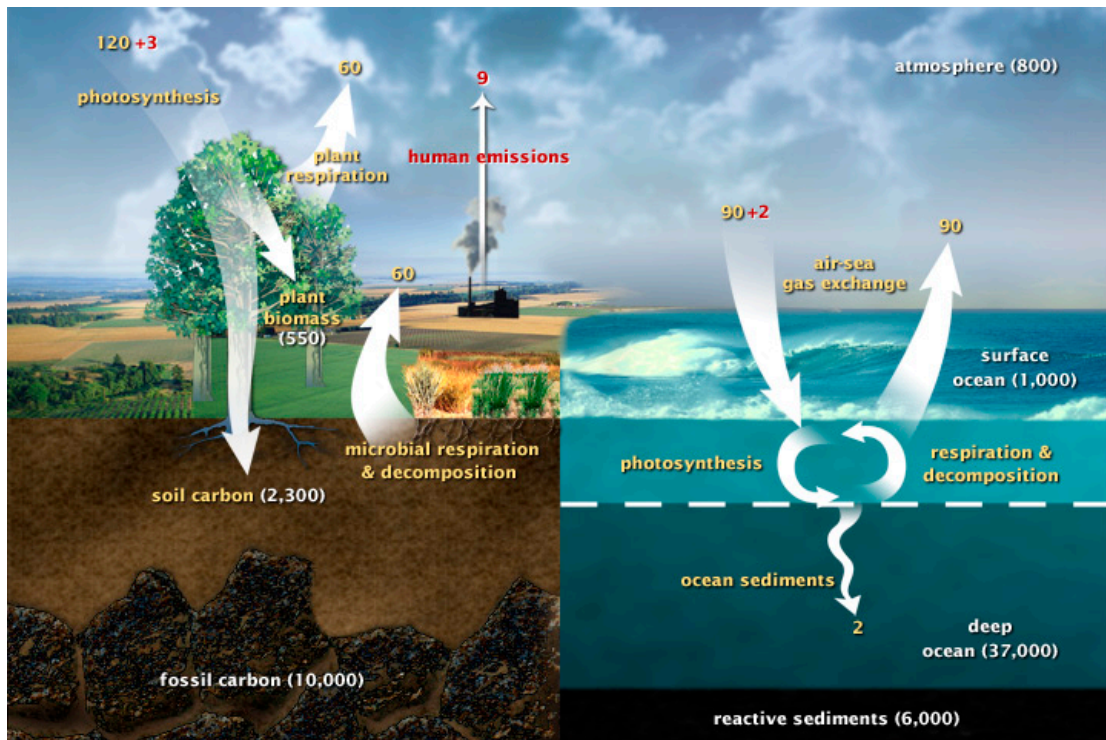


Figure 1.1 The global carbon cycle components. Yellow numbers are natural fluxes, reds are human activities, and white numbers indicate stored carbon in Gt C/year (1 Gt = 1 billion tonnes = 1 Petagram = 1×10^{15} g) (Courtesy: US DOE. Climate Placemat: Energy-Climate Nexus, US Department of Energy Office of Science. (p. 1)).

Climate scientists agree that anthropogenic GHG emissions, especially CO_2 , cause a substantial increasing trend in global temperature over the past 60 years (IPCC, 2014). Based on the up-to-date carbon budget over the last decade (2007-2016), 88% of the increased rate of global CO_2 emissions ($9.4 \pm 0.5 \text{ Gt C yr}^{-1}$, $34.4 \pm 1.8 \text{ Gt CO}_2$) are caused by fossil fuel and industrial process, and 12% resulted from deforestation and land-use changes ($1.3 \pm 0.7 \text{ Gt C yr}^{-1}$, $4.8 \pm 2.6 \text{ Gt CO}_2$, Fig. 3). These CO_2 emissions were partitioned into the following C sinks: 46% of the total CO_2 emissions accumulated in the atmosphere ($4.7 \pm 0.1 \text{ Gt C yr}^{-1}$, $17.2 \pm 0.4 \text{ Gt CO}_2$), 30% in the land ($3.0 \pm 0.8 \text{ Gt C yr}^{-1}$, $11.0 \pm 2.9 \text{ Gt CO}_2$) and 24% in the ocean ($2.4 \pm 0.5 \text{ Gt C yr}^{-1}$, $8.8 \pm 1.8 \text{ Gt CO}_2$) with an imbalance of 5 % (0.6 Gt C yr^{-1} , $2.2 \pm 4.3 \text{ Gt CO}_2$) (Le Quéré et al., 2018). The mismatch between the total sources and sinks (grey line) in Fig. 1.3 implies the knowledge gaps in our understanding of the C cycle. Main causes of C budget imbalance

are mostly likely related to missing processes (e.g., vegetation responses to diffuse radiation and unknown internal variability) and imperfect spatio and temporal data coverage in land and ocean CO₂ sinks. In addition, understanding the behaviour of the terrestrial C cycle under increasing atmospheric CO₂ and changing environmental conditions (e.g. climate change and human activities) is crucial in order to understand the climate system (Matthews et al., 2005).

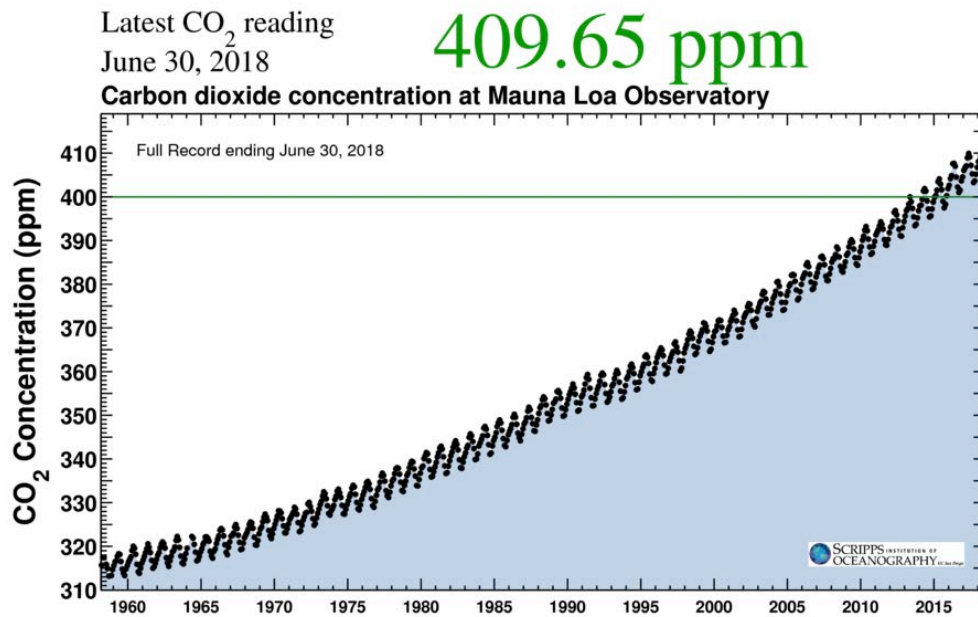


Figure 1.2 Atmospheric CO₂ concentration measured at the Mauna Loa Atmospheric Baseline Observatory (19.5 °N 155.6 °W, 3397 m.a.s.l.) in Hawaii from 1958-2018. Retrieved July 2, 2018, from https://scripps.ucsd.edu/programs/keelingcurve/wp-content/plugins/sio-blumoon/graphs/mlo_full_record.png.

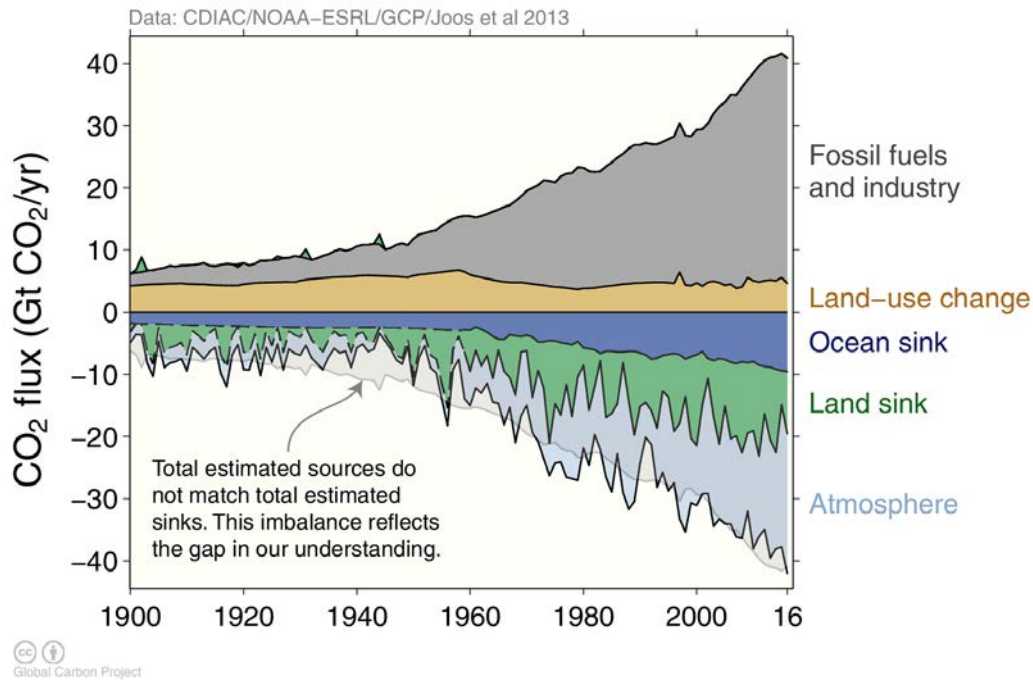


Figure 1.3 The global carbon budget averaged over the period of 1959-2017. The carbon emissions from fossil fuels, industry, and land use change are balanced by the atmosphere and carbon uptakes by land and ocean. Grey line denotes the mean global budget imbalance between the total emissions and the total sinks (atmosphere+land+ocean) (Courtesy: Global Carbon Project. (2017). Supplemental data of Global Carbon Budget 2017 (Version 1.0) [Data set]. Global Carbon Project. <https://doi.org/10.18160/gcp-2017>).

1.2 Terrestrial carbon cycle

The terrestrial biosphere is a crucial component of the C cycle (Fig. 1.1, Fig. 1.3). Gross primary productivity (GPP) is a measure of the amount of CO₂ removed from the atmosphere every year to fuel photosynthesis (Chapin III and Eviner, 2014). Most C taken up by GPP is returned to the atmosphere almost immediately through ecosystem respiration. Ecosystem respiration (R_{eco}) is all C released from the terrestrial ecosystem. Soil respiration (R_s), an important component of ecosystem respiration (R_{eco}), is controlled by plants, microbes, and fauna in the soil (Chapin III and Eviner, 2014). R_s is the sum of below-ground autotrophic respiration (R_A) and heterotrophic respiration (R_H). R_A represents root respiration and rhizosphere activities that mineralize relatively recent photosynthetic assimilates. R_H is the activity of heterotrophic microorganisms that decompose soil organic matter (Trumbore, 2006). Plant respiration is the cellular

respiration of both above and belowground plant biomass. The net primary production (NPP) is the difference between GPP and the plant respiration (McNaughton et al., 1989; Kirschbaum et al. 2001). Other terms often used include the ecosystem productivity (NEP) or net ecosystem exchange (NEE), which are two different terms for the difference between GPP and R_{eco} (Lovvet et al. 2006).

1.3 Boreal ecosystems in central Siberia

Northern Eurasia is located in the subarctic climate zone and is one of the most sensitive areas to rapid climate change. In the past three decades, northern Eurasia has experienced a drastic warming of 1-2 °C, which is higher than the global average of 0.85 °C (IPCC, 2014). This region shows one of the most pronounced surface temperature warming trends over the period of 1881-2008: more than 2 °C for the winter and 1.35 °C for the summer, respectively (Groisman et al. 2009). Substantial air temperature warming over the last three decades for this region has resulted in a longer growing season length and enhanced vegetation productivity (Forkel et al., 2016; Hayes et al., 2011; Myneni et al., 1997; Piao et al., 2008).

Boreal ecosystems are the dominant terrestrial biosphere in northern Eurasia, located approximately between latitudes 50-67 °N (Kasischke, 2000). Globally, forest ecosystems occupy about 27% of the total land surface area (FAO, 1995). Boreal forests make up 33% of the world's forest cover (Ruckstuhl et al., 2008). More than 50% of Russia's land area is covered by boreal forests (Dolman et al., 2012), and these Russian forests (the so-called "taiga") comprise *ca.* 21% of the world's forested area (Tishkov, 2002; Ruckstuhl et al. 2008). Approximately 32% (272 ± 32 Pg C) of C carbon stored in forests globally can be found in boreal forests (Pan et al. 2011). Boreal forests store approximately 85% of the plant's soil C and 60-70% of the total soil C (Ceulemans et al., 1999; Dixon et al. 1994). Another report puts the total C storage in boreal forests even higher, estimating that these ecosystems store 471 Pg of C (Prentice et al. 2001). Thus, investigating the role of boreal forests as a net C sink and their interaction with the changing climate is important to understand the current and future terrestrial C cycles (Bonan, 2008; Gauthier et al., 2015).

Wetlands are ecosystems that consist of excessively waterlogged land. They are characterized by distinct water levels, soil moisture conditions, soil carbon characteristics, and vegetation structure (Schot 1999, Charman, 2002). For instance, Mitsch and Gosselink (1993) classified nine types of wetlands depending on the seasonality of water table and dominant vegetation types: bog, fen, mire, marsh, playa, slough, swamp, wet meadow, and open water. Bogs and fens are classified as organic soil wetlands, whereas marsh and swamp are classified as mineral soil wetlands (Apostolov et al. 2004). Especially, bogs dominated by *Sphagnum* moss can accumulate more than 40 cm of dead plant biomass and organic matter (Bold, 1967). Raised or blanket bogs receive water and nutrients from precipitation, making them ombrotrophic, thus they have acidic water, and low nutrient contents.

Peatlands are wetlands that accumulate partially decomposed organic vegetation. Although peatlands occupy ca. 3% of the land surface, they store roughly 16-33% of the global soil carbon pool (600 Gt C) (Gorham 1991; Bridgham et al. 2006). Approximately 25-30% of peatlands are found in the boreal forests of the northern hemisphere (Gorham, 1991; Wieder et al., 2006) and these boreal peatlands store 270-379 Pg (Turunen et al. 2002). Northern peatlands have low vegetative productivity due to low nutrient concentrations but 5-50 times larger soil carbon pools than other ecosystems due to anaerobic and cold soil conditions (Frolking et al. 1998). The peat area in the boreal region is smaller than in the Arctic permafrost region. However the depths of peat are the deepest in the permafrost-free boreal zone (Kauppi et al. 1997; Beilman et al. 2009). Although peatlands along the Yenisei River in West Siberian Plain in Russia occupy ca. 40-50% of the land surface in Russia, their ecological characteristics and behaviour under changing environments are yet poorly understood (Schulze et al., 2015). Northern peats have accumulated during the Holocene, acting as an atmospheric CO₂ sink throughout that time (Lund et al. 2010; Yu, 2012; Smith et al. 2004). Moreover, peatlands are also the major natural methane source (Moore and Knowles, 1990). The role of peatlands as a net carbon sink under a warming climate is highly uncertain (Abdalla et al., 2016; Limpens et al., 2008). Therefore, measuring C fluxes and investigating their environmental drivers in northern peatlands is crucial for understanding the Eurasian C cycle.

1.4 Wildfires and snowmelt

Wildfires and snowmelt are critical environmental changes in northern Eurasia. These disturbances are directly or indirectly influenced by human induced climate change. Changes in frequency or intensity of wildfires and snowmelt will alter emissions of GHGs in northern Eurasia in the future (Monier et al. 2013).

Wildfire is an important disturbance factor for ecosystem change in boreal ecosystems. The intensity and frequency of wildfires have amplified in Russian and Canadian boreal forests due to fast temperature increases and extension of dry periods (Stocks et al. 1998; Young et al. 2017; Groisman et al. 2009; Tchebakova et al. 2009; Conard and Ivanova, 1997). In 2010, 'mega-heat waves' burned large parts of Russian forests and agricultural lands (Barriopedro et al. 2011). Wildfires become more frequent and stronger due to the warmer and drier climate, thus it is a critical disturbance factors in the taiga (Achard et al., 2008; Vasileva et al., 2011). Fires increase atmospheric concentrations of carbon monoxide (CO), CH₄, and aerosols (Vasileva et al. 2011). Radiation is the vital controlling factor on vegetation growth and productivity. Aerosol particles or smoke plumes induced by fires that remain in the atmosphere for excessive periods of time will change radiation components, influencing vegetation productivity and net CO₂ uptake.

The snow period in northern Eurasia, typically lasts from October to May. In spring (April-May), thick snow cover (> 1 m) in Siberia melts within few weeks. These dramatic changes influence carbon, water, and energy fluxes in terrestrial ecosystems (Groisman et al. 2009). During 1982-2011, snow cover in Eurasia decreased significantly and was strongly correlated with surface air temperature warming trends (Brwon and Derksen, 2013). In addition, changes in timing of snowmelt influence the length of the vegetative growing season and annual carbon budget (McGuire et al, 2002; Lafelur and Humphereys, 2007). For instance, a recent study by Pulliainen et al. (2017) showed that decreasing snow cover and earlier retreat of snow cover consistently resulted in enhanced forest ecosystem productivity. However, during 1997-2006, another boreal Eurasian region showed that vegetation growth decreased compared to 1982-1997 (Piao et al. 2011). Those two studies suggested that the trends of vegetation growth and productivity vary temporally and spatially. Therefore, it is important to keep monitoring the

ecosystem's response to environmental changes to investigate whether or not these ecosystems will continue to play a role as a sink and a potential mitigator of anthropogenic CO₂ emissions (Hayes et al., 2011; Matthews et al., 2005).

1.5 Objectives and research questions

Net vegetation CO₂ uptake rates in central Siberia are influenced by environmental changes, such as spring snowmelt and summer wildfires. The objective of my thesis is to characterize the variability of CO₂ fluxes and its abiotic drivers during the most dynamical seasonal changing periods, spring and summertime. To achieve this objective, CO₂ fluxes were measured by the EC method at a coniferous forest and a bog. Furthermore, EC flux measurements were utilized to evaluate the reliability of regional CO₂ flux estimates from tall tower profile measurements. An overview of research questions is addressed graphically as in Fig. 1.4.

Smoke produced from fires typically increases diffuse radiation resulting in an enhancement of vegetation productivity, particularly in broadleaf deciduous forests and croplands because diffuse radiation makes for favourable sky conditions for photosynthesis. Compared to other regions (e.g. Amazon or temperate ecosystems), the effects of clouds and fire smokes on vegetation productivity in Siberian coniferous forest are not well studied. Chapter 3 characterizes the potential diffuse radiation fertilization effect on forest net ecosystem productivity during wildfires that occurred from 2012-2013.

The research questions for Chapter 3 are:

- 1) What are the major environmental factors controlling the variability of forest net ecosystem productivity (NEP)?
- 2) How does forest net ecosystem productivity (NEP) respond to diffuse radiation caused by smoke particles during wildfires?
- 3) How strong is the diffuse radiation fertilization effect on NEP?

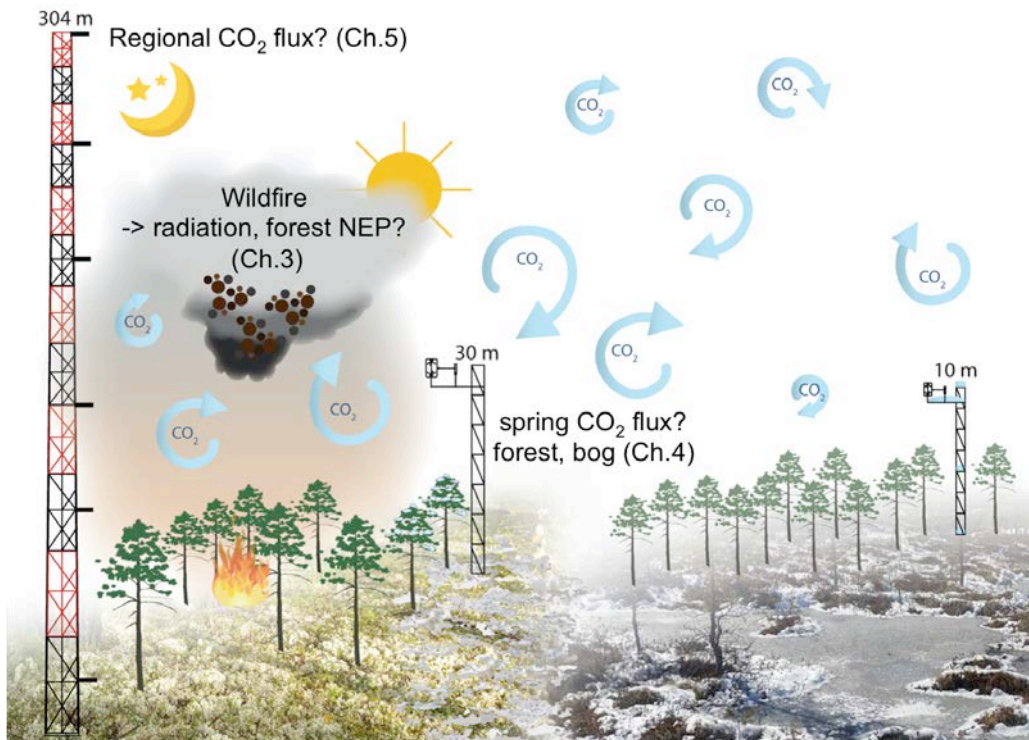


Figure 1.4 Overview of the questions addressed in this thesis. Art work courtesy of Silvana Shott and Iris Möbius.

Chapter 4 focuses on the spring interannual variability of CO_2 fluxes and its abiotic drivers measured at a coniferous forest and bog from 2013-2017. During the spring snowmelt period, solar radiation, air and soil temperatures substantially increase. In addition, air temperature fluctuates greatly with accompanying warm and cold spells. Therefore, the timing of vegetation transition from being a net CO_2 source to being a net CO_2 sink would be influenced by local weather condition and associated environmental changes.

Specific research questions for Chapter 4 are:

- 4) What are the factors controlling the variability of CO_2 at a coniferous forest and bog in spring?
- 5) How do the coniferous forest and bog ecosystems differ in their responses to environmental variables during spring?
- 6) What influence does the very warm spring in 2015 have on the timing of snowmelt, frequency of frost days, and the strengths of net CO_2 sinks?

Chapter 5 investigates the spatial variability of summertime regional CO₂ flux estimates from profile measurements from 2012-2015. Regional CO₂ fluxes were estimated by an alternative EC method using tall tower CO₂ concentration profile measurements, following the identical procedure addressed by Winderlich et al. (2014). To evaluate the reliability of regional CO₂ flux estimations, CO₂ flux measurements at the neighbouring flux towers were used as a reference data.

Research question is:

- 7) How reliable are regional CO₂ flux estimates from profile measurements?

This PhD dissertation consists of the three independent result chapters (Chapter 3 to 5). The contents of Chapter 3 were published in *Agricultural and Forest Meteorology* (Park et al., 2018). The contents of Chapter 4 were submitted to *Boreal Environmental Research*. Chapter 5 is an unpublished manuscript. Details of research background and methodology are demonstrated in each result chapter. Chapter 6 summarizes the key findings and outlook for future research.

1.6 References

- Abdalla M., Hastings A., Truu J., Espenberg M., Mander Ü. and Smith P. 2016. Emissions of methane from northern peatlands: a review of management impacts and implications for future management options. *Ecology and Evolution* 6: 7080–7102.
- Achard F., Eva H.D., Mollicone D. & Beuchle R. 2008. The effect of climate anomalies and human ignition factor on wildfires in Russian boreal forests. *Philosophical transactions of the Royal Society of London. Series B, Biological sciences* 363: 2331–2339.
- Apostolov, S., Hristov, I., Boshnakova, S., Holland, B., Borthwick, F., Jabbor, S., Boingeanu O., Olshanskaya, M., Langerholc, M. 2004. World Wetlands Day 2004 at the Central European University: *From the Mountains to the Sea – Wetlands at Work for Us*. Background paper. [on-line].
URL: http://www.personal.ceu.hu/students/03/nature_conservation/wwddetail/WW_D_2004_CEU-bp-contents.html
- Beilman, D. W., MacDonald, G. M., Smith, L. C., and Reimer, P. J., 2009: Carbon accumulation in peatlands of Est Siberia over the last 2000 yr, *Global Biogeochem. Cy.*, 23, GB1012, 1–12.
- Bold, H.C. *Morphology of Plants*, second ed., Harper and Row, New York (1967), pp. 225-229
- Bonan G.B. 2008. Forests and Climate Change: Forcings, Feedbacks, and the Climate Benefits of Forests. *Science* 320: 1444–1449.
- Bridgham, S.D., Megonigal, J.P., Keller, J.K., Bliss, N.B., Trettin, C., 2006. The carbon balance of North American wetlands. *Wetlands* 26, 889–916. doi:10.1672/0277-5212(2006)26[889:tcbona]2.0.co;2
- Brown R, Derksen C., 2013. Is Eurasian October snow cover extent increasing? *Environ Res Lett* 8:024006
- Chapin F.S., and Eviner V.T., 2014. Biogeochemical Interactions Governing Terrestrial Net Primary Production. In: Holland H.D. and Turekian K.K. (eds.) *Treatise on Geochemistry*, Second Edition, vol. 10, pp. 189-216. Oxford: Elsevier.
- Charman, D. 2002. *Peatlands and environmental change*. J. Wiley & Sons, London &

New York, 301 p.

- Ceulemans R., I.A. J. & Jach M.E. 1999. Effects of CO₂ Enrichment on Trees and Forests : Lessons to be Learned in View. *Annals of Botany* 84: 577–590.
- Ciais, P., C. Sabine, G. Bala, L. Bopp, V. Brovkin, J. Canadell, A. Chhabra, R. DeFries, J. Galloway, M. Heimann, C. Jones, C. Le Quéré, R.B. Myneni, S. Piao and P. Thornton, 2013: Carbon and Other Biogeochemical Cycles. In: Climate Change 2013: The Physical Science Basis. Contribution of Working Group I to the Fifth Assessment Report of the Intergovernmental Panel on Climate Change [Stocker, T.F., D. Qin, G.-K. Plattner, M. Tignor, S.K. Allen, J. Boschung, A. Nauels, Y. Xia, V. Bex and P.M. Midgley (eds.)]. Cambridge University Press, Cambridge, United Kingdom and New York, NY, USA.
- Conard, S.G., Ivanova, G.A., 1997. Wildfire in Russian boreal forests-potential impacts of fire regime characteristics on emissions and global carbon balance rates. *Environ. Pollut.* 98, 305–313.
- Dolman A.J., Shvidenko A., Schepaschenko D., Ciais P., Tchepakova N., Chen T., Molen M.K. Van Der, Beilelli Marchesini L., Maximov T.C., Maksyutov S. & Schulze E.D. 2012. An estimate of the terrestrial carbon budget of Russia using inventory-based, eddy covariance and inversion methods. *Biogeosciences* 9: 5323–5340.
- FAO. 1995. Forest resources assessment 1990. Global synthesis. FAO Forestry Paper 124. Rome. 90p.
- Forkel M., Carvalhais N., Rödenbeck C., Keeling R., Heimann M., Thonicke K., Zaehle S. & Reichstein M. 2016. Enhanced seasonal CO₂ exchange caused by amplified plant productivity in northern ecosystems. *Science* 4971: 696–699.
- France P.C., Willem J., Friedlingstein P. & Munhoven G. 2013. Carbon and Other Biogeochemical Cycles. *Climate Change 2013 - The Physical Science Basis*: 465–570.
- Frolking, S.S., Bubier, J.L., Moore, T.R., Bellisario, L.M., Bhardwaj, A., Carroll, P., Grill, P.M., Lafleur, P.M., McCaughey, J.H., Roulet, N.T., Suyker, A.E., Verma, S.B., Waddington, J.M., Whiting, G.J., 1998. Relationship between ecosystem productivity and photosynthetically active radiation from northern peatlands.PDF.

- Global Biogeochem. Cycles 12, 115–126.
- Gauthier S., Bernier P., Kuuluvainen T., Shvidenko A.Z. & Schepaschenko D.G. 2015. Boreal forest health and global change. *Science* 349: 819–822.
- Gorham, E., 1991. Northern Peatlands: Role in the Carbon Cycle and Probable Responses to Climatic Warming. *Ecol. Appl.* 1, 182–195. doi:10.2307/1941811
- Groisman P. & Soja A.J. 2009. Ongoing climatic change in Northern Eurasia: justification for expedient research. *Environmental Research Letters* 4: 045002.
- Hayes D.J., McGuire a. D., Kicklighter D.W., Gurney K.R., Burnside T.J. & Melillo J.M. 2011. Is the northern high-latitude land-based CO₂ sink weakening? *Global Biogeochemical Cycles* 25: n/a-n/a.
- Heimann M. & Reichstein M. 2008. Terrestrial ecosystem carbon dynamics and climate feedbacks. *Nature* 451: 289–292.
- Huntzinger D.N., Michalak A.M., Schwalm C., Ciais P., King A.W., Fang Y., Schaefer K., Wei Y., Cook R.B., Fisher J.B., Hayes D., Huang M., Ito A., Jain A.K., Lei H., Lu C., Maignan F., Mao J., Parazoo N., Peng S., Poulter B., Ricciuto D., Shi X., Tian H., Wang W., Zeng N. & Zhao F. 2017. Uncertainty in the response of terrestrial carbon sink to environmental drivers undermines carbon-climate feedback predictions. *Scientific Reports* 7: 4765.
- Kasischke, E.S. and Stocks, B.J. 2000. Fire, climate change, and carbon cycling in the boreal forest. Springer-Verlag, New York, NY.
- Kauppi, P. E., Posch, M., Hänninen, P., Henttonen, H. M., Iha-lainen, A., Lappalainen, E., Starr, M., and Tamminen, P.: Car- bon reservoirs in peatlands and forests in the boreal regions of Finland, *Silva Fenn.*, 31, 13–25, 1997.
- Kirschbaum, M.U.F., Eamus, D., Gifford, R.M., Roxburgh, S.H., Sands, P.J., 2001. Definitions of some ecological terms commonly used in carbon accounting. *Coop. Res. Cent. Carbon Account.* 2–6. doi:10.1111/j.1365-2486.2004.00878.x
- Le Quéré, C., Robbie M. Andrew, Pierre Friedlingstein, Stephen Sitch, Julia Pongratz, A.C., Manning, Jan Ivar Korsbakken, Glen P. Peters, Josep G. Canadell, Robert B. Jackson, T.A.B., Pieter P. Tans, Oliver D. Andrews, Vivek K. Arora, Dorothee C. E. Bakker, Leticia Barbero, M., 2018. Global Carbon Budget 2017. *Earth Syst. Sci. Data* 10, 405–448.

- Liou, K. N., 2002: An Introduction to Atmospheric Radiation. Academic Press, 583 pp.
- Lafleur P.M. & Humphreys E.R. 2008. Spring warming and carbon dioxide exchange over low Arctic tundra in central Canada. *Global Change Biology* 14: 740–756.
- Limpens J., Berendse F., Blodau C., Canadell J.G., Freeman C., Holden J., Roulet N., Rydin H. & Schaepman-Strub G. 2008. Peatlands and the carbon cycle: from local processes to global implications – a synthesis. *Biogeosciences* 5: 1475–1491.
- Lovett G.M., Cole J.J. & Pace M.L. 2006. Is net ecosystem production equal to ecosystem carbon accumulation? *Ecosystems* 9: 152–155.
- Lund, M., Lafleur, P.M., Roulet, N.T., Lindroth, A., Christensen, T.R., Aurela, M., Chojnicki, B.H., Flanagan, L.B., Humphreys, E.R., Laurila, T., Oechel, W.C., Olejnik, J., Rinne, J., Schubert, P., Nilsson, M.B., 2010. Variability in exchange of CO₂ across 12 northern peatland and tundra sites. *Glob. Chang. Biol.* 16, 2436–2448. doi:10.1111/j.1365-2486.2009.02104.x
- Matthews H.D., Weaver A.J. & Meissner K.J. 2005. Terrestrial carbon cycle dynamics under recent and future climate change. *Journal of Climate* 18: 1609–1628.
- McGuire A.D., Wirth C., Apps M., Beringer J., Clein J., Epstein H., Kicklighter D.W., Bhatti J., Chapin F.S., Groot B. de, Efremov D., Eugster W., Fukuda M., Gower T., Hinzman L., Huntley B., Jia G.J., Kasischke E., Melillo J., Romanovsky V., Shvidenko A., Vaganov E. & Walker D. 2002. Environmental variation, vegetation distribution, carbon dynamics and water/energy exchange at high latitudes. *Journal of Vegetation Science* 13: 301–314.
- McNaughton S.J., Oosterheld M., Frank D.A. & Williams K.J. 1989. Ecosystem-level patterns of primary productivity and herbivory in terrestrial habitats. *Nature* 341: 142–144.
- Mitsch, W.J. and Gosselink, J.G. 1993. *Wetlands* (2nd ed.). Van Nostrand Reinhold Co., New York.
- Moore, T.R., Knowles, R., 1989. the Influence of Water Table Levels on Methane and Carbon Dioxide Emissions From Peatland Soils. *Can. J. Soil Sci.* 69, 33–38. doi:10.4141/cjss89-004
- Monier, E., Sokolov, A., Schlosser, A., Scott, J., Gao, X., 2013. Probabilistic projections of 21st century climate change over Northern Eurasia. *Environ. Res. Lett.* 8, 1–9.

doi:10.1088/1748-9326/8/4/045008

- Myneni R.B., Keeling C.D., Tucker C.J., Asrar G. & Nemani R.R. 1997. Increased plant growth in the northern high latitudes.pdf.
- Pan, Y., Birdsey, R. a, Fang, J., Houghton, R., Kauppi, P.E., Kurz, W. a, Phillips, O.L., Shvidenko, A., Lewis, S.L., Canadell, J.G., Ciais, P., Jackson, R.B., Pacala, S.W., McGuire, a D., Piao, S., Rautiainen, A., Sitch, S., Hayes, D., 2011. A large and persistent carbon sink in the world's forests. *Science* 333, 988–93.
doi:10.1126/science.1201609
- Piao S., Ciais P., Friedlingstein P., Peylin P., Reichstein M., Luysaert S., Margolis H., Fang J., Barr A., Chen A., Grelle A., Hollinger D.Y., Laurila T., Lindroth A., Richardson A.D. & Vesala T. 2008. Net carbon dioxide losses of northern ecosystems in response to autumn warming. *Nature* 451: 49–52.
- Piao S., Wang X., Ciais P., Zhu B., Wang T. & Liu J. 2011. Changes in satellite-derived vegetation growth trend in temperate and boreal Eurasia from 1982 to 2006. *Global Change Biology* 17: 3228–3239.
- Prentice, I.C., Farquhar, G.D., Fasham, M.J.R., Goulden, M.L., Heiman, M., Jaramillo, V.J., Kheshgi, H.S., Le Quere, C., Scholes, R.J., Wallace, D.W.R., 2001. The carbon cycle and atmospheric carbon dioxide. In: J.T. Houghton, Y. Ding, D.J. Griggs, M. Noguera, P.J. van der Linden, X. Dai, K. Maskell, C.A. Johnson (Editors), *Climate Change 2001: The Scientific Basis, Contribution of Working Group I to the Third Assessment Report of the Intergovernmental Panel on Climate Change*. Cambridge University Press., Cambridge, pp. 183-237.
- Pulliainen J., Aurela M., Laurila T., Aalto T., Takala M., Salminen M., Kulmala M., Barr A., Heimann M., Lindroth A., Laaksonen A., Derksen C., Mäkelä A., Markkanen T., Lemmetyinen J., Susiluoto J., Dengel S., Mammarella I., Tuovinen J.-P. & Vesala T. 2017. Early snowmelt significantly enhances boreal springtime carbon uptake. *Proceedings of the National Academy of Sciences* 114: 201707889.
- Raupach M.R., Gloor M., Sarmiento J.L., Canadell J.G., Frölicher T.L., Gasser T., Houghton R.A., Quéré C. Le & Trudinger C.M. 2014. The declining uptake rate of atmospheric CO₂ by land and ocean sinks. *Biogeosciences* 11: 3453–3475.
- Ruckstuhl K.E., Johnson E. a & Miyanishi K. 2008. Introduction. The boreal forest and

- global change. *Philosophical transactions of the Royal Society of London. Series B, Biological sciences* 363: 2245–2249.
- Schot, P.P. 1999. Wetlands. In, Nath, B. et al. (eds.), *Environmental Management in Practice: Vol. 3*, p. 62-85. Routledge, London & New York, 297 p.
- Schulze E.D., Lapshina E., Filippov I., Kuhlmann I. & Mollicone D. 2015. Carbon dynamics in boreal peatlands of the Yenisey region, western Siberia. *Biogeosciences* 12: 7057–7070.
- Smith, L.C., MacDonald, G.M., Velichko, A.A., Beilman, D.W., Borisova, O.K., Frey, K.E., Kremenetski, K. V., Sheng, Y., 2004. Siberian Peatlands a Net Carbon Sink and Global Methane Source since the Early Holocene. *Science* (80-.). 303, 353–356. doi:10.1126/science.1090553
- Stocks, B.J., Fosberg, M.A., Lynham, T.J., Mearns, L., Wotton, B.M., Yang, Q., Jin, J.-Z., Lawrence, K., Hartley, G.R., Mason, J.A., McKENNEY, D.W., 1998. Climate Change and Forest Fire Potential in Russian and Canadian Boreal Forests. *Clim. Change* 38, 1–13. doi:10.1023/A:1005306001055
- Tishkov A., 2002. Boreal forests. In: Shahgedanova, M. (Ed.), *The physical geography of Northern Eurasia*. Oxford University Press, Oxford, pp. 216–233.
- Trumbore S. 2006. Carbon respired by terrestrial ecosystems - recent progress and challenges. *Global Change Biology* 12: 141–153.
- Turunen J., Tomppo E., Tolonen K., 2002. Estimating carbon accumulation rates of undrained mires in Finland – application to boreal and subarctic regions. *Holocene*, 12, 69-80.
- Vasileva A. V., Moiseenko K.B., Mayer J.C., Jürgens N., Panov A., Heimann M. & Andreae M.O. 2011. Assessment of the regional atmospheric impact of wildfire emissions based on CO observations at the ZOTTO tall tower station in central Siberia. *Journal of Geophysical Research Atmospheres* 116: 1–18.
- Wieder R. K., Vitt D. H., Benscoter B.W., 2006. Peatlands and the Boreal forest. In: *Boreal Peatland Ecosystems*, Ecological Studies 188 (eds Wieder RK, Vitt DH), pp. 1-8. Springer-Verlag, Heidelberg, Germany.
- Winderlich J., Gerbig C., Kolle O. & Heimann M. 2014. Inferences from CO₂ and CH₄ concentration profiles at the Zotino Tall Tower Observatory (ZOTTO) on

- regional summertime ecosystem fluxes. *Biogeosciences* 11: 2055–2068.
- Young, A.M., Higuera, P.E., Duffy, P.A., Hu, F.S., 2017. Climatic thresholds shape northern high-latitude fire regimes and imply vulnerability to future climate change. *Ecography (Cop.)*. 40, 606–617. doi:10.1111/ecog.02205
- Yu, Z.C., 2012. Northern peatland carbon stocks and dynamics: A review. *Biogeosciences* 9, 4071–4085. doi:10.5194/bg-9-4071-2012

Chapter 2 Materials and methods

2.1 Study site

The research station is located in Zotino village (60.48 °N, 89.21 °E) approximately 20 km west of the Yenisei River in the Krasnoyarsk region of Russia. The station is influenced by a strong continental climate with a large temperature amplitude and intermediate precipitation. Based on the long-term weather station measurements from 1937-1989, the average air temperature in January was -26 °C and 22 °C in July. During the wintertime, air temperature can drop below -40 °C, and during summertime air temperature can exceed 35 °C. Annual precipitation is approximately 600 mm. During winter, snow accumulates to approximately 2 m depth (Schulze et al. 2002).

The dominant land cover types at the Zotino site are boreal coniferous forest and peat bog. Flux measurement towers were installed at a Scots pine forest and a sphagnum peat bog. Details of site characteristics are described in Chapter 3.2 and Chapter 4.2.

In the past, many investigations have been conducted to quantify and characterize the seasonal variability in C, water, and energy fluxes at the forest and bog in Zotino. Flux measurements in Zotino were initiated as a part of the EUROSIBERIAN CARBONFLUX project from 1998-2000 and the Terrestrial Carbon Observing Programme-Siberia (TCOS-Siberia) from 2002-2005 (Heimann, 2002; Schulze et al. 2002). This project was a pioneering international research initiative for monitoring the biogeochemical cycle over the European-Russian and western Siberian boreal ecosystems. The project included short-term aircraft measurement campaigns to monitor atmospheric CO₂ and its isotopic composition profile, atmospheric oxygen and nitrogen ratio (O₂/N₂), CH₄ and CO concentrations (Lloyd et al. 2001). In addition, year-round flux measurements were performed to investigate CO₂ and energy fluxes in boreal forests (Kelliher et al. 1998; Valentini et al. 2000; Tchebakova et al. 2002; Lloyd et al., 2001) and in bogs (Arneth et al., 2002; Kurbatova et al. 2002; Arneth et al. 2006). Soil respiration measurements using the chamber technique were also conducted (Shibistova et al. 2002) and the results were published in the journal *Tellus* 54B special issue (Heimann, 2002). However, long-term EC flux measurements were not continued after 2001 in Zotino. In 2012, new EC flux measurement systems were installed to measure

CO₂, water vapour, and energy exchanges at a coniferous forest and bog in the surrounding the Zotino tall tower (Winderlich et al. 2014; Park et al. 2018).

The Zotino Tall Tower Observatory (ZOTTO) is a biogeochemical monitoring station established in 2006 as a German-Russian cooperation project (Heimann et al. 2014). The goal of ZOTTO is to quantify spatio-temporal variations in the long-term regional GHG budget with a robust approach (Kozlova et al. 2008; Heimann et al. 2014).

2.2 Ground-based CO₂ measurements

This section presents a brief overview of the tower-based CO₂ measurements currently being conducted at the Zotino site.

Ground-based CO₂ monitoring systems are vital to quantify C budgets and understand the processes of the C cycle between the terrestrial ecosystems and the atmosphere. These systems provide the spatial and temporal distributions of sources and sinks of GHG by combining various measurement platforms (e.g. space-based and aircraft etc.) and the atmospheric inverse modelling technique (Ciais et al. 2014; Dolman et al. 2008; Haszpra et al. 2005; Barcza et al. 2009; Desai et al. 2015). Synthesizing different approaches reduces the uncertainty in quantifying C budgets at regional to global scales (Lauvaux et al. 2012; Peters et al. 2007; Thomson et al. 2016; Winderlich, 2012; Saeki et al. 2013).

Atmospheric mixing ratio measurements provide the concentrations of atmospheric GHG compositions. The atmospheric GHG observation networks provide reliable and continuous background gas concentrations from daily to multi-decadal scales for a wide temporal range (Lucas et al., 2015). Tall tower platforms (> 200 m) are particularly useful where observation networks are sparse and in vulnerable regions affected by climate change, such as Siberia and the Amazon basin (Winderlich et al. 2010; Sasakawa et al. 2012; Andrea et al. 2016; Kim et al. 2017). Mixing ratio measurement systems at the tall tower can sample the air above the surface layer or at a mixed layer height, minimizing the local source and sink influences from the ground surface (Gloor et al. 2001). Therefore, since early 1990s scientists have used a similar concept to the tall television towers to measure atmospheric GHGs (Tans, 1991; Bakwin et al. 1998; Haszpra et al. 2001; Popa et al. 2010). For instance, tall tower GHG

measurements were used to estimate the source-sink distributions of surface CO₂ flux and carbon budget in northern Eurasia (Winderlich, 2012; Saeki et al. 2013; Kim et al. 2017).

Traditionally, atmospheric GHG observatories measure mole fractions of CO₂ by non-dispersive infrared (NDIR) spectroscopy and CH₄ by Gas Chromatography (GC) (Rella et al. 2013). These techniques were also applied to measure CO₂, CH₄, CO, and N₂O in ZOTTO (Kozlova et al. 2008; Kozlova and Manning, 2009). However, it requires expensive laboratory work and frequent maintenance to handle dry air sample. Therefore, continuous *in-situ* atmospheric GHG measurements at remote observatory would be challenging. Over the past 10 years, the cavity ring-down spectroscopy (CRDS) technique has been developed to improve temporal resolution, precision and accuracy of GHG measurements, and reduce maintenance efforts (Rella et al. 2013; Chen et al. 2010). Since 2009, the same technique has applied at ZOTTO and produce continuous and high quality measurements of dry mole fractions of CO₂ and CH₄ (Winderlich et al. 2010; Timokhina et al. 2018).

A global flux tower network (FLUXNET) has also grown over the past 25 years (Baldocchi et al. 2001). Flux measurements provide information about the local source and sink distributions of different carbon reservoirs on various vegetation types and climate regions (Burba and Anderson, 2010; Baldocchi et al. 2001; Chu et al. 2017). Depending on the measurement height, the EC flux measurements cover on an ecosystem scale of 1-3 km² (spatial scale of 100-2000 m) from daily to annual time scales (Baldocchi, 1997; Schmid, 1994). At present, approximately 900 flux stations are operating all over the world (Chu et al. 2017). However, very few stations exist in Russia despite the fact that this region contains the largest forested area worldwide.

Micrometeorological methods are widely used as a non-destructive, reliable, and quasi-continuous approach to obtain vertical turbulent fluxes on agricultural and forestry applications (Meyers and Baldocchi, 2005). In this thesis, CO₂ fluxes were obtained by two micrometeorological methods. Direct flux measurements at a coniferous forest and bog were obtained by the eddy covariance (EC) method, representing an ecosystem scale (~1 km²) (Chapter 3 and 4). To obtain CO₂ fluxes at a larger scale, a combination of changes in the CO₂ concentration profile at the tall tower with the modified Bowen ratio

(MBR) method were used (Chapter 5). This subsection presents a brief overview of theoretical background of the EC and the MBR methods.

On flux towers, micrometeorological methods are used to measure trace gases, energy, and momentum exchanges between the surface and the atmosphere (Fig. 2.1). One of the most widely used micrometeorological methods is the EC. This method directly measures turbulent fluxes using a fast-responsive sonic anemometer and gas analyzer (measurement frequency of 10-20 Hz) (Baldocchi et al., 2001; Aubinet et al. 2012). Eddy or turbulent flux in the atmospheric surface boundary layer is calculated by the covariance of the vertical wind velocity and the scalar density of atmospheric constituent (Swinbank, 1951; Aubinet et al. 2012):

$$F \approx \overline{\rho_a} \overline{w's'}$$

where $\overline{\rho_a}$ is mean density of atmospheric constituent [mg m^{-3}], s' is perturbation of mixing ratio, and w' is a perturbation of vertical wind velocity [m s^{-1}]. Generally, this equation is expressed simply as $\overline{w'\rho_c'}$ for CO_2 flux when density fluctuations (s') are assumed negligible.

The EC method requires specific assumptions. First, turbulence in surface layer is measured under statistically stationary condition. Under this condition, fluctuations do not change during the averaging time (e.g. 5-60 min but typically 30 min). Second, the terrain surrounding of flux tower is relatively flat, topographically and horizontally homogenous. Third, no strong divergence and convergence flows should dominate during the transport processes, therefore density change is negligible (Aubinet et al. 2012; Meyers and Baldocchi, 2005). In practice, setting measurement stations in heterogeneous landscapes and complex terrains are unavoidable. Therefore, accurate estimates of carbon exchange and carbon budget can be challenging due to horizontal and vertical advections (Finnigan et al. 2003; Kang et al. 2017). However, as the Zotino site is relatively homogeneous and the terrain is flat, advection terms are not considered in my research. Systematic or unknown random errors from the EC method can be minimized through instrumental configurations and flux correction methods (Aubinet et al. 2012; Lee et al. 2004).

The EC method also requires specifications in both hardware and software systems: (1) the capability to measure small sizes of eddies continuously, (2) minimize

flow distortion, (3) low power consumption, (4) large data storage to save raw data, (5) the standardization of post-processing, quality check and quality assurance procedures (Moncrieff et al., 1997). Currently, there are seven software packages for raw data processing and data acquisition (e.g., EddyUH, EddyPro, TK3 and etc.) provide various options for flux calculation, flux corrections, and footprint analysis (Fratini et al. 2014; Mammarella et al. 2015). As each software has strengths and weakness, researchers need to consider the proper flux correction or raw-data processing schemes for their site characteristics and research purposes. In addition, post-processing of half-hourly flux and meteorological data with gap-filling and flux partitioning procedures (e.g., REddyProc) can be used (Wuzler et al. 2018). A brief overview of raw-data and post-processing tools is listed in <https://fluxnet.fluxdata.org/2017/10/10/toolbox-a-rolling-list-of-softwarepackages-for-flux-related-data-processing/>.

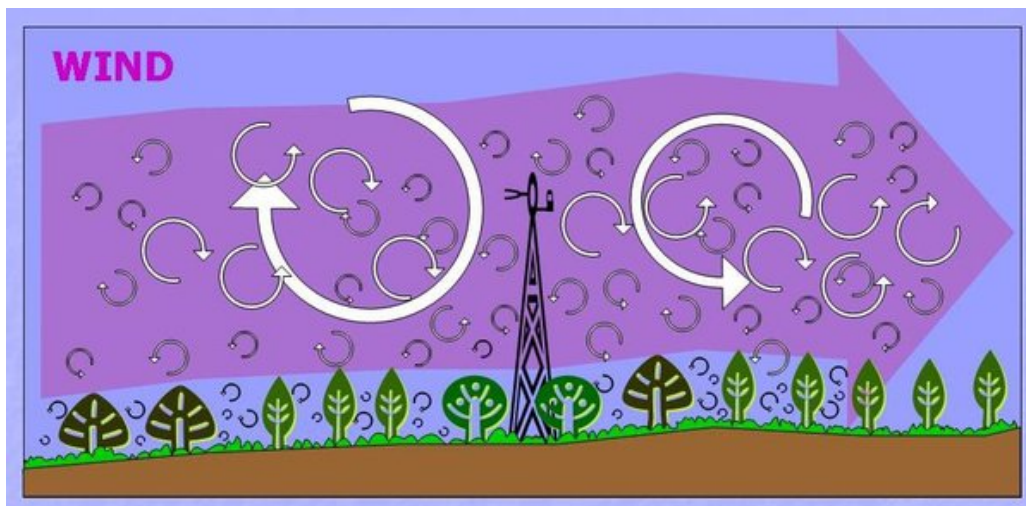


Figure 2.1 The eddy covariance technique directly measures the exchanges of gases, energy, and momentum exchanges between the surface and the atmosphere. In surface layer, the air flow (big arrows) consists of numerous and various sizes of individual eddies and vortices (small arrows). Eddies move in both horizontal and vertical directions. Adopted from Burba and Anderson (2010), [Online image]. Retrieved on December 18, 2017, from https://upload.wikimedia.org/wikipedia/commons/6/65/Pyörrekovarianssi-tekniikan_kaaviokuva.jpg

Fluxes of CO₂, water vapour, and CH₄ are measured by the EC method. However, gas analyzers for some chemical species (e.g. from volatilization fluxes) or particle

depositions (e.g. organic micro pollutants) have a low frequency or require a long sampling time from several hours to several weeks, which do not fulfil the requirements for the EC method (Bolinus et al. 2016; Meyers and Baldocchi, 2005). In this case, alternative micrometeorological methods are used to overcome the specific assumptions of the EC method (e.g. gas species, low response gas analysers etc.) (Pattery et al. 1993; Meyers and Baldocchi, 2005). On such approach is the MBR method for estimating fluxes (Hicks and Wesely, 1978). Originally, the MBR method was used to estimate heat flux (Bowen, 1926; Hicks and Wesely, 1978). Later, this method was applied to lake and forest floor to determine CO₂ and H₂O fluxes (Meyers et al. 1996) as well as other trace gas fluxes (e.g. nitric acid vapour, ammonia, and mercury) and particle composition (e.g., persistent organic pollutants) (Mayer et al. 2011; Meyers and Baldocchi, 2005; Bolinius et al. 2016).

This method is based on Monion-Obukov similarity theory (MOST), assuming the eddy diffusivity (K) of each trace gas is identical to the eddy diffusivity of measured heat flux (Meyers and Baldocchi, 2005; Mayers et al. 1996). The K -theory is a generalized MOST in which turbulent fluxes can be parameterized with the local mean gradient of the transported quantity and a positive eddy-transfer coefficient or eddy diffusivity K (Stull, 1988). This coefficient K is not constant and differs depending on the scalar quantity. It varies with the size of eddies and increases with height. But, K in the similarity theory is assumed to be replaceable for all scalar quantities; therefore the coefficient for calculating one flux can be equal to another flux (Meyers et al., 1996):

$$F_x = K \frac{dc}{dz}$$

The flux of the target gas species (F_x) can be determined by a measure of the concentration gradient (dc) over the same height interval (dz).

For ZOTTO, the measurements system are not suitable for flux measuring fluxes because of flow distortion due to the very long tubing (302 m), the low measurement frequency of CO₂ concentration (0.2 Hz), and the long mixing time inside of the buffers (~40 min) (Winderlich et al., 2014). Therefore, the MBR method can be applied. By combining it with changes in the CO₂ concentrations from surface to the top of the tall tower, the MBR method is only needed to account for fluxes across the top level, when

mixing reaches beyond the observed profile. Detailed procedure to obtain tall-tower based CO₂ fluxes are described in Winderlich et al. (2014) and Chapter 5 in this thesis.

2.3 References

- Andreae M.O., Acevedo O.C., Araùjo A., Artaxo P., Barbosa C.G.G., Barbosa H.M.J., Brito J., Carbone S., Chi X., Cintra B.B.L., Silva N.F. Da, Dias N.L., Dias-Júnior C.Q., Ditas F., Ditz R., Godoi A.F.L., Godoi R.H.M., Heimann M., Hoffmann T., Kesselmeier J., Könemann T., Krüger M.L., Lavric J. V., Manzi A.O., Lopes A.P., Martins D.L., Mikhailov E.F., Moran-Zuloaga D., Nelson B.W., Nölscher A.C., Santos Nogueira D., Piedade M.T.F., Pöhlker C., Pöschl U., Quesada C.A., Rizzo L. V., Ro C.U., Ruckteschler N., Sá L.D.A., Oliveira Sá M. De, Sales C.B., Santos R.M.N. Dos, Saturno J., Schöngart J., Sörgel M., Souza C.M. De, Souza R.A.F. De, Su H., Targhetta N., Tóta J., Trebs I., Trumbore S., Eijck A. Van, Walter D., Wang Z., Weber B., Williams J., Winderlich J., Wittmann F., Wolff S. & Yáñez-Serrano A.M. 2015. The Amazon Tall Tower Observatory (ATTO): Overview of pilot measurements on ecosystem ecology, meteorology, trace gases, and aerosols. *Atmospheric Chemistry and Physics* 15: 10723–10776.
- Arneth A., Kurbatova J., Kolle O., Shibistova O.B., Lloyd J., Vygodskaya N.N. & Schulze E.-D. 2002. Comparative ecosystem-atmosphere exchange of energy and mass in a European Russian and a central Siberian bog II. Interseasonal and interannual variability of CO₂ fluxes. *Tellus B* 54: 514–530.
- Arneth a., Veenendaal E.M., Best C., Timmermans W., Kolle O., Montagnani L. & Shibistova O. 2006. Water use strategies and ecosystem-atmosphere exchange of CO₂ in two highly seasonal environments. *Biogeosciences* 3: 421–437.
- Aubinet M., Vesala T., and Papale D. (eds.), 2012. Eddy Covariance: A Practical Guide to Measurement and Data Analysis, Springer Atmospheric Sciences, DOI 10.1007/978-94-007-2351-1 5, Springer-Verlag, 451 pp.
- Bakwin P.S., Tans P.P., Hurst D.F. & Zhao C. 1998. Measurements of carbon dioxide on very tall towers: Results of the NOAA/CMDL program. *Tellus, Series B: Chemical and Physical Meteorology* 50: 401–415.
- Baldocchi D. 1997. Flux Footprints Within and Over Forest Canopies. *Boundary-Layer Meteorology* 85: 273–292.
- Baldocchi D.D. 2003. Assessing the eddy covariance technique for evaluating carbon dioxide exchange rates of ecosystems: past, present and future. *Global Change Biology* 9: 479–492.
- Baldocchi D., Falge E., Gu L., Olson R., Hollinger D., Running S., Anthoni P., Bernhofer C., Davis K., Evans R., Fuentes J., Goldstein A., Katul G., Law B., Lee X., Malhi Y., Meyers T., Munger W., Oechel W., Paw K.T.U., Pilegaard K., Schmid H.P. & Valentini R. 2001. FLUXNET : A New Tool to Study the Temporal and Spatial Variability of Ecosystem-Scale Carbon Dioxide , Water Vapor , and Energy Flux Densities. : 2415–2434.
- Barcza Z., Kern A., Haszpra L. & Kljun N. 2009. Spatial representativeness of tall tower eddy covariance measurements using remote sensing and footprint analysis. *Agricultural and Forest Meteorology* 149: 795–807.
- Bolinus D.J., Jahnke A. & MacLeod M. 2016. Comparison of eddy covariance and modified Bowen ratio methods for measuring gas fluxes and implications for measuring fluxes of persistent organic pollutants. *Atmospheric Chemistry and Physics* 16: 5315–5322.
- Bowen, I.S., 1926. The ratio fo heat losses by conduction and by evaporation from any

- water surface. *Phys. Rev.*, 27, 779-787.
- Burba, G., and D. Anderson, 2010. A Brief Practical Guide to Eddy Covariance Flux Measurements: Principles and Workflow Examples for Scientific and Industrial Applications. LI-COR Biosciences, Lincoln, Nebraska, USA, 212 pp.: <http://www.licor.com/eddycovariance>.
- Chen H., Winderlich J., Gerbig C., Hoefler A., Rella C.W., Crosson E.R., Pelt A.D. Van, Steinbach J., Kolle O., Beck V., Daube B.C., Gottlieb E.W., Chow V.Y., Santoni G.W. & Wofsy S.C. 2010. High-accuracy continuous airborne measurements of greenhouse gases (CO₂ and CH₄) using the cavity ring-down spectroscopy (CRDS) technique. *Atmospheric Measurement Techniques* 3: 375–386.
- Chu H., Baldocchi D.D., John R., Wolf S. & Reichstein M. 2017. Fluxes all of the time? A primer on the temporal representativeness of FLUXNET. *Journal of Geophysical Research: Biogeosciences* 122: 289–307.
- Ciais P., Dolman A.J., Bombelli A., Duren R., Pregon A., Rayner P.J., Miller C., Gobron N., Kinderman G., Marland G., Gruber N., Chevallier F., Andres R.J., Balsamo G., Bopp L., Bréon F.M., Broquet G., Dargaville R., Battin T.J., Borges A., Bovensmann H., Buchwitz M., Butler J., Canadell J.G., Cook R.B., Defries R., Engelen R., Gurney K.R., Heinze C., Heimann M., Held A., Henry M., Law B., Luyssaert S., Miller J., Moriyama T., Moulin C., Myneni R.B., Nussli C., Obersteiner M., Ojima D., Pan Y., Paris J.D., Piao S.L., Poulter B., Plummer S., Quegan S., Raymond P., Reichstein M., Rivier L., Sabine C., Schimel D., Tarasova O., Valentini R., Wang R., Werf G. Van Der, Wickland D., Williams M. & Zehner C. 2014. Current systematic carbon-cycle observations and the need for implementing a policy-relevant carbon observing system. *Biogeosciences* 11: 3547–3602.
- Desai A.R., Xu K., Tian H., Weishampel P., Thom J., Baumann D., Andrews A.E., Cook B.D., King J.Y. & Kolka R. 2015. Landscape-level terrestrial methane flux observed from a very tall tower. *Agricultural and Forest Meteorology* 201: 61–75.
- Dolman, Han (A.J & Valentini, Riccardo & Freibauer, Annette. (2008). Introduction: Observing the Continental-Scale Greenhouse Gas Balance. 10.1007/978-0-387-76570-9_1.
- Finnigan J.J., Clement R., Malhi Y., Leuning R. & Cleugh H.A. 2003. Techniques Part I: Averaging and Coordinate Rotation. *Boundary-Layer Meteorology* 107: 1–48.
- Foken, T. and B. Wichura, 1996: ‘Tools for quality assessment of surface-based flux measurements’. *Agricultural and Forest Meteorology*, vol. 78(1-2): pp. 83–105.
- Fratini G. & Mauder M. 2014. Towards a consistent eddy-covariance processing: An intercomparison of EddyPro and TK3. *Atmospheric Measurement Techniques* 7: 2273–2281.
- Gloor M., Bakwin P., Hurst D., Lock L., Draxler R. & Tans P. 2001. What is the concentration footprint of a tall tower? *Journal of Geophysical Research* 106: 17831.
- Haszpra L., Barcza Z., Bakwin P.S., Berger B.W., Davis K.J. & Weidinger T. 2001. Measuring system for the long-term monitoring of biosphere/atmosphere exchange of carbon dioxide. *Journal of Geophysical Research Atmospheres* 106: 3057–3069.
- Haszpra L., Barcza Z., Davis K.J. & Tarczay K. 2005. Long-term tall tower carbon dioxide flux monitoring over an area of mixed vegetation. *Agricultural and Forest*

- Meteorology* 132: 58–77.
- Heimann M., 2002. Forword: The EUROSIBERIAN CARBONFLUX project. *Tellus* 54B, : 417–419.
- Heimann M., Schulze E.-D., Winderlich J., Andreae M.O., Chi X., Gerbig C., Kolle O., Kuebler K., Lavrič J. V., Mikhailov E., Panov A., Park S., Rödenbeck C. & Skorochood A. 2014. The Zotino Tall Tower Observatory (ZOTTO): Quantifying large scale biogeochemical changes in Central Siberia. *Nova Acta Leopoldina* 117: 51–64.
- Hicks B. B. and Wesely M. L. (1978) An examination of some micrometeorological methods for measuring dry deposition. U. S. EPA Report, EPA-600/7-78-116, Research Triangle Park, North Carolina.
- Kang M., Ruddell B.L., Cho C., Chun J. & Kim J. 2017. Identifying CO₂ advection on a hill slope using information flow. *Agricultural and Forest Meteorology* 232: 265–278.
- Kelliher F.M., Lloyd J., Arneth A., Byers J.N., McSeveny T.M., Milukova I., Grigoriev S., Panforyov M., Sogatchev A., Varlargin A., Ziegler W., Bauer G. & Schulze E.-D. 1998. Evaporation from a central Siberian pine forest. *Journal of Hydrology* 205: 279–296.
- Kim J., Kim H.M., Cho C.-H., Boo K.-O., Jacobson A.R., Sasakawa M., Machida T., Arshinov M. & Fedoseev N. 2017. Impact of Siberian observations on the optimization of surface CO₂ flux. *Atmospheric Chemistry and Physics* 17: 2881–2899.
- Kozlova E. a. & Manning a. C. 2009. Methodology and calibration for continuous measurements of biogeochemical trace gas and O₂ concentrations from a 300-m tall tower in central Siberia. *Atmospheric Measurement Techniques* 2: 205–220.
- Kozlova E.A., Manning A.C., Kisilyakhov Y., Seifert T. & Heimann M. 2008. Seasonal, synoptic, and diurnal-scale variability of biogeochemical trace gases and O₂ from a 300-m tall tower in central Siberia. *Global Biogeochemical Cycles* 22: 1–16.
- Kurbatova B.J., Arneth A., Vygodskaya N.N. & Kolle O. 2002. Comparative ecosystem – atmosphere exchange of energy and mass in a European Russian and a central Siberian bog I . Interseasonal and interannual variability of energy and latent heat fluxes during the snowfree period. : 497–513.
- Lauvaux T., Schuh A.E., Bocquet M., Wu L., Richardson S., Miles N. & Davis K.J. 2012. Network design for mesoscale inversions of CO₂ sources and sinks. *Tellus, Series B: Chemical and Physical Meteorology* 64.
- Lee, X., W. Massman, and B. Law (Eds.), 2004. “Handbook of Micrometeorology: A Guide for Surface Flux Measurement and Analysis”. Springer-Verlag, 250 pp.
- Lloyd J., Francey R.J., Mollicone D., Raupach M.R., Sogachev A., Arneth A., Byers J.N., Kelliher F.M., Rebmann C., Valentini R., Wong S.-C., Bauer G. & Schulze E.-D. 2001. estimates for CO₂ and its 3C/nC ratio and for water vapor above. *Global Biogeochemical Cycles* 15: 267–284.
- Lloyd, J., Shibistova, O., Zolotoukhine, D., Kolle, O., Arneth, A., Wirth, C., Styles, J.M., Tchebakova, N.M., Schulze, E.-D., 2002. Seasonal and annual variations in the photosynthetic productivity and carbon balance of a central Siberian pine forest. *Tellus B* 54, 590–610. doi:10.1034/j.1600-0889.2002.01487.x
- Lucas D.D., Yver Kwok C., Cameron-Smith P., Graven H., Bergmann D., Guilderson

- T.P., Weiss R. & Keeling R. 2015. Designing optimal greenhouse gas observing networks that consider performance and cost. *Geoscientific Instrumentation, Methods and Data Systems* 4: 121–137.
- Mammarella I., Nordbo A., Rannik Ü., Haapanala S., Levula J., Laakso H., Ojala A., Peltola O., Heiskanen J., Pumpanen J. & Vesala T. 2015. Carbon dioxide and energy fluxes over a small boreal lake in Southern Finland. *Journal of Geophysical Research: Biogeosciences* 120: 1296–1314.
- Mayer, J.C., Bargsten, A., Rummel, U., Meixner, F.X., Foken, T., 2011. Distributed Modified Bowen Ratio method for surface layer fluxes of reactive and non-reactive trace gases. *Agric. For. Meteorol.* 151, 655–668.
doi:10.1016/j.agrformet.2010.10.001
- Meyers T.P., Hall M.E., Lindberg S.E. & Kim K. 1996. Use of the modified Bowen-ratio technique to measure fluxes of trace gases. *Atmospheric Environment* 30: 3321–3329.
- Meys, Tilden P. and Baldocchi, Dennis D., "Current Micrometeorological Flux Methodologies with Applications in Agriculture" (2005). Publications, Agencies and Staff of the U.S. Department of Commerce. 500.
<http://digitalcommons.unl.edu/usdeptcommercepub/500>.
- Moncrieff, J.B., Massheder, J.M., De Bruin, H., Elbers, J., Friborg, T., Heusinkveld, B., Kabat, P., Scott, S., Soegaard, H., Verhoef, A., 1997. A system to measure surface fluxes of momentum, sensible heat, water vapour and carbon dioxide. *J. Hydrol.* 188–189, 589–611. doi:10.1016/S0022-1694(96)03194-0
- Park S.-B., Knohl A., Lucas-Moffat A.M., Migliavacca M., Gerbig C., Vesala T., Peltola O., Mammarella I., Kolle O., Lavrič J.V., Prokushkin A. & Heimann M. 2018. Strong radiative effect induced by clouds and smoke on forest net ecosystem productivity in central Siberia. *Agricultural and Forest Meteorology* 250–251: 376–387.
- Peters W., Jacobson A.R., Sweeney C., Andrews A.E., Conway T.J., Masarie K., Miller J.B., Bruhwiler L.M.P., Pétron G., Hirsch A.I., Worthy D.E.J., Werf G.R. van der, Randerson J.T., Wennberg P.O., Krol M.C. & Tans P.P. 2007. An atmospheric perspective on North American carbon dioxide exchange: CarbonTracker. *Proceedings of the National Academy of Sciences of the United States of America* 104: 18925–18930.
- Popa M.E., Gloor M., Manning A.C., Jordan A., Schultz U., Haensel F., Seifert T. & Heimann M. 2010. Measurements of greenhouse gases and related tracers at Bialystok tall tower station in Poland. *Atmospheric Measurement Techniques* 3: 407–427.
- Rella C.W., Chen H., Andrews A.E., Filges A., Gerbig C., Hatakka J., Karion A., Miles N.L., Richardson S.J., Steinbacher M., Sweeney C., Wastine B. & Zellweger C. 2013. High accuracy measurements of dry mole fractions of carbon dioxide and methane in humid air. *Atmospheric Measurement Techniques* 6: 837–860.
- Saeki T., Maksyutov S., Sasakawa M., Machida T., Arshinov M., Tans P., Conway T.J., Saito M., Valsala V., Oda T., Andres R.J. & Belikov D. 2013. Carbon flux estimation for Siberia by inverse modeling constrained by aircraft and tower CO₂ measurements. 118: 1100–1122.
- Sasakawa, M., Machida, T., Tsuda, N., Arshinov, M., Davydov, D., 2013. Aircraft and

- tower measurements of CO₂ concentration in the planetary boundary layer and the lower free troposphere over southern taiga in West Siberia : Long-term records from 2002 to. doi:10.1002/jgrd.50755
- Schmid H.P. 1994. Source areas for scalars and scalar fluxes. *Boundary-Layer Meteorology* 67: 293–318.
- Schulze E.-D., Vygodskaya N.N., Tchebakova N.M., Czimeczik C.I., Kozlov D.N., Lloyd J., Mollicone D., Parfenova E., Sidorov K.N., Varlagin A. V. & Wirth C. 2002. The eurosiberian transect: an introduction to the experimental region. *Tellus B* 54: 421–428.
- Shibistova O., Lloyd J., Zrazhevskaya G., Arneth A., Kolle O., Knohl A., Astrakhantchva N., Shijneva I. & Schmerler J. 2002. Annual ecosystem respiration budget for a *Pinus sylvestris* stand in central Siberia. *Tellus B* 54: 568–589.
- Stull, R. (1988): An introduction to boundary layer meteorology. 1997th ed. Dordrecht: Kluwer Academic Publishers.
- Swinbank C.W. 1951. The measurement of vertical transfer of heat and water vapor by eddies in the lower atmosphere. : 135–145.
- Tans P.P. 1991. Uncertainties in the Global Carbon Cycle. *Pure Appl. Chem.* 63: 766–768.
- Tchebakova, N.M., Kolle, O., Zolotoukhine, D., Arneth, A., Styles, J.M., Vygodskaya, N.N., Schulze, E.-D., Shibistova, O., Lloyd, J., 2002. Inter-annual and seasonal variations of energy and water vapour fluxes above a *Pinus sylvestris* forest in the Siberian middle taiga. *Tellus B* 54, 537–551. doi:10.1034/j.1600-0889.2002.01337.x
- Thompson R.L., Sasakawa M., Machida T., Aalto T., Worthy D., Lavric J. V., Myhre C.L. & Stohl A. 2017. Methane fluxes in the high northern latitudes for 2005–2013 estimated using a Bayesian atmospheric inversion. *Atmospheric Chemistry and Physics* 17: 3553–3572.
- Timokhina A. V., Prokushkin A.S., Panov A. V., Kolosov R.A., Sidenko N. V., Lavric J. & Heimann M. 2018. Interannual Variability of Atmospheric CO₂ Concentrations over Central Siberia from ZOTTO Data for 2009–2015. *Russian Meteorology and Hydrology* 43: 288–294.
- Thompson R L et al 2016 Top-down assessment of the Asian carbon budget since the mid 1990s *Nat. Commun.* 7 10724
- Valentini R., Dore S., Marchi G., Mollicone D., Panfyorov M., Rebmann C., Kolle O. & Schulze E.-D. 2000. Carbon and water exchanges of two contrasting central Siberia landscape types: regenerating forest and bog. *Functional Ecology* 14: 87–96.
- Winderlich J., Chen H., Gerbig C., Seifert T., Kolle O., Lavrič J. V., Kaiser C., Höfer A. & Heimann M. 2010. Continuous low-maintenance CO₂/CH₄/H₂O measurements at the Zotino Tall Tower Observatory (ZOTTO) in Central Siberia. *Atmospheric Measurement Techniques* 3: 1113–1128.
- Winderlich J., Gerbig C., Kolle O. & Heimann M. 2014. Inferences from CO₂ and CH₄ concentration profiles at the Zotino Tall Tower Observatory (ZOTTO) on regional summertime ecosystem fluxes. *Biogeosciences* 11: 2055–2068.
- Winderlich, J.: Setup of a CO₂ and CH₄ measurement system in Central Siberia and modeling of its results, Technical Report Vol. 26, ISSN 1615–7400, Max-Planck Institute for Biogeochemistry, Jena, 2012.
- Wutzler T., Lucas-Moffat A., Migliavacca M., Knauer J., Sickel K., Šigut L., Menzer O.

& Reichstein M. 2018. Basic and extensible post-processing of eddy covariance flux data with REddyProc. *Biogeosciences* 15: 5015–5030.

Chapter 3 Strong radiative effect induced by clouds and smoke on forest net ecosystem productivity in central Siberia

published in *Agricultural and Forest Meteorology*

Sung-Bin Park, Alexander Knohl, Antje M. Lucas-Moffat, Mirco Migliavacca, Christoph Gerbig, Timo Vesala, Olli Peltola, Ivan Mammarella, Olaf Kolle, Jošt Valentin Lavrič, Anatoly Prokushkin, Martin Heimann. Strong radiative effect induced by clouds and smoke on forest net ecosystem productivity in central Siberia, *Agricultural and Forest Meteorology*, Volumes 250–251, 2018, Pages 376-387, <http://dx.doi.org/10.1016/j.agrformet.2017.09.009>.

3.1 Introduction

The high northern latitudes ($> 55^{\circ}\text{N}$) are one of the largest carbon sink regions and have become warmer and drier due in recent decades to rising temperatures (Forkel et al., 2016). Moreover, boreal forests in Russia, so-called “taiga”, comprise about 21 % of the world’s forest area (Tishkov, 2002). Despite its importance to the terrestrial carbon cycle, this area is one of the most data-deficient regions because of its remoteness. One of the critical disturbance factors in the taiga are large wildfires induced by a combination of human activity and climate change (Achard et al., 2008; Vasileva et al., 2011). Since 1996 a significant increase in the number and frequency of wildfires, as well as burned areas, has been observed (Ponomarev et al., 2016; Antamoshkina and Korets, 2015). For instance, heavy smoke from wildfires covered central Siberia in the summers of 2012 and 2013 (Ponomarev, 2013). This heavy smoke resulted in reduced incoming solar radiation and caused changes in the surface radiation balance (Schafer et al. 2002a; Schafer et al. 2002b).

Solar radiation, in particular photosynthetically active radiation (PAR: 400-700 nm), controls canopy processes related to photosynthesis such as gross primary productivity (GPP), net ecosystem exchange of CO_2 (NEE), and light use efficiency (LUE). Determining the biophysical and physiological mechanisms influencing canopy photosynthesis under cloudy and smoky conditions has been difficult due to the interaction among multiple environmental factors such as incoming radiation, diffuse radiation or diffuse fraction, leaf temperature, air humidity, and/or surface wetness (Dengel and Grace, 2010; Doughty et al., 2010; Gu et al., 2002, 1999; Hollinger et al., 1994; Knohl and Baldocchi, 2008; Misson et al., 2005; Rocha et al., 2004). Under cloudy, overcast or high fire-related aerosol load conditions, the total radiation reaching the canopy is reduced, typically resulting in a reduction in photosynthesis (Cirino et al., 2014; Yamasoe et al., 2006).

The diffuse radiation fertilization (DRF) effect is an increase in photosynthesis that results from a trade-off between decreased solar radiation and increased light scattering, both caused by clouds or smoke (Mercado et al., 2009; Rap et al., 2015; Roderick et al., 2001). Diffuse radiation enhances photosynthesis because diffuse light can more effectively penetrate the canopy (Dengel et al., 2015; Doughty et al., 2010;

Knohl and Baldocchi, 2008; Urban et al., 2007; Yamasoe et al., 2006). This effect, however, depends on properties of vegetation structure properties, such as canopy architecture, and leaf area index (LAI), and plant functional type (Alton et al., 2007; Kanniah et al., 2012; Knohl and Baldocchi, 2008; Niyogi et al., 2004). Under diffuse light conditions, the efficiency of canopy photosynthesis increased over 50 % for both crops and temperate forests (Choudhury, 2001; Gu et al., 2002; Hollinger et al., 1994), but not in wetlands due to their low canopy height and low LAI (Letts et al., 2005). Synthetic and data-based modelling studies have also shown that results differ significantly for the same plant functional type, which may be explained by differing model assumptions, treatment of radiation, and the complexity level of each model (Alton, 2008; Alton et al., 2007; Knohl and Baldocchi, 2008; Matsui et al., 2008; Mercado et al., 2009; Rap et al., 2015; Still et al., 2009). Therefore, it is still an open question how forest ecosystems respond to various light regimes (Cheng et al., 2015; Dengel and Grace, 2010; Kanniah et al., 2012; Min, 2005; Misson et al., 2005; Oliphant et al., 2011; Strada et al., 2015).

Aerosol particles have a significant influence on photosynthesis by increasing diffuse radiation, exhibiting favorable conditions for photosynthesis similar to those created by cloudy conditions (Gu et al., 2003; Niyogi et al., 2004; Rap et al., 2015). The aerosol scattering effect may increase the amount of diffuse light, enhancing the CO₂ uptake of forests at midday by up to 8 %, without reducing incoming solar radiation (Misson et al., 2005). This effect is more pronounced in forests and croplands than in grasslands (Jing et al., 2010; Niyogi et al., 2004). Another grassland study did not find significant increases of CO₂ uptake due to aerosol loading (Kanniah et al., 2010). In tropical forests, an increase of aerosol optical depth (AOD) results in an increase of CO₂ uptake, particularly in the sub-canopy (Doughty et al., 2010; Yamasoe et al., 2006). However, if AOD is very high (> 2) or cloud cover is thick, CO₂ uptake decreases due to the reduction of incoming radiation (Cirino et al., 2014; Oliveira et al., 2007a; Yamasoe et al., 2006). This suggests that moderate aerosol concentrations increase CO₂ uptake at ecosystem scales because of the diffuse radiation fertilization effect, whereas high levels of aerosols reduce CO₂ uptake by blocking solar radiation (Kanniah et al., 2012; Strada and Unger, 2016).

In this study, we use flux measurements obtained by the eddy covariance (EC) technique at the ZOTINO Tall Tower Observatory (ZOTTO) site in central Siberia (Heimann et al., 2014; Kozlova et al., 2008; Winderlich et al., 2010) to understand the underlying processes of the DRF effect in a boreal forest during wildfire events. To our knowledge, no other study has investigated the effect of smoke and clouds on NEP at an ecosystem scale in central Siberia.

The objectives of this study are: (1) to characterise the environmental controls of Net Ecosystem Productivity (NEP) and (2) to examine the impact of clouds and smoke on radiation partitioning and its influence on NEP. To address these objectives we first identified the environmental drivers of NEP using an Artificial Neural Networks (ANNs) model (Moffat et al., 2010). We then tested the hypothesis that different levels of smoke particles influence NEP, enhancing it at intermediate levels and decreasing it at higher smoke levels.

3.2 Materials and methods

3.2.1 Study site

The research area is situated on the western side of the Yenisei river basin in the middle taiga subzone (Heimann et al., 2014; Kozlova et al., 2008; Winderlich et al., 2010; Fig. 3.1 bottom). Long-term energy and mass exchange measurements based on the EC technique in this region were performed quasi-continuously from 1998-2000 and 2002-2005 (Arneth et al., 2006; Kelliher et al., 1999; Lloyd et al., 2002a; E.-D. Schulze et al., 2002; Tchebakova et al., 2015). A new flux tower (60°48'25''N, 89°21'27''E, 180 m a.s.l.) was erected at a distance of 900 m from the tall tower site in mid-June 2012 (Winderlich et al., 2014; Fig. 3.1 top). This station is located in a homogeneous Scots pine (*Pinus sylvestris* L.) forest, with an average canopy height of 20 m, similar to the former site. However, the average tree age is estimated to be more than 100 years younger compared to the old site (82-107 and 230 years, respectively). The forest around Zotino is an open stand with sparse understory and a lichen-dominated ground cover (Wirth et al., 1999). The LAI value may be lower than the values reported at the old station (1.3 m² m⁻² for minimum and 3.5 m² m⁻² for maximum) due to the more sparse canopy structure (Alton et al., 2005; Los et al., 2000; Shibistova, 2002; Wirth et al.,

1999). The forest is located on alluvial sandy mineral soil with no underlying permafrost (Kelliher et al., 1999; Lloyd et al., 2002a).

3.2.2 Measurement systems

3.2.2.1 Eddy covariance flux measurements

The EC system consists of a three-axis ultrasonic anemometer USA-1 (METEK GmbH, Elmshorn, Germany) to measure three wind components as well as sonic temperature, and a closed-path infrared gas analyzer LI-7200 (LI-COR Biosciences, Lincoln, NE, USA) to measure CO₂ and H₂O concentrations. The sampling intake line consists of a 1 m stainless steel tube with an inner diameter of 7.7 mm (a 3/8'' tube). The flow rate inside the sampling line was 15 L min⁻¹, which should provide turbulent airflow inside the tubing to minimize frequency losses. The horizontal and vertical sensor separations were 25 cm and 5 cm, respectively. The voltage signals for CO₂ and H₂O concentrations (dry mole fractions) of the gas analyzer were connected to the analog input channels of the sonic anemometer. After the analog-to-digital conversion by the converter inside the anemometer, these signals were added to the digital data stream sent from the sonic anemometer to the computer via serial data transmission at a sampling rate of 20 Hz. Storage of the raw data was managed by the program EddyMeas as part of the EddySoft package (Kolle and Rebmann, 2007). Additionally the LI-7200 was directly connected to the computer via RS-232 and the program LI7200Log collected all status information and measured data from the gas analyzer at a rate of 1 Hz and stored them as 30 min averages.

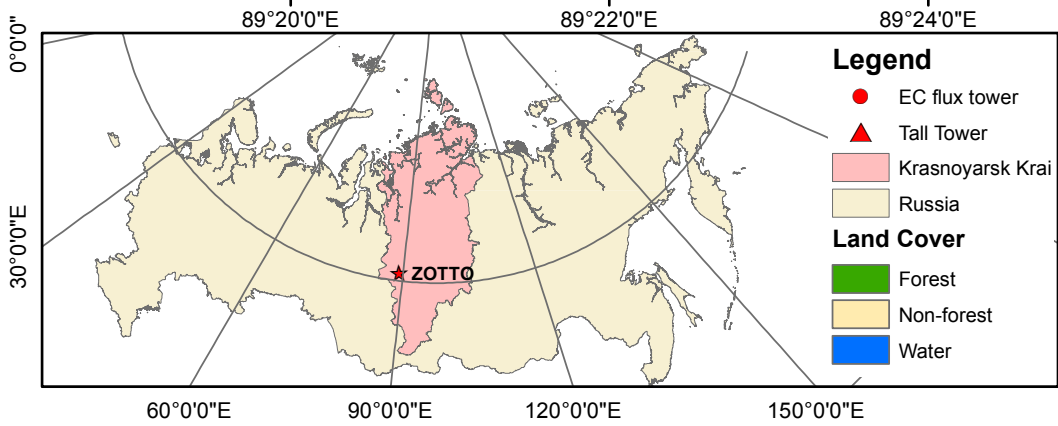
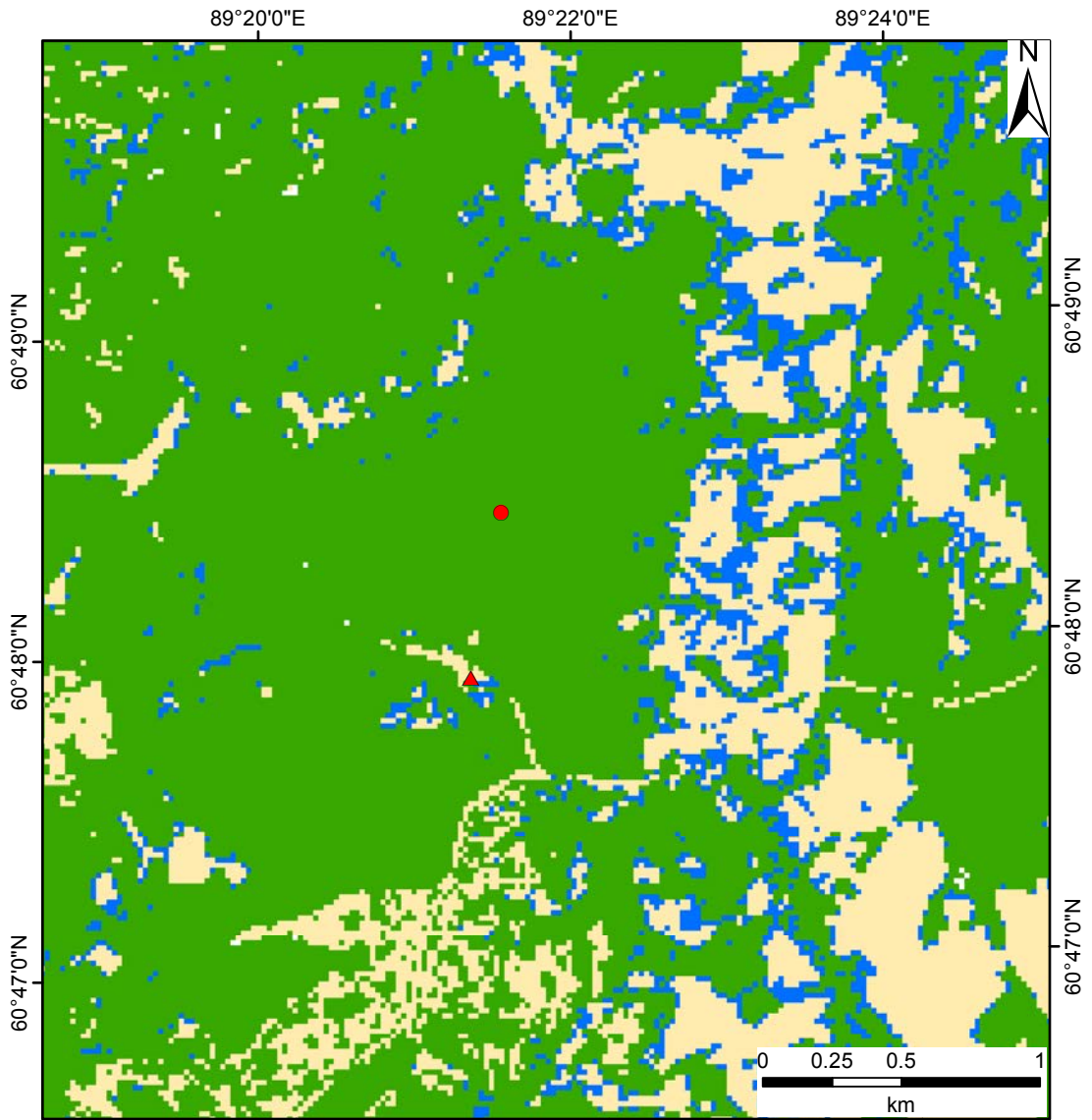


Figure 3.1 Land cover (top) and geographical location (bottom) of the ZOTTO site. Land cover map derived from 30-meter Landsat-8 imagery. Round circle and triangle shapes indicate the forest eddy covariance flux tower and the tall tower sites.

In order to determine the CO₂ storage flux below the EC measurement height, ambient CO₂ concentrations were measured at nine heights (0.1, 0.3, 1, 2, 5, 9, 15, 22, 29.2 m) with a GMP343 probe (Vaisala, Helsinki, Finland). A CR10X data logger (Campbell Scientific, Logan, UT, USA) was used to control the gas-switching unit and to collect the data from the probe. Air was drawn through equal length tubes at a rate of 7 L min⁻¹, with each height being sampled for 1 min (the lowest level was sampled for 2 min). Readings were taken at a rate of 1 Hz over the last 50 sec (110 sec for lowest level) of sampling at each height and then averaged for each 10 min cycle before being stored. Storage fluxes of CO₂ below the flux measurement level were determined as the time change of an integrated spline function through the CO₂ profile measurements. Manual calibration of the LI-7200 and replacement of new filters were performed periodically (April, June, and September) in each measurement year.

3.2.2.2 Auxiliary measurements

Along with the flux measurements, meteorological data were collected. Air temperature (T_a) and relative humidity (RH) were measured at a height of 29.7 m a.g.l. with a KPK1/6-ME-H38 sensor (MELA Sensortechnik GmbH, Galltec, Germany). Atmospheric pressure was measured with a barometric pressure sensor (61302V – RM Young Co., Traverse City, MI, USA) both above the canopy and inside of the measurement cabin. The atmospheric vapor pressure deficit (VPD) was calculated as the difference between the saturation and actual vapor pressure. Average wind velocity and wind direction were recorded using the sonic anemometer of the EC system mounted at the top of the tower. The short- and longwave radiation components were measured with a CNR1 net radiometer (Kipp & Zonen, Kipp & Zonen, Delft, The Netherlands) above the canopy. Up- and downward PAR were measured using a quantum sensor PQS1 (Kipp & Zonen, Delft, Netherlands). Diffuse and total PAR at 2 m height was measured using a BF-3 (Delta-T Devices Ltd., Cambridge, UK) at the tall tower station (Fig. 3.1 top) since 2009 (Winderlich et al., 2010).

Soil temperature was measured with PT100 probes (Jumo GmbH, Germany) at six depths (0.02, 0.04, 0.08, 0.16, 0.32, and 0.64 m). Soil moisture probes (ML-2x, DeltaT Devices, Cambridge, UK) were installed at depths of 0.08 (two replicates), 0.16, 0.32, and 0.64 m. Soil heat fluxes were measured using 5 soil heat flux plates, (HF3/CN3, McVan Instruments, Australia) installed at a depth of 0.03 m. Precipitation was collected by a heated tipping-bucket rain gauge (5.4032.35.009, Adolf Thies GmbH, Germany) at a height of 1.5 m above the ground. All ancillary measurements were collected every 10 sec and then averaged every 10 min using a CR3000 data logger (Campbell Scientific, Logan, UT, USA).

For the daily AOD at 550 nm, we used the MODIS Level 3 (MOD08_D3.051) data containing the ZOTTO site from 2007 to 2013, which has a spatial resolution of 1° by 1° (<http://giovanni.gsfc.nasa.gov/>).

3.2.3 Data processing and quality control

EC data were post-processed with the EddyUH software (Mammarella et al., 2016). Data processing and flux calculations were performed in a similar manner to Mammarella et al. (2015). The high frequency CO₂ and H₂O concentration data were despiked by comparing two adjacent data points: if their differences were larger than 5 ppm and 10 mmol mol⁻¹, the following point was replaced with the same value as in the previous point. A double rotation method was performed during the half-hourly averaging period. A cross-wind correction was applied point by point to the sonic temperature data (Liu et al., 2001). A primary value for the time lag between the vertical wind velocity and scalar measurements was estimated for each 30 min averaging period by maximizing the covariance. The obtained values were later fine-tuned using the time lag optimizer (Mammarella et al., 2016). Fluxes were corrected for high- and low-frequency losses due to the limited frequency responses of the EC system. The response times used in correcting fluxes for low-pass filtering with a transfer function are described by Horst (1997). The transfer function of the high-pass filtering was performed as described in Rannik and Vesala (1999). The transfer function for H₂O was calculated from different classes of relative humidity (Mammarella et al., 2009).

The flux data were screened to remove erroneous values, which did not fulfil the theoretical requirements of the EC method. Half-hourly flux data were flagged as low quality if the absolute values of the skewness of the related concentration or vertical wind velocity were outside of the range (-2, 2), or if the kurtosis was outside of the range (1, 8) (Vickers and Mahrt, 1997). Furthermore, the non-steady state and the integral turbulent characteristics tests were applied following Foken and Wichura (1996). A 2-D coordinate rotation method was applied to data from the sonic anemometer coordinate system. To avoid erroneous data due to malfunction of the gas analyzer, mole fractions of CO₂ and H₂O were taken in the range of [370, 450 ppmv] and [0, 30 mmol mol⁻¹], respectively. In addition to these criteria, the LI-7200 data were screened based on the diagnostic values provided by the instrument. Periods were excluded if 1) the half-hourly mean values for the diagnosis of the chopper and the detector of the gas analyzer were not zero, 2) the signal strength was detected for less than 50 % of the time, 3) the signal strength deteriorated with time, or 4) the signal strength was unstable. A threshold of 0.2 m s⁻¹ for friction velocity (u_*) was determined based on the summer period of the first year using the algorithm described in (Papale et al., 2006) and implemented in REddyProc package in R (ver. 3.2.3: R Core Team, 2016), then applied to the entire dataset. In this study we did not apply gap-filling and only used good quality measured data. The dataset contained on average 55 % high quality CO₂ flux measurements.

Net ecosystem productivity (NEP) was used to describe the negative sign of measured NEE (Kirschbaum et al., 2001; Lovett et al., 2006). Positive values indicate CO₂ uptake by forests whereas negative values indicate CO₂ released to the atmosphere. In order to avoid additional uncertainty introduced by flux partitioning based on night-time ecosystem respiration, we used direct measurements of NEP instead of GPP.

3.2.4 Data selection

Data analysis was focused on daylight hours (potential global radiation, $R_{pot} > 20$ W m⁻²) during the summer of 2012 and 2013. The data covered a measurement period from June 19 to September 30, 2012 and from June 1 to September 4, 2013. PAR_t measurements at EC tower and tall tower sites are very similar (R^2 of 0.97) during daylight hours, however we used the EC site PAR measurements which has less scattered

data. Diffuse fraction (f_{dif}) is the fractional ratio of the diffuse PAR to the total PAR (Dengel and Grace, 2010; Niyogi et al., 2004; Roderick et al., 2001). The diffuse PAR sensor at the tall tower had offsets of about $3 \mu\text{mol photon m}^{-2} \text{ s}^{-1}$; however, we used the original data without calibration. We replaced f_{dif} with 1 if it exceeded 1. Data points with missing T_a and VPD were discarded. A clearness index (CI) was computed as the ratio between actual global radiation (R_g) and R_{pot} . In this study, CI is the same concept as atmospheric transmittance (Knobl and Baldocchi, 2008) and relative irradiance (Cirino et al., 2014; Oliveira et al., 2007a). CI was used to determine the reduction of total incident PAR due to clouds and/or smoke particles and associated with changes in NEP, temperature, and humidity (Cirino et al. 2014).

3.2.5 Artificial Neural Networks

To characterize the environmental drivers of NEP, we used a methodology based on artificial neural networks (ANNs) developed for ecological datasets (Moffat et al., 2010). ANNs are a data-driven approach just like machine-learning techniques. The hierarchy of environmental controls and functional relationships are identified directly from the half-hourly measurements. During the training process, the correlations and relationships of environmental drivers with the ecosystem response are mapped onto the ANNs.

Fourteen environmental drivers were used as input variables (Table 3.1) to model the NEP response. The ANN requires a complete set of input and output drivers. In total, 2542 half-hourly data points were used for ANN training (1089 for 2012, 1453 for 2013).

ANNs training scenarios consisted of different sets of input variables. First, the ANNs were trained with all fourteen drivers and the potential model performance with all available input drivers was used as a benchmark. Then, the ANNs were trained with one input driver at a time to determine the primary drivers. Finally, the ANNs were trained with the dominant primary driver plus each of other input variables as secondary drivers. Tertiary drivers were identified by fixing both the primary and the secondary drivers. A detailed example of this procedure can be found in Moffat (2012).

In the next step, the functional relationships of the three most important drivers (PAR_t , VPD, f_{dif}) were extracted from the ANNs. The ANNs trained on the summer data

represent a model of the dependence of mean ecosystem behaviour on these three drivers. The sensitivity of the ecosystem to changes in these environmental drivers under different AOD values was investigated using this the ANNs.

Table 3.1 List of environmental variables used for ANN trainings.

NEP	Net ecosystem productivity ($\mu\text{mol CO}_2 \text{ m}^{-2}\text{s}^{-1}$)
PAR _t	Downward total photosynthetically active radiation ($\mu\text{mol photon m}^{-2}\text{s}^{-1}$)
PAR _{dir}	Direct PAR ($\mu\text{mol photon m}^{-2}\text{s}^{-1}$)
PAR _{dif}	Diffuse PAR ($\mu\text{mol photon m}^{-2}\text{s}^{-1}$)
Rg	Global radiation (W m^{-2})
VPD	Vapor pressure deficit (hPa)
RH	Relative humidity (%)
SWC	Soil water content at 0.32 m depth (%)
T _a	Air temperature (°C)
Ts1, Ts2	Soil temperature at 0.04 m and 0.32 m depth (°C)
G	Ground heat flux (W m^{-2})
WD	Wind direction (°)
WS	Horizontal wind speed (m s^{-1})
u*	Friction velocity (m s^{-1})
f _{dif}	Diffuse fraction

3.3 Results

3.3.1 Meteorological conditions and NEP

Mean daily T_a ranged between 8.1 and 27.1 °C in 2012, and between 4.4 and 26.9 °C in 2013 (Fig. 3.2a). For the periods between June 19 and June 23, the mean daily T_a was about 17.5 °C in both years. During this period, the maximum temperature in 2012 was reached 4 days later than in 2013. T_a for June 2012 (18.1 °C) was warmer and drier than the same period in 2013. T_a reached its peak towards the end of July. Maximum values of VPD (25.3 hPa on 22 July, 2012; 22.7 hPa on 17 July, 2013) were observed at the same time as the maxima of T_a (Fig. 3.2a). In both years, both T_a and VPD started to decrease in the middle of August.

From mid-July to the end of August the total rainfall was 28.1 mm in 2012 and about five times higher in 2013 (139.3 mm; Fig. 3.2b). In the time before the installation of the EC tower in 2012, precipitation was very low as recorded at the neighboring tall tower site with similar soil characteristics resulting in very dry soil conditions compared to 2013. The precipitation average of 5 mm in July 2012 was not enough to increase the low soil moisture contents. Maximum soil water content (SWC) at a depth of 0.32 m was two times higher in 2013 (15.5 %) than in 2012 (8.6 %).

Mean daily PAR_t in 2012 ($350.0 \mu\text{mol m}^{-2}\text{s}^{-1}$) was about $50 \mu\text{mol m}^{-2}\text{s}^{-1}$ lower than in 2013 ($400.3 \mu\text{mol m}^{-2}\text{s}^{-1}$), whereas the maximum value of about $625 \mu\text{mol m}^{-2}\text{s}^{-1}$ in 2013 was $25.4 \mu\text{mol m}^{-2}\text{s}^{-1}$ higher than in 2012 ($600 \mu\text{mol m}^{-2}\text{s}^{-1}$). The averaged maximum daily PAR_t in both years was similar at about $700 \mu\text{mol m}^{-2}\text{s}^{-1}$. A daily averaged CI of 0.42 during daylight hours indicates that the conditions at the study site were mostly cloudy or overcast in both years.

Daily NEP varied between -7.00 and $3.38 \mu\text{mol CO}_2 \text{m}^{-2}\text{s}^{-1}$ in 2012, whereas it fell between -3.68 and $8.38 \mu\text{mol CO}_2 \text{m}^{-2}\text{s}^{-1}$ in 2013. The daily averaged NEP reached a minimum of $3.54 \mu\text{mol CO}_2 \text{m}^{-2}\text{s}^{-1}$ on the 25th of June 2012. Monthly averaged NEP was $-0.55 \mu\text{mol CO}_2 \text{m}^{-2}\text{s}^{-1}$ in July of 2012 and $1.88 \mu\text{mol CO}_2 \text{m}^{-2}\text{s}^{-1}$ in July of 2013. The situation for August was the opposite, with NEP of $0.66 \mu\text{mol CO}_2 \text{m}^{-2}\text{s}^{-1}$ in 2012 and $0.44 \mu\text{mol CO}_2 \text{m}^{-2}\text{s}^{-1}$ in 2013.

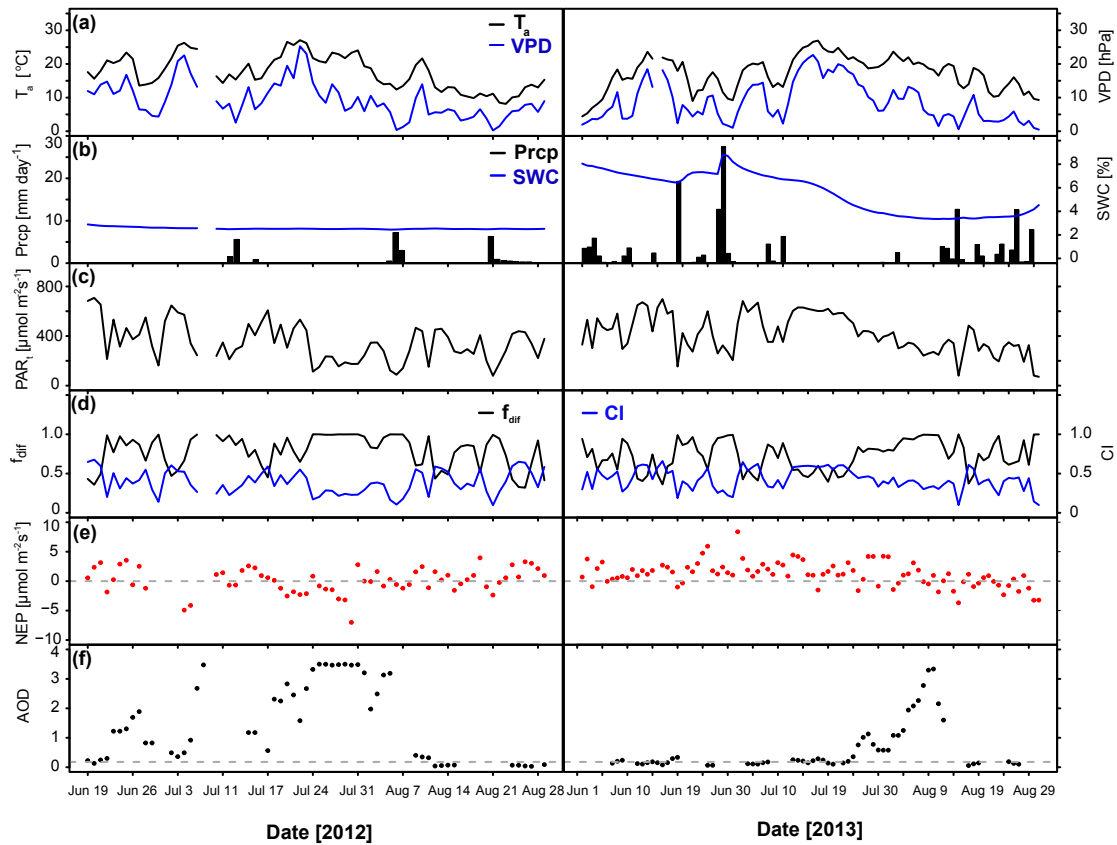


Figure 3.2 Time series of daily observation at ZOTTO. (a) Air temperature (T_a , black), vapor pressure deficit (VPD, blue), (b) total precipitation (Prcp, black), soil moisture at 0.32 m (SWC, blue), (c) total incident photosynthetic active radiation (PAR_t), (d) diffuse fraction (f_{dif} , black), clearness index (CI, blue), (e) net ecosystem productivity (NEP, red), and (f) AOD from June 19 to September 4, 2012 (left) and June 1 to September 4, 2013 (right). Only f_{dif} and CI are averaged in daylight hours ($R_{pot} > 20 \text{ Wm}^{-2}$). The horizontal grey dashed line of (f) is the mean background AOD value of 0.18 during June - August in Siberia (Remer et al., 2008).

3.3.2 Wildfire

In general, fires in central Siberia occur between July and late August (Valendik et al., 2014). However, in 2012 they started already in late June and lasted until the first week of August. Summer of 2012 was recorded as a mega-fire in Siberia due to a stable anticyclone that result in high temperatures and low precipitation (Zhuravleva et al., 2017). In 2012, about 83 % of the surface area (7111 km²) in a 100 km radius around ZOTTO burned (Antamoshkina and Korets, 2015). During the 2000-2014 period, the highest fire occurrences (33 fire events) were in lichen forests within a 100 km radius around the ZOTTO site. Conversely, in 2013, the burnt area was the 5th largest (237 km²) fire in this period, and the fire season was less active (8 fire events) than in 2012.

We used AOD as a smoke aerosol proxy, which revealed that the aerosol particle number concentrations increased along with the atmospheric carbon monoxide (CO) concentration, in agreement with previous observations (Chi et al., 2013). We observed overall phasing and similar amplitudes of AOD and CO mixing ratio (not shown) similar to those observed by Konovalov et al. (2014), suggesting that our use of AOD is an appropriate indicator of fire emissions during these periods. Hence, we assumed that AOD is mainly driven by smoke from fire. At ZOTTO, for the period from June to August in 2012 and 2013, the daily MODIS AOD was available in total for 85 days. The maximum baseline AOD (2007-2011) was 0.95 and the present AOD in 2012-2013 was 3.5.

3.3.3 Drivers of NEP

The benchmark ANN trained with all 14 drivers indicated that modelled NEP generally agrees well with observation, but with lower variability (Fig. 3.3a). The coefficient of determination (R^2) was 0.64 with a standard deviation of the model residuals of $\pm 2.58 \mu\text{mol CO}_2 \text{ m}^{-2}\text{s}^{-1}$ (Fig. 3.3b).

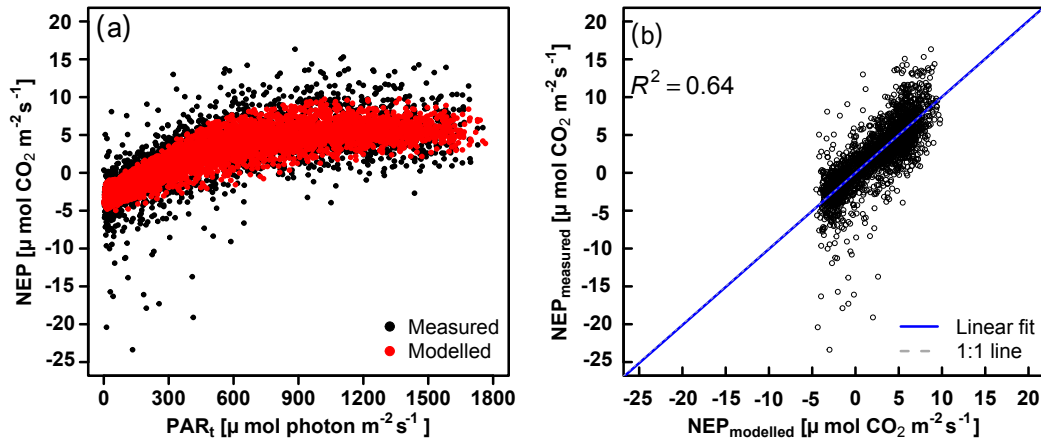


Figure 3.3 Results of the ANN benchmarked with all fourteen environmental drivers: (a) Measured (black) and modelled (red) daytime NEP response projected onto PAR. (b) Scatterplot of measured versus modelled daytime NEP. The linear regression fit (blue solid line) is close to the 1:1 line (grey dashed line). Positive NEP values indicate CO₂ uptake by forests whereas negative values indicate CO₂ released to the atmosphere. See Table 1 for details on the environmental drivers.

The analysis of the hierarchy of the environmental drivers identified PAR as the dominant primary driver, VPD as the main secondary driver, and soil temperatures at 0.08 and 0.32 m depth (Ts1 and Ts2) or f_{dif} as tertiary drivers (Fig. 3.4). For ANNs trained with single drivers (Fig. 3.4a), PAR_t had a higher model performance (R^2 of 0.54) than any of the other radiative drivers (*e.g.*, R^2 of 0.53 for R_g, 0.32 for PAR_{dir}, and 0.49 for PAR_{dif}). Adding VPD explained an additional $\sim 4\%$ of the variability (R^2 of 0.59, Fig. 3.4b). VPD is calculated from RH and T_a, which have similar relevance as secondary drivers. Including f_{dif} as a tertiary driver explains about 2% of the additional variability of NEP (R^2 of 0.60), and allows us to approach the benchmark of 0.64 (Fig. 3.4c). The importance of Ts1 and Ts2 is similar to that of f_{dif} . All other environmental variables showed smaller improvements as tertiary drivers. The influence of the micrometeorological variables (WS, WD, and u^*) was only marginal, which is expected for a cleaned dataset.

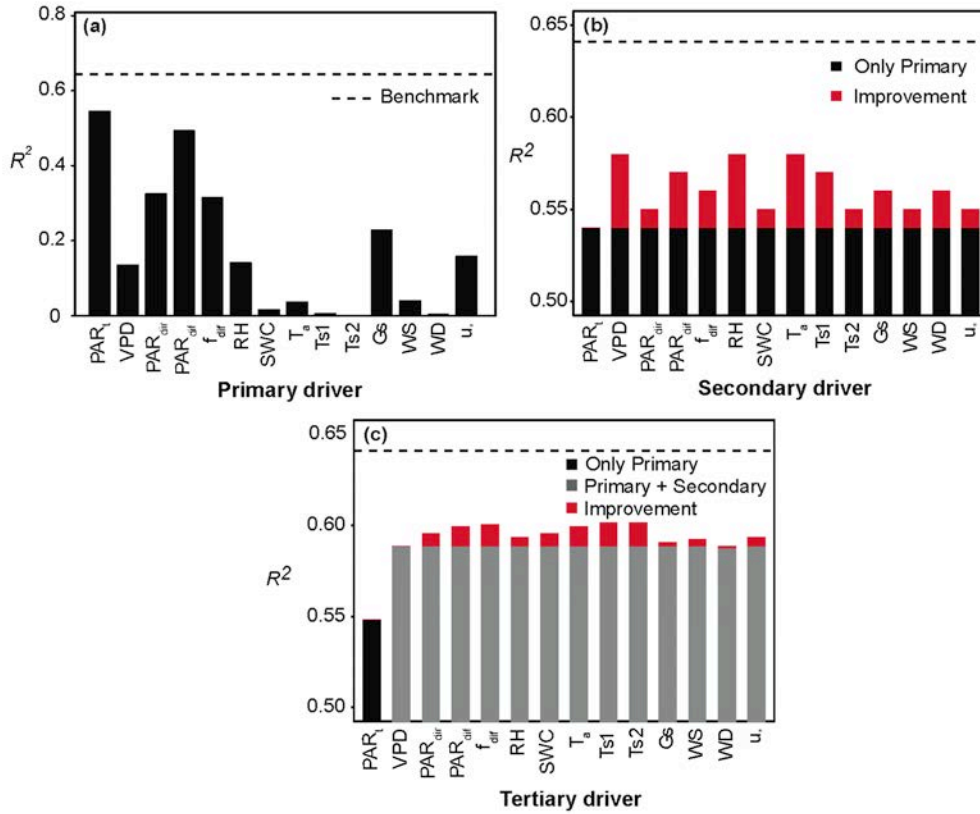


Figure 3.4 Performance (R^2) of the ANNs trained with 14 input drivers: (a) with a single (primary) driver at a time, (b) with PAR plus a secondary driver, and (c) with PAR and VPD plus a tertiary driver. The performance improvement (red) indicates the relevance of the secondary and tertiary drivers. The horizontal dotted line is the benchmark performance with all 14 drivers.

The ANNs trained with the three main drivers (PAR_t , VPD and f_{dif}) can be used to analyze the functional relationships between these drivers and NEP. Light response shows the expected behaviour (Fig. 3.5a): for low light, the partial derivative of NEP with PAR_t (*i.e.*, LUE), is constantly around $0.015 \mu\text{mol CO}_2 / \mu\text{mol photons}$, translating to an almost linear slope in the beginning at low values of PAR_t . NEP values are negative (indicating respiration) around $-3 \mu\text{mol CO}_2 \text{ m}^{-2}\text{s}^{-1}$. At higher levels of PAR_t , the NEP response levels off, saturating with the derivative approaching zero and optimum NEP values around $+6 \mu\text{mol CO}_2 \text{ m}^{-2}\text{s}^{-1}$.

The NEP response exhibits a decrease (negative derivative) with increasing air dryness over the entire range of VPD (Fig. 3.5b). The partial derivative of NEP with f_{dif}

is positive over the full range of f_{dif} values, indicating a positive effect of diffuse light on NEP (Fig. 3.5c).

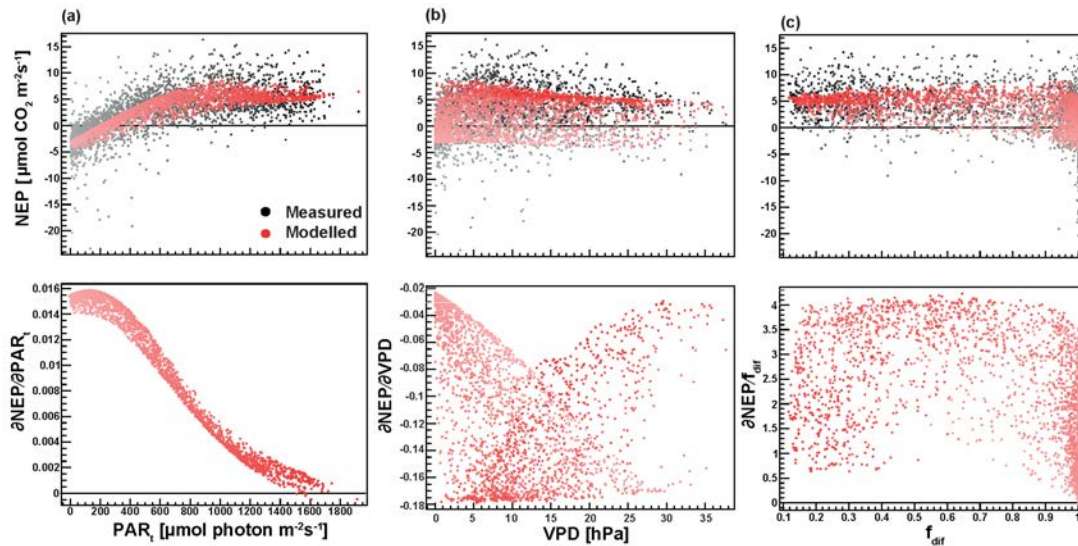


Figure 3.5 Daytime NEP response (upper panel) and partial derivatives (lower panel) modelled with three drivers PAR_t (a), VPD (b), and f_{dif} (c). The modelled (red circles) and measured (black circles) NEP values are shown in gradient colours from light to dark denoting low to high PAR_t .

3.3.4 How do clouds and smoke affect the partitioning of PAR?

Both f_{dif} and CI describe the behavior of the light intensity due to clouds and smoke particles (Fig. 3.6a). Overall, 75.4 % of half-hourly data where $f_{\text{dif}} > 0.3$ are influenced by clouds and smoke particles. A linear negative relationship between CI and f_{dif} exists for f_{dif} values lower than 0.95. If CI is lower than 0.5, f_{dif} saturates to 1, indicating a reduction of incoming PAR due to thick clouds (overcast conditions) or very thick smoke. Incoming PAR shows a strong and significant ($p < 0.001$) negative correlation with f_{dif} , indicating an increase PAR_t with clearer skies (Fig. 3.6b). The relationship between PAR_{dif} and f_{dif} is nonlinear; PAR_{dif} increases with f_{dif} , reaching its maximum at around $f_{\text{dif}} = 0.9$, then decreases at higher values of f_{dif} .

We observed a significant reduction of incoming PAR due to AOD, whereas PAR_{dif} first increases up to a critical value due to the aerosol scattering effect, then decreases at high levels of smoke intensity due to reduced PAR_t (Fig. 3.7a). The relationships between PAR_t and f_{dif} and between PAR_t and AOD are strong and significant. In general, f_{dif} increase with AOD, but it saturates to 1 at values of AOD greater than 2 (Fig. 3.7b). Overall, AOD explains about 76 % of variability in f_{dif} , but with large scatter at low AOD, indicating an additional influence of clouds. Values of $f_{dif} > 0.3$ are seen on cloudy or overcast days, showing the influence of clouds at low smoke conditions.

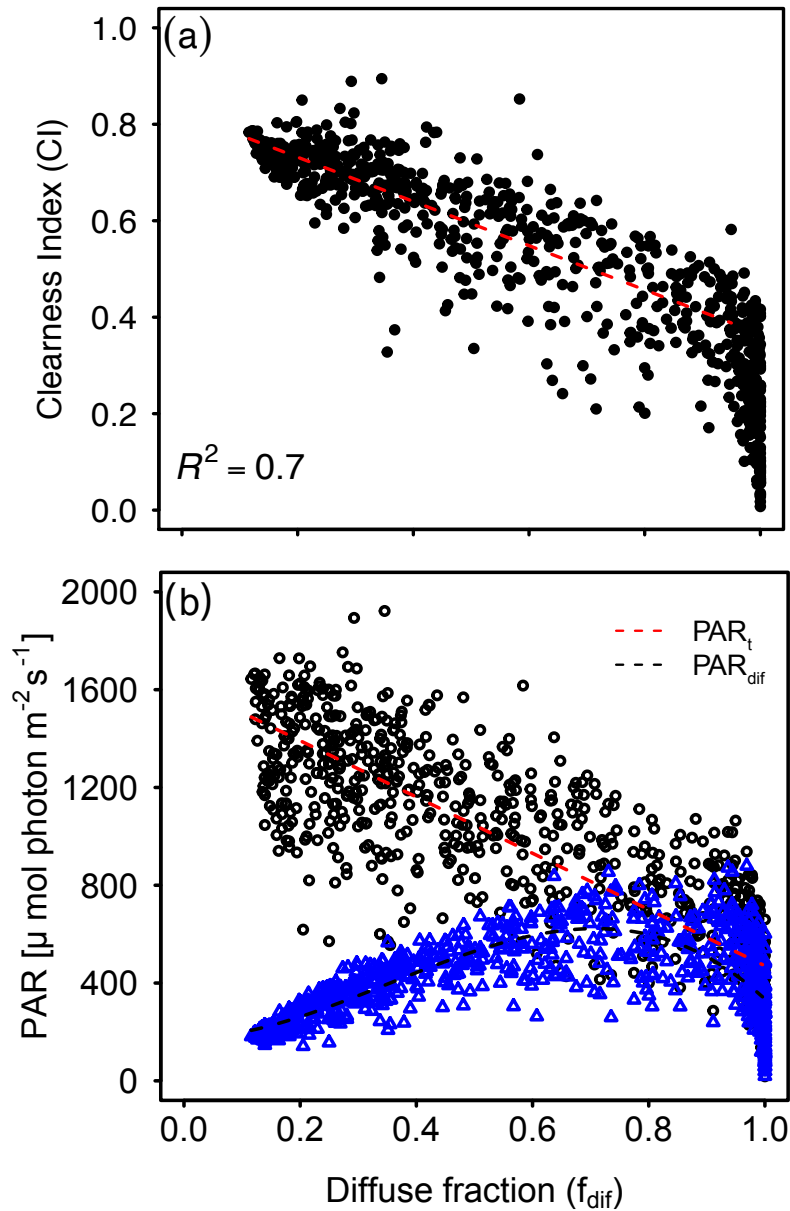


Figure 3.6 (a) Relationship between proportion of diffuse to total PAR (f_{dif}) and clearness index (CI) at midday (11:00-15:00) in summer (Linear fit [red dashed line] of $f_{dif} < 0.95$; $\text{CI} = 0.823363 - 0.458292 * f_{dif}$, $R^2 = 0.70$, $p < 0.001$, $n = 539$), and (b) between f_{dif} and total (black circles) and diffuse (blue triangles) PAR. Linear fit (red dashed line) of total PAR ($\text{PAR}_t = 1652.11 - 1154.17 * f_{dif}$, $R^2 = 0.75$, $p\text{-value} < 0.001$) and 3rd polynomial fit (black dashed line) of PAR_{dif} ($\text{PAR}_{dif} = 172.99 + 44.74 * f_{dif} + 2637.56 * (f_{dif})^2 - 2502.92 * (f_{dif})^3$, $R^2 = 0.56$, $p < 0.001$, $n = 730$).

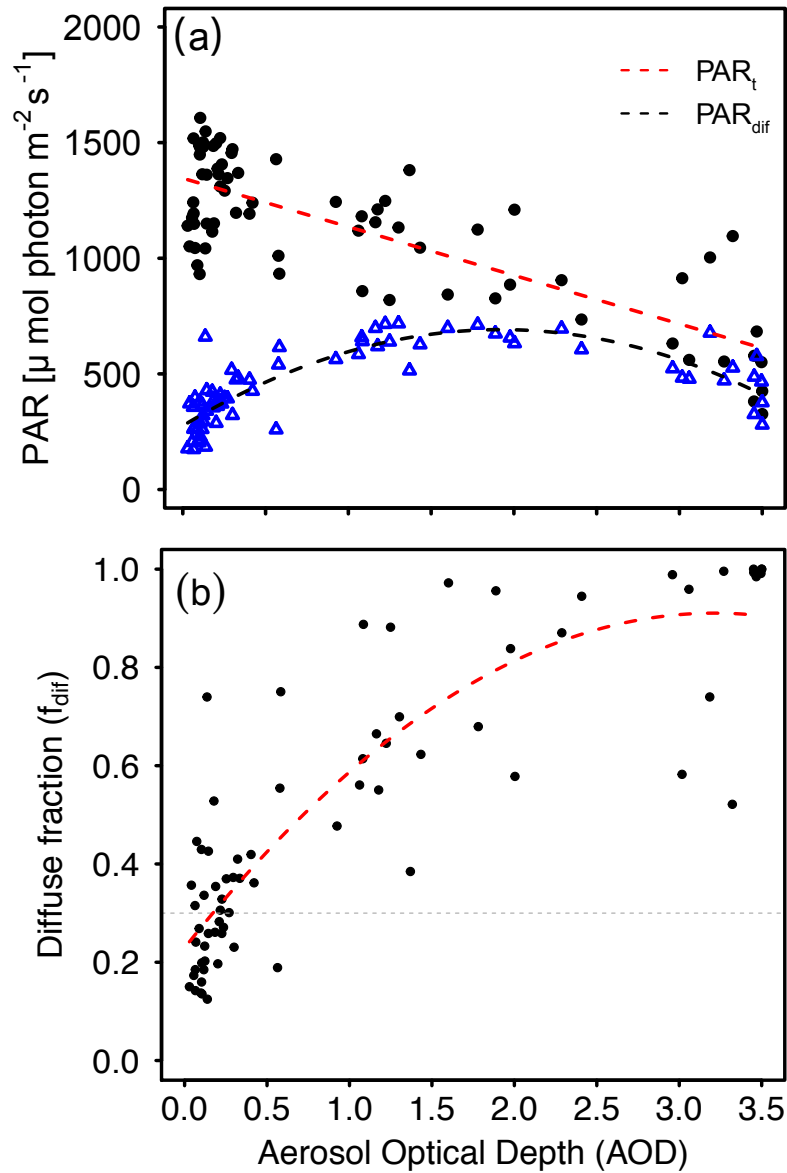


Figure 3.7 (a) Relationship between daily AOD and PAR components and (b) between a fraction of diffuse PAR at midday (11:00-15:00) in summer. Black circles and blue triangles denote PAR_t and PAR_{dif} , respectively. The linear fit of PAR_t (red dashed line) of (a) is $\text{PAR}_t = 1345.92 - 209.89 \cdot \text{AOD}$, $R^2 = 0.64$, $p\text{-value} < 0.001$, the 2nd polynomial fit of PAR_{dif} is $\text{PAR}_{\text{dif}} = 275.53 + 433.05 \cdot \text{AOD} - 112.74 \cdot (\text{AOD})^2$, $R^2 = 0.71$, $p\text{-value} < 0.001$. The 2nd polynomial fit of f_{dif} and AOD is $f_{\text{dif}} = 0.22924 + 0.42387 \cdot (\text{AOD}) - 0.06593 \cdot (\text{AOD})^2$, $R^2 = 0.76$, $p\text{-value} < 0.001$. The total sample size is 72. The grey dashed line at $f_{\text{dif}} = 0.3$ indicates a threshold of clear sky conditions.

3.3.5 How relevant is the effect of smoke on NEP?

We performed a sensitivity analysis to predict the normalized midday mean NEP during summer using data on changes in meteorological drivers (Table 3.2). Overall, reductions in PAR_t have a much greater impact on NEP than increases in f_{dif} . Reductions of 10 to 30 % in PAR_t decreased normalized midday mean NEP compared with the measured NEP. Increases in NEP are also caused by f_{dif} but only if PAR_t reduction is not more than 20 %.

An increase in f_{dif} of 150 % increases NEP \sim 20 %, whereas a reduction in PAR_t of 60 % decreases NEP \sim 24 %. No scenarios that we tested (increases in f_{dif} up to 150 %) increased NEP when PAR_t was reduced by 30 % or more.

Theoretically, without reduction in PAR_t , NEP increases from 4 to 37 % due to the f_{dif} enhancement (up to 400 %). Conversely, NEP would decrease from 6 to 83 % due to reductions in $PAR_t \sim$ 60 %. However, actual NEP responds differently due to the compensation of PAR_t for f_{dif} and vice versa. For instance, a forest experiencing a 10 % reduction in PAR_t and a 50 % increase in f_{dif} is predicted to be 2 % less productive compared with the measured NEP. However a forest experiencing the same reduction in PAR_t and 100-400 % increase in f_{dif} is predicted to be 2 to 33 % more productive compared with the measured NEP. When PAR_t is reduced by 15 %, NEP enhancement requires an increase in f_{dif} greater than 150 %. When PAR_t is reduced by 40 %, NEP enhancement requires an increase in f_{dif} greater than 350 % (corresponding to $PAR_t = 959.6 \mu\text{mol photon m}^{-2}\text{s}^{-1}$ and f_{dif} of 0.9). When PAR_t is reduced by 50 %, no increase in f_{dif} is sufficient to sustain forest productivity.

Overall, the decrease in PAR_t overwhelms the increase in f_{dif} caused by high AOD during fires (Fig. 3.7). At low to moderate levels of AOD (0.3-1), forests experiencing a 7-11 % reduction in PAR_t and a 41-67 % increase in f_{dif} resulting in a 1.45 % increase in NEP. However, at higher levels of AOD (2-3.5), NEP decreases about 7 % due to a 28 % reduction in PAR_t and despite a 132 % increase in f_{dif} . This is most pronounced at the maximum AOD of 3.5 during fires, which results in a \sim 42 % reduction in NEP due to a 52 % reduction in PAR_t and despite an increase in f_{dif} up to 158 %.

Table 3.2 Midday (11:00-15:00) normalized mean NEP during summer was estimated by considering the percentage decreases and increases in PAR_t and f_{dif}. VPD variation is fixed. All values are percentage changes in NEP relative to our measured midday mean NEP during summer. Zero is the measured NEP with no change in meteorology. We simulated 10 - 60 % decreases in PAR_t by increasing f_{dif} from 50 to 400 %. Corresponding PAR_t values for the relative changes decrease 10 – 60 % from 1400 to 600 $\mu\text{mol photon m}^{-2}\text{s}^{-1}$ at a rate of 100 $\mu\text{mol photon m}^{-2}\text{s}^{-1}$ (Fig. 3.6b). In the same manner, relative increases from 0.2 to 1 in f_{dif} range from 50 to 400 % in increments of 0.1. The first column indicates NEP considering the reduction of PAR_t, while the first row indicates NEP only considering the f_{dif} increase. Increasing AOD from 0.3 to 0.7, 1, 1.5, 2, and 3.5, the relative changes in PAR_t decrease by about 7, 11.5, 19.6, 27.8, and 52.4 %, respectively (Fig. 3.7a). Similarly, the relative increases in f_{dif} from 50 to 200 % with AOD are 41, 67.5, 104.5, 132, 158.3 %, respectively (Fig. 3.7b). The thick bold line indicates the line between negative and positive effects due to PAR_t and f_{dif} changes.

NEP change [%]		f _{dif} changes								
		0%	+50%	+100%	+150%	+200%	+250%	+300%	+350%	+400%
PAR _t changes	0%	0	3.6	7.5	11.8	16.4	21.2	26.3	31.6	37.0
	-10%	-5.7	-1.8¹⁾	2.3²⁾	6.8	11.6	16.7	21.8	27.2	32.7
	-15%	-9.4	-5.5	-1.2	3.4	8.3	13.4	18.6	24.1	29.6
	-20%	-13.9	-9.8	-5.4³⁾	-0.7	4.2	9.4	14.7	20.1	25.6
	-35%	-32.0	-27.6	-23.0	-18.1⁴⁾	-13.0	-7.8	-2.4	2.0	8.3
	-40%	-40.0	-35.5	-30.8	-25.9	-20.8	-15.5	-10.2	-4.9	0.4
	-50%	-60.0	-54.7	-49.9	-44.9⁵⁾	-39.8	-34.6	-29.4	-24.2	-19.2
	-60%	-83.3	-78.7	-73.8	-68.8	-63.7	-58.7	-53.6	-48.7	-44.0

Values are obtained from Fig. 3.7

- 1): NEP where AOD increases from 0.3 to 0.7, decreasing PAR_t 7 % ($1198.0 \mu\text{mol photon m}^{-2}\text{s}^{-1}$) and increasing f_{dif} 41 % (0.49)
- 2): NEP where AOD increases from 0.3 to 1, decreasing PAR_t 11.5 % ($1136.03 \mu\text{mol photon m}^{-2}\text{s}^{-1}$) and increasing f_{dif} 67.5 % (0.59)
- 3): NEP where AOD increases from 0.3 to 1.5, decreasing PAR_t 19.6 % ($1031.09 \mu\text{mol photon m}^{-2}\text{s}^{-1}$) and increasing f_{dif} 104.5 % (0.72)
- 4): NEP where AOD increases from 0.3 to 2, decreasing PAR_t 27.8 % ($926.14 \mu\text{mol photon m}^{-2}\text{s}^{-1}$) and increasing f_{dif} 132 % (0.81)
- 5): NEP where AOD increases from 0.3 to 3.5, decreasing PAR_t 52.40 % ($611.31 \mu\text{mol photon m}^{-2}\text{s}^{-1}$) and increasing f_{dif} 158.37 % (0.91)

3.4. Discussion

3.4.1 Environmental drivers of NEP identified by the ANNs

We can explain 60 % of the benchmark of 64 % variation in NEP using data on PAR_t , VPD, and f_{dif} or soil temperatures. Light intensity, VPD, and T_a are known to be key controls of photosynthesis (Goulden et al. 1997; Jarvis et al. 1997; Chen et al. 1999). A wide range of VPD implies that water vapour quickly evaporates due to the strong influence of air dryness (Fig. 3.2 and Fig. 3.5b). With the optimum temperature range for evergreen coniferous trees of 10-25 °C (Larcher, 2003), an increase in VPD at water-limited sites causes a reduction in productivity because of the closing of stomata to prevent water loss (Fig. 3.5b, (Dengel and Grace, 2010; Kelliher et al., 1997; Lloyd et al., 2002a; Shibistova et al., 2002). At VPD above 10 hPa, the stomata begin to close, thus reducing photosynthesis and transpiration rates in boreal trees (Dang et al. 1997; Hogg et al. 1997).

In general, temperature controls the distinct seasonality of photosynthesis and respiration rates (Lloyd et al., 2002a). Due to the tight coupling between temperature and humidity, temperature sensitivity may have similar down-regulating effects as VPD. Similar to Alton et al. (2007), we suggest that stomata might not be fully open at high humidity conditions (low VPD) if the light intensity is too low for photosynthesis.

When light is saturated, NEP can be interpreted as a proxy for, but not equal to, the ecosystem photosynthetic capacity (Musavi et al., 2016; Reichstein et al., 2014). Light responses (Fig. 3.3b) show that an ecosystem at high northern latitudes quickly reaches the light saturation point. For instance, NEP in tropical forests reaches its maximum saturation when PAR_t is around 1550-1870 $\mu\text{mol m}^{-2}\text{s}^{-1}$ (Cirino et al., 2014), whereas in the ZOTTO forest, the maximum NEP is reached when PAR_t is around 700-900 $\mu\text{mol m}^{-2}\text{s}^{-1}$.

3.4.2 Effects of clouds and smoke on radiation

Incoming PAR decreases significantly at very high levels of f_{dif} and AOD (Fig. 3.6 and Fig. 3.7). A similar correlation between f_{dif} and CI (Fig. 3.6a) is also found at other sites (Knohl and Baldocchi, 2008; Roderick et al., 2001), although the ZOTTO site has a higher CI regime (~ 0.45) compared to other sites (~ 0.2). Diffuse PAR and f_{dif} are values defined at wavelengths relevant for photosynthesis, whereas the definition of CI includes a wider range of wavelengths. Using CI may have more confounding effects or overestimate the influence of clouds and aerosols on ecosystem responses (Cohan et al., 2002; Kanniah et al., 2010; Letts et al., 2005).

Clouds play a more significant role in determining PAR_t than AOD (Fig. 3.6b, Fig. 3.7a), as found in modeling studies (Min, 2005; Schafer et al., 2002b). However, the separation of a reduction in PAR_t caused by aerosol effect and that caused by clouds is not possible (Cirino et al., 2014).

An increase of PAR_{dif} and f_{dif} with increase in AOD up to ~ 2 , and a decrease of both parameters at higher AOD values (Fig. 3.7) are consistent with previous studies (Cirino et al., 2014; Jing et al., 2010; Kanniah et al., 2010; Min, 2005; Moon et al., 2009; Oliphant et al., 2011; Oliveira et al., 2007; Schafer et al., 2002b; Steiner et al., 2013; Strada et al., 2015). The peak of PAR_{dif} at values of f_{dif} around 0.9 (Fig. 3.7b) may be due to the fact that on overcast days more light is scattered than on days with more patchy cloud cover (Cohan et al., 2002; Min, 2005). Large scatter of f_{dif} during low smoke (AOD < 0.3) conditions implies that cloud effects on f_{dif} may play a role in the DRF effect (Fig. 3.7b). Previous studies have shown that a moderate level of f_{dif} is predominately caused by aerosols or thin clouds, although the effects of the two are confounded (Min, 2005; Oliphant et al. 2011).

The size distribution and concentration of water vapor droplets in clouds depends on the types of aerosols present, changing cloud microphysics and radiative fluxes. For instance, clouds induced by smoke particles embrace more and smaller size water droplets compared to smoke-free clouds under the same conditions, leading to an increase in cloud cover of up to 5 % (Kaufman and Koren, 2006). Also, MODIS AOD is known to be overestimated at 550 nm (Levy et al., 2010). Several studies have shown that fine

resolution ground-based aerosol measurements (*e.g.*, size distribution, light scattering coefficients, AOD) help to understand the role of smoke particles on clouds and the radiation budget (Oliphant et al., 2011; Yamasoe et al., 2006). However, the influence of AOD on incoming radiation may not be as pronounced as that of clouds because it responds indirectly to photosynthesis (Fig. 3.6 and Fig. 3.7). An insignificant relationship between NEP and AOD supports this hypothesis (not shown). In other words: as shown by ANNs analysis, the environmental drivers PAR_t , VPD, and f_{dif} play a more important role than AOD in explaining NEP (Fig. 3.4). Therefore, the predicting NEP without AOD as a training driver of ANNs is appropriate.

Maximum NEP enhancement occurs when PAR_{dif} reaches its maximum ($638.2 \mu\text{mol photon m}^{-2}\text{s}^{-1}$) at f_{dif} of 0.7. However, at this light level, total PAR is $844.2 \mu\text{mol photon m}^{-2}\text{s}^{-1}$ lower than the maximum value with no cloud cover (Fig. 3.7b and Fig. 3.4a). The forest ecosystem is still productive under low light conditions, because of the NEP increase caused by increasing f_{dif} (Fig. 9c); however, the relative change in NEP is less than $\sim 10\%$ (Table 3.2). Moreover, at very large AOD values (> 2), we found that NEP is reduced by 50 % due to the strong reduction of PAR_t although separating the effect of clouds and smoke on this reduction is not possible (Cirino et al., 2014).

3.4.3 Requirements of the diffuse radiation fertilization (DRF) effect

Our sensitivity analysis showed that a DRF effect in the ZOTTO forest is theoretically possible, but that it is not often observed due to the overall strong reduction in PAR_t by clouds and smoke (Table 3.2). One possible explanation of why the DRF effect at our site is not as pronounced as in other forests (Doughty et al., 2010; Knohl and Baldocchi, 2008; Mercado et al., 2009; Niyogi et al., 2004; Oliveira et al., 2007; Rap et al., 2015; Still et al., 2009; Yamasoe et al., 2006) might be the sparse canopy and the low LAI. Our results also provide evidence that within the same plant functional type, the DRF effect is not as pronounced in forests with lower LAI (Gu et al., 2002).

Kanniah et al. (2012) concluded that ecosystems with low LAI may not experience positive effects of diffuse light on vegetation productivity. This is particularly true in open canopy ecosystems, such as grasslands (Niyogi et al., 2004; Wohlfahrt et al.,

2008) and wetlands (Letts et al., 2005). A simulation using a multi-layer canopy model showed that the DRF effect decreases with decreasing LAI and it also depends on leaf clumping and leaf angle (Knobl and Baldocchi, 2008). However, substantial increase of CO₂ uptake due to thick clouds were found in a grassland with very low LAI (~ 0.37; Jing et al., 2010) as well as in some forests with low LAI (~ 2; Migliavacca et al., 2009; Misson et al., 2005). Observations in multi-layered arctic shrub ecosystems with low LAI (~1.5) support our argument that the importance of canopy structure on DRF effects is independent from of LAI (Williams et al., 2014). Therefore, we argue that canopy structure may be a more crucial factor than LAI in determining DRF effects.

In our Siberian forest at very high levels of AOD (> 3), both PAR_t and PAR_{dif} are ~ 700 μmol photon m⁻²s⁻¹ and f_{dif} is high (> 0.6; Fig. 3.7). High f_{dif} can be caused by both overcast conditions (thick clouds) or by the presence of smoke (Fig. 3.6b, Fig. 3.7b). Although it is not possible to separate smoke from cloud effects, higher aerosol loading and thick cloud cover have a large impact on forest NEP by changing the amount of incoming PAR reaching the surface (Oliveria et al. 2007; Cirino et al. 2014). A possible explanation for a strong reduction of PAR_t may be to the fact that smoke absorbs solar radiation and suppresses the formation of clouds (Andreae et al., 2004; Koren et al., 2004). Our results support those of Alton et al. (2008), namely that increases ecosystem productivity due to diffuse radiation are less than 10 %.

3.5. Conclusion

Due to increased drying and warming, the Siberian taiga is increasingly exposed to fires. However, the ecosystem NEP response may be non-linear depending on the complex interaction among clouds and aerosol types, canopy structure, the magnitude of fires, and associated meteorological conditions. Here, we combine eddy covariance flux measurements and data-driven modelling in order to understand the environmental drivers of forest NEP and investigate the impact of smoke and clouds on diffuse and direct components of radiation partitioning.

The ANNs analysis suggest that the f_{dif} did increase NEP, however, it was more sensitive to a strong reduction of PAR_t than to diffuse light enrichment due to clouds or

high smoke. The overall effect of a potential increase in NEP due to thick clouds or high aerosol loading minimized by the low light intensity, sparse canopy structure and low LAI. The ANNs have the benefit of quantifying the impact of diffuse radiation on NEP without additional canopy structure parameters. This represents an important advance in understanding ecosystem functional properties and their effects on photosynthesis. Moving forward, our results suggest that, in the particular case of sparse canopies with low LAI (e.g., grasslands and wetlands), the DRF effect should be included in biogeochemical models and coupled Earth System models in order to better describe net ecosystem productivity.

3.6. References

- Achard, F., Eva, H.D., Mollicone, D., Beuchle, R., 2008. The effect of climate anomalies and human ignition factor on wildfires in Russian boreal forests. *Philos. Trans. R. Soc. Lond. B. Biol. Sci.* 363, 2331–2339. doi:10.1098/rstb.2007.2203
- Alton, P.B., North, P., Kaduk, J., Los, S., 2005. Radiative transfer modeling of direct and diffuse sunlight in a Siberian pine forest. *J. Geophys. Res. Atmos.* 110. doi:10.1029/2005JD006060
- Alton, P.B., North, P.R., Los, S.O., 2007. The impact of diffuse sunlight on canopy light-use efficiency, gross photosynthetic product and net ecosystem exchange in three forest biomes. *Glob. Chang. Biol.* 13, 776–787. doi:10.1111/j.1365-2486.2007.01316.x
- Alton, P.B., 2008. Reduced carbon sequestration in terrestrial ecosystems under overcast skies compared to clear skies. *Agric. For. Meteorol.* 148, 1641–1653. doi:10.1016/j.agrformet.2008.05.014
- Andreae, M.O., Rosenfeld, D., Artaxo, P., Costa, A.A., Frank, G.P., Longo, K.M., Silva-Dias, M.A.F., 2004. Smoking Rain Clouds over the Amazon. *Science* (80-). 303, 1337–1342. doi:10.1126/science.1092779
- Antamoshkina, O.A., Korets, M.A., 2015. Vegetation monitoring within the ZOTTO tall tower coverage area using remote sensing data. *Vestnik SibGAU* 16 (4), 814–818 (In Russian).
- Arneeth, A., Lloyd, J., Shibistova, O., Sogachev, A., Kolle, O., 2006. Spring in the boreal environment : observations on pre- and post-melt energy and CO₂ fluxes in two central Siberian ecosystems. *Boreal Environ. Res.* 11, 311–328.
- Chen, J.Q., Falk, M., Euskirchen, E., Suchanek, T.H., Ustin, S.L., Bond, B.J., Brosofske, K.D., Phillips, N., Bi, R.C., 2002. Biophysical controls of carbon flows in three successional Douglas-fir stands based on eddy-covariance measurements. *Tree Physiol.* 22, 169–177.
- Cheng, S.J., Bohrer, G., Steiner, A.L., Hollinger, D.Y., Suyker, A., Phillips, R.P., Nadelhoffer, K.J., 2015. Variations in the influence of diffuse light on gross primary productivity in temperate ecosystems. *Agric. For. Meteorol.* 201, 98–110. doi:10.1016/j.agrformet.2014.11.002
- Chi, X., Winderlich, J., Mayer, J.C., Panov, A. V., Heimann, M., Birmili, W., Heintzenberg, J., Cheng, Y., Andreae, M.O., 2013. Long-term measurements of aerosol and carbon monoxide at the ZOTTO tall tower to characterize polluted and pristine air in the Siberian taiga. *Atmos. Chem. Phys.* 13, 12271–12298. doi:10.5194/acp-13-12271-2013
- Choudhury, B.J., 2001. Estimating gross photosynthesis using satellite and ancillary data: Approach and preliminary results. *Remote Sens. Environ.* 75, 1–21. doi:10.1016/S0034-4257(00)00151-6
- Cirino, G.G., Souza, R.A.F., Adams, D.K., Artaxo, P., 2014. The effect of atmospheric aerosol particles and clouds on net ecosystem exchange in the Amazon. *Atmos. Chem. Phys.* 14, 6523–6543. doi:10.5194/acp-14-6523-2014
- Cohan, D.S., Xu, J., Greenwald, R., Bergin, M.H., Chameides, W.L., 2002. Impact of atmospheric aerosol light scattering and absorption on terrestrial net primary productivity. *Glob. Biogeochem. Cycles* 4. doi:10.1029/2001GB001441
- Dang, Q.L., Margolis, H.A., Coyea, M.R., Sy, M., Collatz, G.J., 1997. Regulation of branchlevel gas exchange of boreal trees: roles of shoot water potential and

- vapour pressure difference. *Tree Physiol.* 17, 521–535.
- Dengel, S., Grace, J., 2010. Carbon dioxide exchange and canopy conductance of two coniferous forests under various sky conditions. *Oecologia* 164, 797–808. doi:10.1007/s00442-010-1687-0
- Dengel, S., Grace, J., MacArthur, A., 2015. Transmissivity of solar radiation within a *Picea sitchensis* stand under various sky conditions. *Biogeosciences* 12, 4195–4207. doi:10.5194/bg-12-4195-2015
- Doughty, C.E., Flanner, M.G., Goulden, M.L., 2010. Effect of smoke on subcanopy shaded light, canopy temperature, and carbon dioxide uptake in an Amazon rainforest. *Global Biogeochem. Cycles* 24, GB3015. doi:10.1029/2009GB003670
- Foken, Th. and Wichura, B., 1996. Tools for quality assessment of surface-based flux measurements. *Agric. For. Meteorol.* 78, 83–105. doi:10.1016/0168-1923(95)02248-1
- Forkel, M., Carvalhais, N., Rödenbeck, C., Keeling, R., Heimann, M., Thonicke, K., Zaehle, S., Reichstein, M., 2016. Enhanced seasonal CO₂ exchange caused by amplified plant productivity in northern ecosystems. *Science* (80-.). 4971, 696–699. doi:10.1126/science.aac4971
- Furyaev, V.V., Vaganov, E.A., Thebakova, N.M., Valendik, E.N., 2001. Effects of fire and climate on successions and structural changes in the Siberian boreal forest. *Eurasian J. For. Res.* 2, 1–15.
- Goulden, M.L., Daube, B.C., Fan, S.-M., Sutton, D.J., Bazzaz, A., Munger, J.W., Wofsy, S.C., 1997. Physiological responses of a black spruce forest to weather. *J. Geophys. Res.* 102, 28987–28996. <http://dx.doi.org/10.1029/97JD01111>.
- Gu, L., Baldocchi, D., Verma, S.B., Black, T.A., Vesala, T., Falge, E.M., Dowty, P.R., 2002. Advantages of diffuse radiation for terrestrial ecosystem productivity. *J. Geophys. Res. Atmos.* 107, 4050. doi:10.1029/2001JD001242
- Gu, L., Baldocchi, D.D., Wofsy, S.C., Munger, J.W., Michalsky, J.J., Urbanski, S.P., Boden, T.A., 2003. Response of a deciduous forest to the Mount Pinatubo eruption: Enhanced photosynthesis 299, 2035–2038.
- Gu, L., Shugart, H.H., Fuentes, J.D., Black, T.A., Shewchuk, S.R., 1999. Micrometeorology, biophysical exchanges and NEE decomposition in a two-story boreal forest — development and test of an integrated model. *Agric. For. Meteorol.* 94, 123–148. doi:10.1016/S0168-1923(99)00006-4
- Heimann, M., Schulze, E.-D., Winderlich, J., Andreae, M.O., Chi, X., Gerbig, C., Kolle, O., Kuebler, K., Lavrič, J. V., Mikhailov, E., Panov, A., Park, S., Rödenbeck, C., Skorochod, A., 2014. The Zotino Tall Tower Observatory (ZOTTO): Quantifying large scale biogeochemical changes in Central Siberia. *Nov. Acta Leopoldina* 117, 51–64.
- Hogg, E.H., Hurdle, P.A., 1997. Sap flow in trembling aspen: implications for stomatal responses to vapor pressure deficit. *Tree Physiol.* 17, 501–509.
- Hollinger, D.Y., Kelliher, F.M., Byers, J.N., Hunt, J.E., McSeveny, T.M., Weir, P.L., 1994. Carbon dioxide exchange between an undisturbed old-growth temperate forest and the atmosphere. *Ecology* 75, 134–150.
- Horst, T.W., 1997. A simple formula for attenuation of eddy fluxes measured with first-order-response scalar sensors. *Boundary-Layer Meteorol.* 82, 219–233. doi:10.1023/A:1000229130034
- Jarvis, P.G., Massheder, J.M., Hale, S.E., Moncrieff, J.B., Rayment, M., Scott, S.L., 1997. Seasonal variation of carbon dioxide, water vapor, and energy exchanges of a boreal black spruce forest. *J. Geophys. Res.* 102, 28953–28966.

- <http://dx.doi.org/10.1029/97JD01176>.
- Jing, X., Huang, J., Wang, G., Higuchi, K., Bi, J., Sun, Y., Yu, H., Wang, T., 2010. The effects of clouds and aerosols on net ecosystem CO₂ exchange over semi-arid Loess Plateau of Northwest China. *Atmos. Chem. Phys.* 10, 8205–8218. doi:10.5194/acp-10-8205-2010
- Kanniah, K., Beringer, J., North, P., Hutley, L., 2012. Control of atmospheric particles on diffuse radiation and terrestrial plant productivity: A review. *Prog. Phys. Geogr.* 36, 209–237. doi:10.1177/0309133311434244
- Kanniah, K.D., Beringer, J., Tapper, N.J., Long, C.N., 2010. Aerosols and their influence on radiation partitioning and savanna productivity in northern Australia. *Theor. Appl. Climatol.* 100, 423–438. doi:10.1007/s00704-009-0192-z
- Kaufman, Y.J., Koren, I., 2006. Smoke and pollution aerosol effect on cloud cover. *Science* 313, 655. <http://dx.doi.org/10.1126/science.1126232>.
- Kelliher, F.M., Hollinger, D.Y., Schulze, E.D., Vygodskaya, N.N., Byers, J.N., Hunt, J.E., McSeveny, T.M., Milukova, I., Sogatchev, A., Varlargin, A., Ziegler, W., Arneth, A., Bauer, G., 1997. Evaporation from an eastern Siberian larch forest. *Agric. For. Meteorol.* 85, 135–147. [http://dx.doi.org/10.1016/S0168-1923\(96\)02424-0](http://dx.doi.org/10.1016/S0168-1923(96)02424-0).
- Kelliher, F.M., Lloyd, J., Arneth, A., Lühker, B., Byers, J.N., Mcseveny, T.M., Milukova, I., Grigoriev, S., Panfyorov, M., Sogatchev, A., Varlargin, A., Ziegler, W., Bauer, G., Wong, S.-C., Schulze, E.-D., 1999. Carbon dioxide efflux density from the floor of a central Siberian pine forest. *Agric. For. Meteorol.* 94, 217–232. [http://dx.doi.org/10.1016/S0168-1923\(99\)00014-3](http://dx.doi.org/10.1016/S0168-1923(99)00014-3).
- Kirschbaum, M.U.F., Eamus, D., Gifford, R.M., Roxburgh, S.H., Sands, P.J., 2001. Definitions of some ecological terms commonly used in carbon accounting. *Coop. Res. Cent. Carbon Account.* 2–6. doi:10.1111/j.1365-2486.2004.00878.x
- Knohl, A., Baldocchi, D.D., 2008. Effects of diffuse radiation on canopy gas exchange processes in a forest ecosystem. *J. Geophys. Res. Biogeosciences* 113, 1–17. doi:10.1029/2007JG000663
- Kolle, Olaf and Rebmann, C., 2007. Eddysoft by meteoools: Documentation of Eddy Covariance Software 1–88.
- Kononov, I.B., Berezin, E. V., Ciais, P., Broquet, G., Beekmann, M., Hadji-Lazaro, J., Clerbaux, C., Andreae, M.O., Kaiser, J.W., Schulze, E.D., 2014. Constraining CO₂ emissions from open biomass burning by satellite observations of co-emitted species: A method and its application to wildfires in Siberia. *Atmos. Chem. Phys.* 14, 10383–10410. doi:10.5194/acp-14-10383-2014
- Koren, I., Kaufman, Y.J., Remer, L.A., Martins, J.V., 2004. Measurement of the Effect of Amazon Smoke on Inhibition of Cloud Formation. *Science* (80-). 303, 1342–1345. doi:10.1126/science.1089424
- Kozlova, E.A., Manning, A.C., Kisilyakhov, Y., Seifert, T., Heimann, M., 2008. Seasonal, synoptic, and diurnal-scale variability of biogeochemical trace gases and O₂ from a 300-m tall tower in central Siberia. *Global Biogeochem. Cycles* 22, 1–16. doi:10.1029/2008GB003209
- Larcher, W., 2003. *Physiological Plant Ecology: Ecophysiology and Stress Physiology of Functional Groups*. Springer Verlag, Berlin. <http://dx.doi.org/10.1007/978-3-662-05214-3>.
- Letts, M.G., Lafleur, P.M., Roulet, N.T., 2005. On the relationship between cloudiness and net ecosystem carbon dioxide exchange in a peatland ecosystem. *Ecoscience* 12, 53–59. doi:10.2980/i1195-6860-12-1-53.1
- Levy, R.C., Remer, L.A., Kleidman, R.G., Mattoo, S., Ichoku, C., Kahn, R., Eck,

- T.F., 2010. Global evaluation of the Collection 5 MODIS dark-target aerosol products over land. *Atmos. Chem. Phys.* 10, 10399–10420. doi:10.5194/acp-10-10399-2010
- Liu, H., Peters, G., Foken, T., 2001. New equations for sonic temperature variance and buoyancy heat flux with an omnidirectional sonic anemometer. *Boundary-Layer Meteorol.* 100, 459–468.
- Lloyd, J., Shibistova, O., Zolotoukhine, D., Kolle, O., Arneth, A., Wirth, C., Styles, J.M., Tchebakova, N.M., Schulze, E.-D., 2002. Seasonal and annual variations in the photosynthetic productivity and carbon balance of a central Siberian pine forest. *Tellus B* 54, 590–610. doi:10.1034/j.1600-0889.2002.01487.x
- Los, S.O., Collatz, G.J., Sellers, P.J., Malmström, C.M., Pollack, N.H., DeFries, R.S., Bounoua, L., Parris, M.T., Tucker, C.J., Dazlich, D.A., 2000. A global 9-yr biophysical land surface dataset from NOAA AVHRR data. *J Hydrometeorol* 1, 183–199. doi:10.1175/1525-7541(2000)001<0183:AGYBLS>2.0.CO;2
- Lovett, G.M., Cole, J.J., Pace, M.L., 2006. Is net ecosystem production equal to ecosystem carbon accumulation? *Ecosystems* 9, 152–155. doi:10.1007/s10021-005-0036-3
- Mammarella, I., Launiainen, S., Gronholm, T., Keronen, P., Pumpanen, J., Rannik, Ü., Vesala, T., 2009. Relative humidity effect on the high-frequency attenuation of water vapor flux measured by a closed-path eddy covariance system. *J. Atmos. Ocean. Technol.* 26, 1856–1866. doi:10.1175/2009JTECHA1179.1
- Mammarella, I., Peltola, O., Nordbo, A., Järvi, L., Rannik, Ü., 2016. Quantifying the uncertainty of eddy covariance fluxes due to the use of different software packages and combinations of processing steps in two contrasting ecosystems. *Atmos. Meas. Tech.* 9, 4915–4933. doi:10.5194/amt-9-4915-2016
- Matsui, T., Beltra'n-Przekurat, A., Niyogi, D., Pielke Sr., R.A., Coughenou, M., 2008. Aerosol light scattering effect on terrestrial plant productivity and energy fluxes over the eastern United States. *J. Geophys. Res.* 113, 1–17. doi:10.1029/2007JD009658
- Mercado, L.M., Bellouin, N., Sitch, S., Boucher, O., Huntingford, C., Wild, M., Cox, P.M., 2009. Impact of changes in diffuse radiation on the global land carbon sink. *Nature* 458. doi:10.1038/nature07949
- Migliavacca, M., Meroni, M., Manca, G., Matteucci, G., Montagnani, L., Grassi, G., Zenone, T., Teobaldelli, M., Godeed, I., Colombo, R., Seufert, G., 2009. Seasonal and interannual patterns of carbon and water fluxes of a poplar plantation under peculiar eco-climatic conditions. *Agric. For. Meteorol.* 149, 1460–1476. doi:10.1016/j.agrformet.2009.04.003
- Min, Q., 2005. Impacts of aerosols and clouds on forest-atmosphere carbon exchange. *J. Geophys. Res. D Atmos.* 110, 1–12. doi:10.1029/2004JD004858
- Misson, L., Lunden, M., McKay, M., Goldstein, A.H., 2005. Atmospheric aerosol light scattering and surface wetness influence the diurnal pattern of net ecosystem exchange in a semi-arid ponderosa pine plantation. *Agric. For. Meteorol.* 129, 69–83. doi:10.1016/j.agrformet.2004.11.008
- Moffat, A.M., Beckstein, C., Churkina, G., Mund, M., Heimann, M., 2010. Characterization of ecosystem responses to climatic controls using artificial neural networks. *Glob. Chang. Biol.* 16, 2737–2749. doi:10.1111/j.1365-2486.2010.02171.x
- Moffat, A.M., 2012. A new methodology to interpret high resolution measurements of net carbon fluxes between terrestrial ecosystems and the atmosphere. PhD Thesis. Friedrich-Schiller-Universität, Jena.

- Moon, K.J., Kim, J., Cho, H.K., Lee, J., Hong, S.Y., Jeong, M.J., 2009. Effect of Aerosol Optical Depth on Diffuse Photosynthetically Active Solar Irradiance. *Asia-pacific J. Atmos. Sci.* 45, 307–317.
- Moore, T.R., Lafleur, P.M., Poon, D.M.I., Heumann, B.W., Seaquist, J.W., Roulet, N.T., 2006. Spring photosynthesis in a cool temperate bog. *Glob. Chang. Biol.* 12, 2323–2335. doi:10.1111/j.1365-2486.2006.01247.x
- Möttus, M., Sulev, M., 2006. Radiation fluxes and canopy transmittance: Models and measurements inside a willow canopy. *J. Geophys. Res.* 111, D02109. doi:10.1029/2005JD005932
- Musavi, T., Migliavacca, M., van de Weg, M.J., Kattge, J., Wohlfahrt, G., van Bodegom, P.M., Reichstein, M., Bahn, M., Carrara, A., Domingues, T.F., Gavazzi, M., Gianelle, D., Gimeno, C., Granier, A., Gruening, C., Havránková, K., Herbst, M., Hrynkiw, C., Kalhori, A., Kaminski, T., Klumpp, K., Kolari, P., Longdoz, B., Minerbi, S., Montagnani, L., Moors, E., Oechel, W.C., Reich, P.B., Rohatyn, S., Rossi, A., Rotenberg, E., Varlagin, A., Wilkinson, M., Wirth, C., Mahecha, M.D., 2016. Potential and limitations of inferring ecosystem photosynthetic capacity from leaf functional traits. *Ecol. Evol.* 6, 7352–7366. doi:10.1002/ece3.2479
- Niyogi, D., Chang, H.I., Saxena, V.K., Holt, T., Alapaty, K., Booker, F., Chen, F., Davis, K.J., Holben, B., Matsui, T., Meyers, T., Oechel, W.C., Pielke, R.A., Wells, R., Wilson, K., Xue, Y., 2004. Direct observations of the effects of aerosol loading on net ecosystem CO₂ exchanges over different landscapes. *Geophys. Res. Lett.* 31, 1–5. doi:10.1029/2004GL020915
- Oliphant, A.J., Dragoni, D., Deng, B., Grimmond, C.S.B., Schmid, H.-P., Scott, S.L., 2011. The role of sky conditions on gross primary production in a mixed deciduous forest. *Agric. For. Meteorol.* 151, 781–791. doi:10.1016/j.agrformet.2011.01.005
- Oliveira, P.H.F., Artaxo, P., Pires, C., De Lucca, S., Procópio, A., Holben, B., Schafer, J., Cardoso, L.F., Wofsy, S.C., Rocha, H.R., 2007. The effects of biomass burning aerosols and clouds on the CO₂ flux in Amazonia, in: *Tellus, Series B: Chemical and Physical Meteorology*. doi:10.1111/j.1600-0889.2007.00270.x
- Papale, D., Reichstein, M., Aubinet, M., Canfora, E., Bernhofer, C., Kutsch, W., Longdoz, B., Rambal, S., Valentini, R., Vesala, T., Yakir, D., 2006. Towards a standardized processing of Net Ecosystem Exchange measured with eddy covariance technique: algorithms and uncertainty estimation. *Biogeosciences* 3, 571–583. doi:10.5194/bg-3-571-2006
- Ponomarev, E., Kharuk, V., Ranson, K., 2016. Wildfires dynamics in Siberian larch forests. *Forests* 7, 125. doi:10.3390/f7060125
- Ponomarev, E.I., 2013. Radiative power of wildfires in Siberia on the basis of TERRA/MODIS imagery processing. *Folia For. Pol. Ser. A - For.* 55, 102–110. doi:10.2478/ffp-2013-0001
- R Core Team 2016, 2016. R: A Language and Environment for Statistical Computing. R Foundation for Statistical Computing, Vienna, Austria URL. <https://www.R-project.org/>.
- Rannik, Ü., Vesala, T., 1999. Autoregressive filtering versus linear detrending in estimation of fluxes by the eddy covariance method. *Boundary-Layer Meteorol.* 91, 259–280. <http://dx.doi.org/10.1023/A:1001840416858>.
- Rap, A., Spracklen, D. V., Mercado, L., Reddington, C.L., Haywood, J.M., Ellis, R.J., Phillips, O.L., Artaxo, P., Bonal, D., Coupe, N.R., Butt, N., 2015. Fires increase

- Amazon forest productivity through increases in diffuse radiation. *Geophys. Res. Lett.* 42, 1–9. doi:10.1002/2015GL063719
- Reichstein, M., Bahn, M., Mahecha, M.D., Kattge, J., Baldocchi, D.D., 2014. Linking plant and ecosystem functional biogeography. *Proc. Natl. Acad. Sci.* 111, 13697–13702. doi:10.1073/pnas.1216065111
- Rocha, A. V, Su, H.-B., Vogel, C.S., Schmid, H.P., Curtis, P.S., 2004. Photosynthetic and water use efficiency responses to diffuse radiation by an aspen-dominated northern hardwood forest.
- Roderick, M.L., Farquhar, G.D., Berry, S.L., Noble, I.R., 2001. On the direct effect of clouds and atmospheric particles on the productivity and structure of vegetation. *Oecologia* 129, 21–30. doi:10.1007/s004420100760
- Schafer, J.S., Eck, T.F., Holben, B.N., Artaxo, P., Yamasoe, M.A., Procopio, A.S., 2002a. Observed reductions of total solar irradiance by biomass-burning aerosols in the Brazilian Amazon and Zambian Savanna. *Geophys. Res. Lett.* 29, 2–5. doi:10.1029/2001GL014309
- Schafer, J.S., Holben, B.N., Eck, T.F., Yamasoe, M.A., Artaxo, P., 2002b. Atmospheric effects on insolation in the Brazilian Amazon: Observed modification of solar radiation by clouds and smoke and derived single scattering albedo of fire aerosols. *J. Geophys. Res. D Atmos.* 107, 1–15. doi:10.1029/2001JD000428
- Schulze, E.-D., Vygodskaya, N.N., Tchebakova, N.M., Czimeczik, C.I., Kozlov, D.N., Lloyd, J., Mollicone, D., Parfenova, E., Sidorov, K.N., Varlagin, A. V., Wirth, C., 2002. The eurosiberian transect: an introduction to the experimental region. *Tellus B* 54, 421–428. doi:10.1034/j.1600-0889.2002.01342.x
- Shibistova, O., Lloyd, J., Zrazhevskaya, G., Arneht, A., Kolle, O., Knohl, A., Astrakhantchva, N., Shijneva, I., Schmerler, J., 2002. Annual ecosystem respiration budget for a *Pinus sylvestris* stand in central Siberia. *Tellus B* 54, 568–589. doi:10.3402/tellusb.v54i5.16688
- Steiner, A.L., Mermelstein, D., Cheng, S.J., Twine, T.E., Oliphant, A., 2013. Observed impact of atmospheric aerosols on the surface energy budget. *Earth Interact.* 17, 1–22. doi:10.1175/2013EI000523.1
- Still, C.J., Riley, W.J., Biraud, S.C., Noone, D.C., Buening, N.H., Randerson, J.T., Torn, M.S., Welker, J., White, J.W.C., Vachon, R., Farquhar, G.D., Berry, J.A., 2009. Influence of clouds and diffuse radiation on ecosystem-atmosphere CO₂ and CO₁₈O exchanges. *J. Geophys. Res. Biogeosciences* 114, 1–17. doi:10.1029/2007JG000675
- Strada, S. and Unger, N., 2016. Potential sensitivity of photosynthesis and isoprene emission to direct radiative effects of atmospheric aerosol pollution. *Atmos. Chem. Phys.* 16, 4213–4234. doi:10.5194/acp-16-4213-2016
- Strada, S., Unger, N., Yue, X., 2015. Observed aerosol-induced radiative effect on plant productivity in the eastern United States. *Atmos. Environ.* 122, 463–476. doi:10.1016/j.atmosenv.2015.09.051
- Tautenhahn, S., Lichstein, J.W., Jung, M., Kattge, J., Bohlman, S.A., Heilmeyer, H., Prokushkin, A., Kahl, A., Wirth, C., 2016. Dispersal limitation drives successional pathways in Central Siberian forests under current and intensified fire regimes. *Glob. Change Biol.* 22, 2178–2197. <http://dx.doi.org/10.1111/gcb.13181>.
- Tchebakova, N.M., Vygodskaya, N.N., Arneht, A., Marchesini, L.B., Kolle, O., Kurbatova, Y.A., Parfenova, E.I., Valentini, R., Vaganov, E.A., Schulze, E.-D., 2015. Energy and mass exchange and the productivity of main Siberian

- ecosystems (from Eddy covariance measurements). 1. heat balance structure over the vegetation season. *Biol. Bull.* 42, 570–578.
doi:10.1134/S1062359015660012
- Tishkov, A., 2002. Boreal forests. In: Shahgedanova, M. (Ed.), *The physical geography of Northern Eurasia*. Oxford University Press, Oxford, pp. 216–233.
- Urban, O., D. Janouš, M. Acosta, R. Czerný, I. Marková, M. Navrátil, M. Pavelka, R. Pokorný, M. Šprtová, R. Zhang, V. Špunda, J. Grace, M.V.M., 2007. Ecophysiological controls over the net ecosystem exchange of mountain spruce stand. Comparison of the response in direct vs. diffuse solar radiation. *Glob. Chang. Biol.* 13, 157–168. doi:10.1111/j.1365-2486.2006.01265.x
- Valendik, E.N., Verkhovets, S. V., Ponomarev, E.I., Ryzhkova, V.A., Kisilyakhov, Y.K., 2014. Large wildfires in taiga subzones of central Siberia. *J. Sib. Fed. Univ.* 1, 43–56.
- Vasileva, A. V., Moiseenko, K.B., Mayer, J.C., Jürgens, N., Panov, A., Heimann, M., Andreae, M.O., 2011. Assessment of the regional atmospheric impact of wildfire emissions based on CO observations at the ZOTTO tall tower station in central Siberia. *J. Geophys. Res. Atmos.* 116, 1–18. doi:10.1029/2010JD014571
- Vickers, D. and Mahrt, L., 1997. Quality control and flux sampling problems for tower and aircraft data. *J. Atmos. Ocean. Technol.* 14, 512–526.
doi:10.1175/1520-0426(1997)014<0512:QCAFSP>2.0.CO;2
- Williams, M., Rastetter, E.B., Van der Pol, L., Shaver, G.R., 2014. Arctic canopy photosynthetic efficiency enhanced under diffuse light, linked to a reduction in the fraction of the canopy in deep shade. *New Phytol.* 202, 1267–1276.
doi:10.1111/nph.12750
- Winderlich, J., Chen, H., Gerbig, C., Seifert, T., Kolle, O., Lavrič, J. V., Kaiser, C., Höfer, A., Heimann, M., 2010. Continuous low-maintenance CO₂/CH₄/H₂O measurements at the Zotino Tall Tower Observatory (ZOTTO) in Central Siberia. *Atmos. Meas. Tech.* 3, 1113–1128. doi:10.5194/amt-3-1113-2010
- Winderlich, J., Gerbig, C., Kolle, O., Heimann, M., 2014. Inferences from CO₂ and CH₄ concentration profiles at the Zotino Tall Tower Observatory (ZOTTO) on regional summertime ecosystem fluxes. *Biogeosciences* 11, 2055–2068.
doi:10.5194/bg-11-2055-2014
- Wirth, A.C., Schulze, E.-D., Schulze, W., Stünzner-Karbe, D. von, Ziegler, W., Miljukolva, I.M., Sogatchev, A., Varlagin, A.B., Panvyorov, M., Grigoriev, S., Kusnetzova, W., M., S., Harges, G., Zimmermann, R., Vygodskaya, N.N., 1999. Above-ground biomass and structure of pristine Siberian Scots Pine forests as controlled by competition and fire. *Int. Assoc. Ecol.* 121, 66–80.
doi:10.1007/s004420050908
- Wohlfahrt, G., Hammerle, A., Haslwanter, A., Bahn, M., Tappeiner, U., Cernusca, A., 2008. Disentangling leaf area and environmental effects on the response of the net ecosystem CO₂ exchange to diffuse radiation. *Geophys. Res. Lett.* 35, 1–5.
doi:10.1029/2008GL035090
- Yamasoe, M., von Randow, C., Manzi, A.O., Schafer, J.S., Eck, T.F., Holben, B.N., 2006. Effect of smoke on the transmissivity of photosynthetically active radiation inside the canopy. *Atmos. Chem. Phys.* 6, 1645–1656.
doi:10.5194/acp-6-1645-2006
- Zhuravleva, T.B., Kabanov, D.M., Nasrtdinov, I.M., Russkova, T. V., Sakerin, S.M., Smirnov, A., Holben, B.N., 2017. Radiative characteristics of aerosol under smoke mist conditions in Siberia during summer 2012. *Atmos. Meas. Tech. Discuss.* 10, 179–198. doi:10.5194/amt-2016-244

Chapter 4 Beginning of snowmelt and surface soil thaw determine spring CO₂ fluxes in boreal forest and bog in central Siberia

Manuscript was submitted to *Boreal Environmental Research*

Sung-Bin Park, Alexander Knohl, Mirco Migliavacca, Tea Thum, Timo Vesala, Olli Peltola, Ivan Mammarella, Anatoly Prokushkin, Olaf Kolle, Jošt Valentin Lavrič, Martin Heimann. Beginning of snowmelt and surface soil thaw determine spring CO₂ fluxes in boreal forest and bog in central Siberia, *Boreal Environmental Research*.

4.1 Introduction

Boreal forests and peatlands are the major terrestrial biomes in northern Eurasia. More than 50% of Russia's land area is covered by forests, and a further 25% by peatlands and tundra (Dolman *et al.* 2012; Schulze *et al.* 2015). Boreal forests store 395 -559 Pg of C (Malhi *et al.* 1999; Prentice *et al.* 2001). Boreal and subarctic peatlands store 220-460 Pg of C (Gorham 1991; Turunen *et al.* 2001; Prentice *et al.* 2001). Both ecosystems are considered to be important sinks of atmospheric carbon dioxide (CO₂) (Lafleur *et al.* 2003; Smith 2004).

In spring, plant physiological processes are controlled by rapidly increasing radiation, temperature, and water availability. As incoming solar radiation increases, air temperature starts to increase and snow begins to melt. These changes in abiotic environmental conditions trigger plant activity as boreal evergreen trees require positive air temperature and available soil water for photosynthesis (Arneth *et al.* 2006). As a result, CO₂ uptake rates gradually increase due to the increase in photochemical efficiency from April to May (Ottander *et al.* 1995; Ensminger *et al.* 2004). The photosynthetic apparatus of boreal forests is adapted to quickly respond to above zero temperatures and spring snowmelt, resulting in fast recovery of physiological activity (Arneth *et al.* 2006). Similarly, a reactivation of photosynthesis for peat mosses occurs immediately after the mosses are exposed from the snow cover (Stoop, 2011). At the beginning of snowmelt surface soil temperature exceeds 0 °C, but remains close to 0 °C until snowmelt completion (Arneth *et al.* 2006; Moore *et al.* 2006). Once the snow melts, soil temperature rapidly increases and a diurnal cycle becomes pronounced. Overall, photosynthetic capacity of both boreal forests and peatlands may be strongly influenced by interannual variability of environmental conditions (Bergh and Linder 1999; Flanagan, 2014).

Based on the regional to global scale studies, the effect of spring warming on vegetation productivity in high-northern latitudes is likely to be different before and after the 2000s. Warming accelerated after 1998 in high-northern latitudes, resulting in earlier start of phenology (Post *et al.* 2018). Several studies found that the spring warming before 2000s accelerated due to warming, resulting in early snow thawing and increase vegetation productivity (Dye and Tucker 2003; Smith *et al.* 2004). In contrast, the trend in spring warming after 2000s slowed down, resulting in smaller increase in vegetation productivity compared to the period of 1980-1990s, especially

in Siberia (Piao *et al.* 2011; Park *et al.* 2018a). A study by Pulliainen *et al.* (2017) based on remote sensing data collected from 1979-2014 showed that earlier snowmelt increased spring ecosystem productivity in boreal forests. This implies that the effect of temperature warming on vegetation productivity is non-linear and region-dependent. Therefore, monitoring spring vegetation carbon uptake on local scale during the present days is essential to understand what causes environmental changes on vegetation productivity.

However, an extension of the growing season length induced by temperature warming may leave plants more exposed to frost conditions in both spring and fall (Liu *et al.* 2018). Similarly, previous studies have shown that frost damages the photosynthetic apparatus of boreal forests, results in inhibition of plant growth and reduction in photosynthesis (Ottander *et al.* 1995; Thum *et al.* 2009; Wallin *et al.* 2013). Wallin *et al.* (2013) proposed that the effects of spring frost and start of soil thawing on boreal forest on spring CO₂ uptake in boreal forests can be nonlinear under the warming future climate. On the contrary, another study found that the effect of warming of growing season temperature on freeze-thaw cycle was not substantial in boreal forests (Ögren 2001). Overall, previous studies suggest that the boreal ecosystem's response to changing climate may be largely dependent on ecosystem types and local climate conditions.

Long-term and continuous flux measurements using the eddy covariance (EC) technique can provide direct information about vegetation responses to changes in abiotic conditions (Lindroth *et al.* 1998; Bowling *et al.* 1998; Pulliainen *et al.* 2017). However, EC flux data are still sparse in central Siberia (Alekseychik *et al.* 2017). Seasonal and annual variability of photosynthesis in Siberian boreal forests (Tanja *et al.* 2003; Ensminger *et al.* 2004; Bartsch *et al.* 2007) as well as Siberian bogs (Arneeth *et al.*, 2002; Schulze *et al.*, 2002) have been highlighted in the past. Particularly, peatlands show a wide range of intensity and magnitude of CO₂ exchange, depending on the type of peatlands and their hydrological conditions (Bubier *et al.* 1998; Lafleur *et al.* 2003; Lund *et al.* 2010; Korrensalo *et al.* 2016, 2017). Local flux observations during springtime are essential to evaluate biophysical and biogeochemical processes in carbon cycle models (Arneeth *et al.* 2006).

Since mid-June of 2012, EC flux measurements have been taken in the two major ecosystem types in central Siberia, i.e. a coniferous forest and a bog. The sites are adjacent to the Zotino Tall Tower Observatory (ZOTTO) (Heimann *et al.* 2014;

Winderlich *et al.* 2014), which is located about 100 km south of the Yenisei river. The five years of data (2013-2017) provide an opportunity to investigate the role of changes in abiotic conditions during springtime for CO₂ exchange of these two important ecosystem types.

The key questions of this study are the following:

- 1) What are the factors controlling the net CO₂ uptake of coniferous forest and bog in spring?
- 2) How do the coniferous forest and bog ecosystems differ in their responses to environmental variables during spring?
- 3) What influence does the very warm spring in 2015 have on the timing of snowmelt, frequency of frost days, and the strengths of net CO₂ sinks?

There was no significant linear increasing or decreasing trend in air temperature during the study period. However, season-average (April-May) air temperature in 2015 was the highest during the study period. Thus, we hypothesize that both ecosystems would show the largest net CO₂ uptakes in the very warm spring because of the earlier termination of snowmelt, earlier start of the net CO₂ uptake and a reduced frequency of frost days.

4.2 Materials and methods

4.2.1 Study site

The Zotino forest flux tower (hereafter ZF, 60°48'25" N, 89°21'27" E, elevation 110 m a.s.l.) is situated 900 m to the north-northeast of the Zotino Tall Tower Observatory (ZOTTO). The average canopy height of the forest is about 20 m, the measurement height is 30.3 m (Table 4.1, Fig. 4.1). The dominant tree species is Scots pine (*Pinus sylvestris*) ranging in age from 80 to 180 years old. Understory vegetation (vegetation height of less than 5 m) consists mostly of regrowth of Scots pine. The main ground vegetation within the footprint area is lichen (*Cladina stellaris* and *Cladina rangiferina*) with patches of dwarf shrub (*Vaccinium vitis-idaea*).

The Zotino bog flux tower (hereafter ZB, 60°49' 03" N, 89°23' 20" E, 66m a.s.l.) is located about 2 km to the northeast of the ZOTTO. The average canopy height at the site is about 2.5 m, and the measurement height is 9.9 m (Table 4.1, Fig. 4.1). The ZB is defined as an ombrotrophic bog (Limpens *et al.* 2008) and also called a raised bog. The landscape is covered by a pine-dwarf shrub-sphagnum (in Siberia called 'ryam') hollow-ridge complex. The ridges make up 70% of the bog area. They are the height of 0.4-0.6 m and covered by plant communities consisting of dwarf pine (*Pinus sylvestris f. litwinowii*), which dominates the trees, and dwarf shrubs (*Chamaedaphne caliculata*). The calibrated absolute age of the peat at the bottom of the bog ranges from 9397 ± 134 y BP at the edges to 13617 ± 190 y BP in the bog center. The peat depth varies from 1.60 m to 5.10 m, increasing toward the center of the bog.

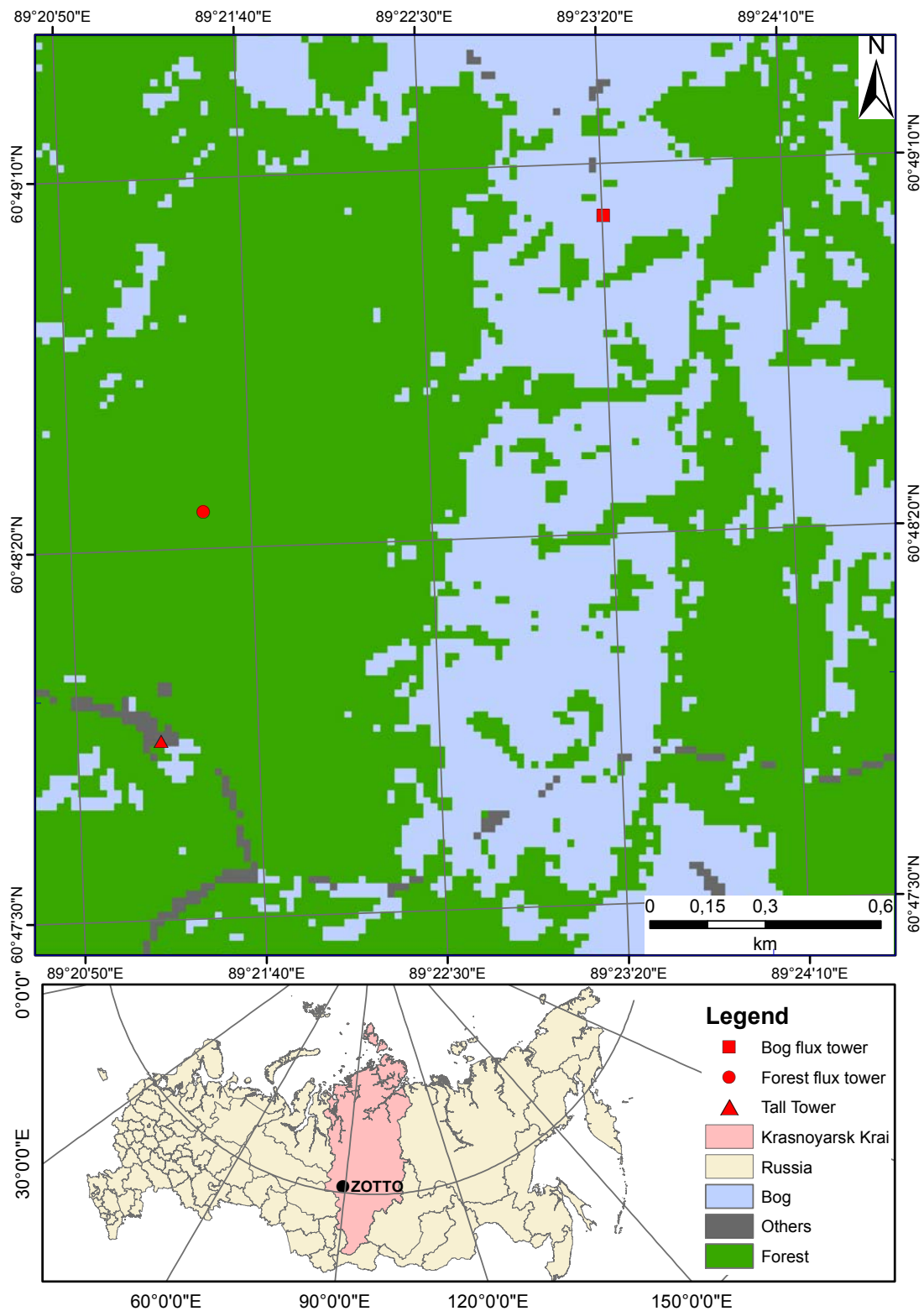


Figure 4.1 Land cover maps and geographical location of forest (ZF; red circle), bog flux towers (ZB; red rectangle), and tall tower (red triangle) at Zotino (black circle). 14 initial land cover types have been reclassified into 3 types. Forests include reforestation, regrowth, lichen with pines, bogs containing shrubs, flooded and wet body. Other classes include clear-cut/barren, burned, sand, and sparse vegetation.

4.2.2 Measurement system

Identical micrometeorological measurement systems were installed at the forest and bog sites (Table 4.2). The EC system consisted of a three-dimensional ultra-sonic anemometer (Metek USA-1, METEK GmbH, Elmshorn, Germany) with integrated 55 W heating and closed-path infrared gas analyzer (LI-7200, LI-COR, Lincoln, USA) to measure CO₂ and H₂O fluxes at 20 Hz frequency. An external diaphragm vacuum pump (N940, KNF Neuberger GmbH, Freiburg, Germany) transported air to the gas analyzer with a flow rate of 13 L min⁻¹ at ambient atmospheric pressure. At the top of the towers, sensors measure the four radiation components and photosynthetically active radiation (PAR), air temperature, relative humidity, and atmospheric pressure. Soil temperature was measured by PT100 soil temperature probes at six depths (0.02, 0.04, 0.08, 0.16, 0.32, and 0.64 m for forest and 0.04, 0.08, 0.16, 0.32, 0.64, and 1.28 m for bog, respectively). Soil moisture was measured at six depths: two sensors at 0.08 m, and one sensor at a depth of 0.16, 0.32, 0.64, 1.28 m for forest, six sensors at a depth of 0.08 m for bog. Data collected from the EC system and meteorological measurements were stored on a data logger (CR3000, Campbell Sci. Inc., Logan, UT, USA). Details of the EC system and data processing are described in Park *et al.* (2018b). Snow depths at both sites were measured manually at locations nearby the towers; however, the measurement intervals were irregular.



Figure 4.2 Eddy covariance flux towers (a) at the Zotino Forest (ZF) site in growing season and (b) snow season and (c) Zotino Bog (ZB) site in growing season and (d) snow season. The measurement heights are 30.3 m and 9.9 m, respectively. Details of the instrumentation are shown in Table 4.2.

Table 4.1 Site characteristics of the flux measurement sites at Zotino.

	ZF	ZB
Geographical location	60.48'25''N, 89.21'27''E	60.49'03''N, 89.23'20''E
Elevation altitude (m a.s.l)	110	66
Vegetation type	Pine forest	Ombrotrophic bog
LAI (m ⁻² m ⁻²)	1-3.5 ¹⁾	not available
Soil type	Podzol	Histosol
Vegetation height (m)	20	2.5 for pine trees 0.5 for dwarf shrubs
Measurement height ²⁾ (m)	29.7	10.1
Tower height ³⁾ (m)	29.4	9.8
Zero plan displacement (m)	13.4	1.675
Roughness length (m)	2	0.25

1) Values from previous ground-based and remote-sensing measurements (Los et al. 2000; Wirth et al. 1999)

2) Measurement heights are the height to the centre of the sonic anemometers

3) Tower heights are the distance between the ground fundament panels to the top of the tower plate

Table 4.2 Instrument setup and sensor types of the flux towers at the Zotino flux sites.

	Zotino Forest (ZF)	Zotino Bog (ZB)
Sonic anemometer	USA-1, METEK GmbH, Elmshorn, Germany	
CO ₂ /H ₂ O gas analyzer	LI-7200, LiCor Biosciences, Lincoln NE, USA	
Time lag	0.8 (CO ₂), 1.2 (H ₂ O)	0.9 (CO ₂), 1.3 (H ₂ O)
Flow rate (L/min)	15	
Sampling frequency (Hz)	20	
Long/short wave up/downwelling radiation	CNR1, Kipp & Zonen, Deft, The Netherlands	
Up/downward photosynthetically active radiation	PQS1, Kipp & Zonen, Deft, The Netherlands	
Air temperature and relative humidity	KPK 1/6-ME-H38, Mela, Bondorf, Germany	
Barometric pressure	Pressure Transmitter, 61302 V, R.M. Young Company, Traverse City, USA	
Soil temperature	RTD temperature probe, Pt100, JUMO	
Soil moisture	ThetaProbe ML2x, Delta-T devices, Cambridge, England	
Ground heat flux	Heat flux plates RIMCO HP3/CN3, McVan Instruments, Mulgrave, Victoria, Australia	
Precipitation	Tipping bucket rain gauge, Adolf Thies GmbH & Co. KG, Göttingen, Germany	

4.2.3 Post-processing and data quality control

Post-processing of the high-frequency data and calculation of half-hourly turbulent fluxes were performed using the EddyUH software (Mammarella *et al.* 2016). The thresholds of friction velocity (u^*) for ZF and ZB were 0.2 m s^{-1} and 0.1 m s^{-1} , respectively. Details of the data post-processing and quality control procedure are described in Park *et al.* (2018b). High quality data were available about 40-60% of the year before the gap-filling procedure (Table 4.3). Only days with 70% of coverage after gap-filling (flag 0-1 from the quality flag criterion in the REddyProc, see also Wutzler *et al.* 2018) were used to calculate cumulative and daily CO_2 flux. The entire 5 years of data were used for ZF, whereas 3 years (2014-2016) of data were used for ZB, because of a long-term data gap during November 2012 to April 2013. In addition, in 2017, data availability was less than 20% for ZB due to a malfunction of the gas analyser. Thus, for this site, we used flux data from 2013-2016 only (i.e., Table 4.4 and Fig. 4.4). Although half-hourly CO_2 fluxes during early April in 2013 were missing the period of source-sink transition at ZB was detectable. Therefore we include the data in 2013 for Table 4.5 and Fig. 4.5.

Table 4.3 The percentages (%) of high quality flux data during spring season (April-June) at the Zotino forest (ZF) and Zotino bog (ZB) sites.

Year	Zotino Forest (ZF)	Zotino Bog (ZB)
2013	44	41
2014	42	51
2015	59	38
2016	60	46
2017	61	19

4.2.3.1 Definition of metrics and analysis

For both sites, the analyses were based on the daily mean CO₂ flux and meteorology data. Daily CO₂ fluxes were summed for each 24-hour period with gap-filled data. The start of CO₂ uptake was identified as the point when a 3-day moving average of daily CO₂ flux fell below zero for the first time. As for EC convention, negative NEE means net CO₂ uptake by the forest and bog, while positive NEE indicates CO₂ release from the ecosystems to the atmosphere.

The four metrics were used to determine the start of CO₂ uptake (SCU, expressed in DOY): 1) air temperature (SCU_{T5(5 °C)}), 2) surface soil temperature (SCU_{Ts04(0 °C)}), 3) the beginning of the snowmelt (SCU_{Bsnow}), and 4) the final day of the snowmelt (SCU_{Fsnow}). For instance, air temperature warming index (SCU_{T5(5 °C)}) is the day on which the 5-day moving average of T_a exceeds 5 °C for a consecutive 3-day period. In previous study, SCU_{T5(5 °C)} was reported as the most relevant known triggers of spring photosynthetic recovery in boreal forests (Tanja *et al.* 2003; Thum *et al.* 2009), thus we used the same definition. The start day of surface soil or peat warming index (SCU_{Ts04(0 °C)}) is the first day when the 3-day moving average of soil or peat temperatures (T_{s04}) at a depth of 0.04 m rose above 0 °C. Because of irregular measurement intervals of snow depth, surface albedo data was used as a proxy for the status of snowmelt. SCU_{Bsnow} refers to the beginning of snowmelt as defined by Thum *et al.* (2009). By visual inspection, the threshold values of albedo were set to the point on which the 3-day moving average of albedo fell below 0.2 (20%) for ZF and 0.5 (50%) for ZB, respectively. SCU_{Fsnow} is the final day of snowmelt and the day when the three-day moving average of surface albedo fell below 0.15 for the first time. In another previous study, SCU_{Fsnow} was determined by the surface soil or peat temperature measurements (T_{s04} or T_{s04(0 °C)}) started showing a distinct diurnal pattern (Shibistova *et al.* 2002). SCU_{Fsnow} using albedo threshold or soil temperature threshold were almost same. Thus we presented the SCU_{Fsnow} using surface soil temperature (Appendix Table S4.3).

The total number of frost days is the number of days on which the daily minimum air temperature fell below 0 °C (Liu *et al.* 2018). Late frost is defined as frost days after the beginning of snowmelt.

4.2.3.2 Statistical analysis

In order to investigate the impacts of frost on CO₂ fluxes and ecosystem recovery from frost, the maximum photosynthetic capacity (A_{max}) and the net ecosystem productivity at PAR of 1500 $\mu\text{mol photon m}^{-2} \text{s}^{-1}$ (NEP_{1500}) were compared among three periods (i.e., pre-frost days, frost days, and post-frost days). The functional relationship between radiation and CO₂ flux was examined with a rectangular hyperbolic light-response function with daytime data ($R_{pot} > 20 \text{ W m}^{-2}$) (Michalelis and Menten, 1913; Ruimy *et al.* 1995; Falge *et al.* 2001):

$$NEP = \frac{\alpha \cdot A_{max} \cdot PAR}{A_{max} + \alpha \cdot PAR} + R_d$$

where PAR ($\mu\text{mol photon m}^{-2} \text{s}^{-1}$) is the incident photosynthetically active radiation, A_{max} ($\mu\text{mol CO}_2 \text{ m}^{-2} \text{s}^{-1}$) is the light-saturation point of CO₂ uptake, and α is the initial slope of the photosynthetic light response curve. This is also known as light use efficiency or quantum yield. R_d is the ecosystem respiration during the day. For the light response analysis, we used the net ecosystem productivity (NEP), which is the same as $-NEE$. Light response model parameters were estimated for selected periods (i.e., pre-frost days, frost days, and post-frost days) using measured NEP data. Parameters were estimated using the Levenberg-Marquardt method, implemented in the `minpack.lm` routine in R (version 3.5.1). NEP_{1500} was calculated with obtained three parameters and fixing PAR of 1500 $\mu\text{mol photon m}^{-2} \text{s}^{-1}$. The definition of NEP_{1500} was identical to that used by Falge *et al.* (2001) and Musavi *et al.* (2016). The standard deviations of NEP_{1500} were calculated from the value of the combinations of minimum and maximum for each parameter.

To identify which abiotic variables are important to explain the variability in daily CO₂ flux, we used the Multivariate Adaptive Regression Splines (MARS) regression model (Friedman and Roosen, 1995) in the “earth” package in R 3.3.0 software (<https://cran.r-project.org/web/packages/earth/index.html>). Daily CO₂ fluxes with corresponding abiotic variables were used as training data for both sites from DOY 99-155 in 2013-2017 for ZF and the same days in 2014-2016 for ZB, respectively. For ZF, nine abiotic measurements were used as training data: photosynthetically active radiation (PAR), surface albedo (Alb), air temperature (T_a), midday vapour pressure deficit (VPD), soil temperatures at the depths of 0.04m (T_{s04}),

0.08m (T_{s08}), 0.16m (T_{s16}), 0.32m (T_{s32}), and 0.64m (T_{s64}). For ZB, a total of six abiotic variables were used as a training data, excluding T_{s08} and T_{s16} due to the long-term gaps (> 3 months). Only VPD was represented by midday (11:00-15:00) averages; and the rest of values were daily mean values.

The MARS is a non-parametric regression method, dealing with both linear and nonlinear relationships and interactions between variables in the data using hinge functions (Park *et al.* 2017). Variable selection algorithms search the variables using both forward and backward stepwise selections. Variable importance is determined by a selection algorithm and is based on the number of model subsets (*nsubsets*), generalized-cross validation (GCV) score, and residual sum of squares (RSS).

$$RSS = \sum_{i=1}^n (y_i - \hat{y}_i)^2$$

, where y_i is a measured CO₂ flux and \hat{y}_i is a modelled CO₂ flux.

$$GCV = \frac{RSS}{N * (1 - \text{effective number of paramete}/N)^2}$$

, where effective number of parameters is the sum of the number of input features and patently * (number of input features -1)/2, N is the number of observations. GCV is the method for choosing the smoothing parameter (Green and Silverman, 1993) and the best model is selected based on GCV. GCV and RSS range from 0-100. Higher GCV scores indicate variables with more explanatory power. Adding a variable can sometimes increase the GCV. The largest summed decrease of the RSS is scaled to 100, therefore a larger net decrease in the RSS is more important. Higher *nsubsets* means that variables are included in more subsets because they are important. Further statistical theory and application are described in detail at <http://www.milbo.org/doc/earth-notes.pdf>.

For both sites, a total of 9 variables (i.e. air temperature (T_a), soil temperatures at 0.04 m (T_{s04}), 0.08 m (T_{s08}), 0.16 m (T_{s16}), 0.32 m (T_{s32}), 0.64 m (T_{s64}), surface albedo (Alb), photosynthetic active radiation (PAR), and vapour pressure deficit (VPD)) were used as predictors. Only VPD was represented by midday (11:00-15:00) averages; and the rest of values were daily mean values.

To quantify the relative contributions and importance of each variable in determining CO₂ fluxes in spring, we used the well-known “lmg” relative importance method developed by Lindemann, Merenda and Gold (1980) and implemented in “relaimpo” R package (Groemping, 2016, <https://cran.r->

project.org/web/packages/relaimpo/index.html). This method was applied only to the variables selected with the MARS model explained before. Additionally, 95% confidence intervals for relative importance were calculated using a bootstrapping procedure.

4.3. Results

4.1 The abiotic controls of spring CO₂ fluxes

This subsection shows both the overall and relative importance of variables that influence CO₂ fluxes in spring. Examples for forest and bog are shown, followed by analysis and discussion of the site differences.

ZF: The MARS model identified the following six variables: Alb, PAR, T_{s04}, T_{s16}, T_{s64}, and T_a among the nine variables analysed as the important influences on CO₂ fluxes (Fig. 4.3, Appendix Table S4.1). The relative importance of the six variables evaluated by “lmg” method explained 71.78% of the variability in springtime CO₂ flux in forest (Fig. 4.3). Alb and PAR were equal as the most important controlling factors of springtime CO₂ fluxes (both 14.8%). PAR contained a larger uncertainty ([12.14, 18.20]) than Alb ([10.68, 19.70]) with a significance level at 95%. The other explanatory variables (i.e. T_{s04}, T_{s16}, T_{s64}, and T_a) explained 7-12% of CO₂ fluxes. The three soil temperatures (T_{s04}, T_{s16}, T_{s64}) explained 10-12% of the variability in CO₂ fluxes. The least important driver was T_a.

ZB: The MARS model identified the following five drivers: T_{s04}, Alb, T_{s64}, PAR, and T_{s32} among the nine variables analysed as the important influences on CO₂ fluxes (Appendix Table S4.2). Both T_a and VPD were not important drivers of CO₂ fluxes. This indicates that the peat temperatures regulate CO₂ fluxes stronger than air temperature. The selected five variables explained 80.64% of the variability in springtime CO₂ fluxes in bog (Fig. 4.4). The relative contributions of T_{s04}, T_{s32}, T_{s64}, Alb, and PAR to CO₂ fluxes were 21.84%, 18.16%, 16.30%, 15.01%, and 9.33%, respectively. In contrast to ZF, peat temperatures were more important drivers than radiative drivers (i.e. Alb and PAR).

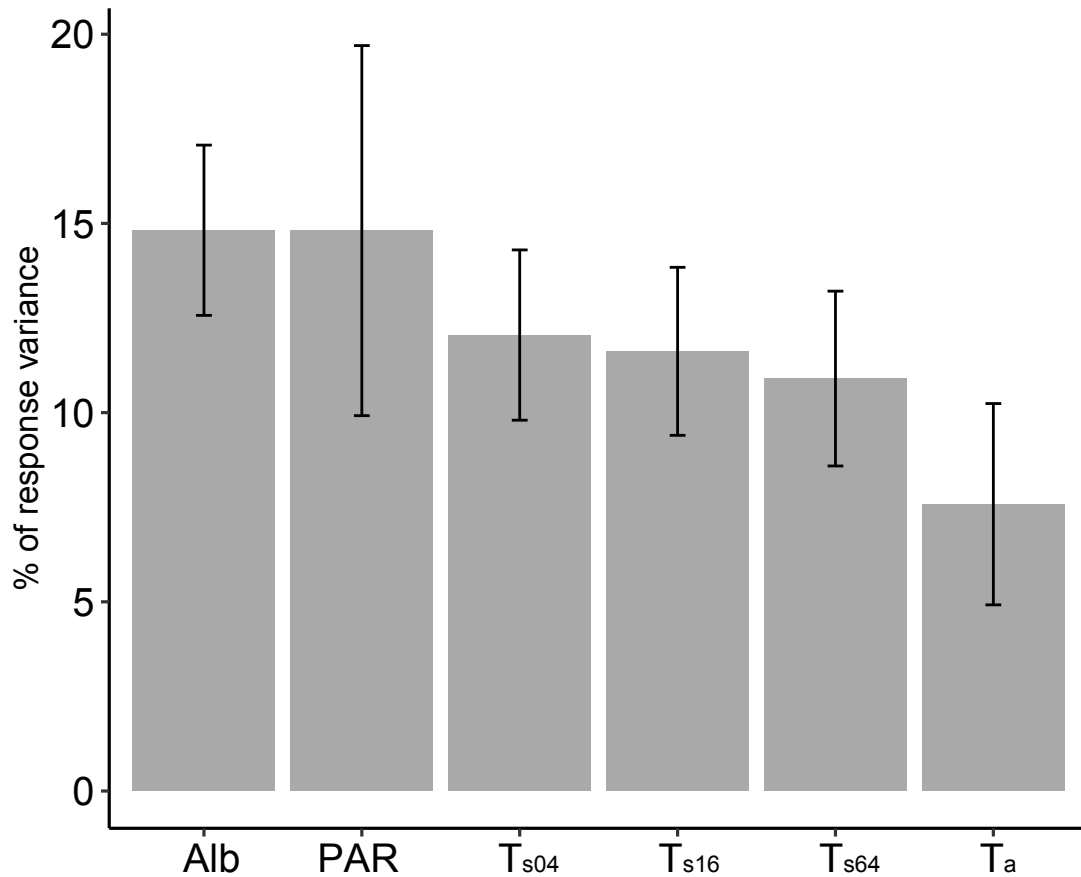


Figure 4.3 Relative importance of six abiotic variables for CO₂ fluxes for the Zotino forest (ZF) with bootstrapped 95% confidence intervals. Bootstrap replicates (n) were set to 1000 and overall R² was 71.78%, which is the sum of the percentage of response variance. The variables are denoted in the importance: surface albedo (Alb), photosynthetically active radiation (PAR), surface soil temperature (T_{s04}), soil temperature at the depth of 0.16m (T_{s16}) and 0.64m (T_{s64}), and air temperature (T_a). Total 285 daily mean values from DOY 99-155 during 2013-2017 were used.

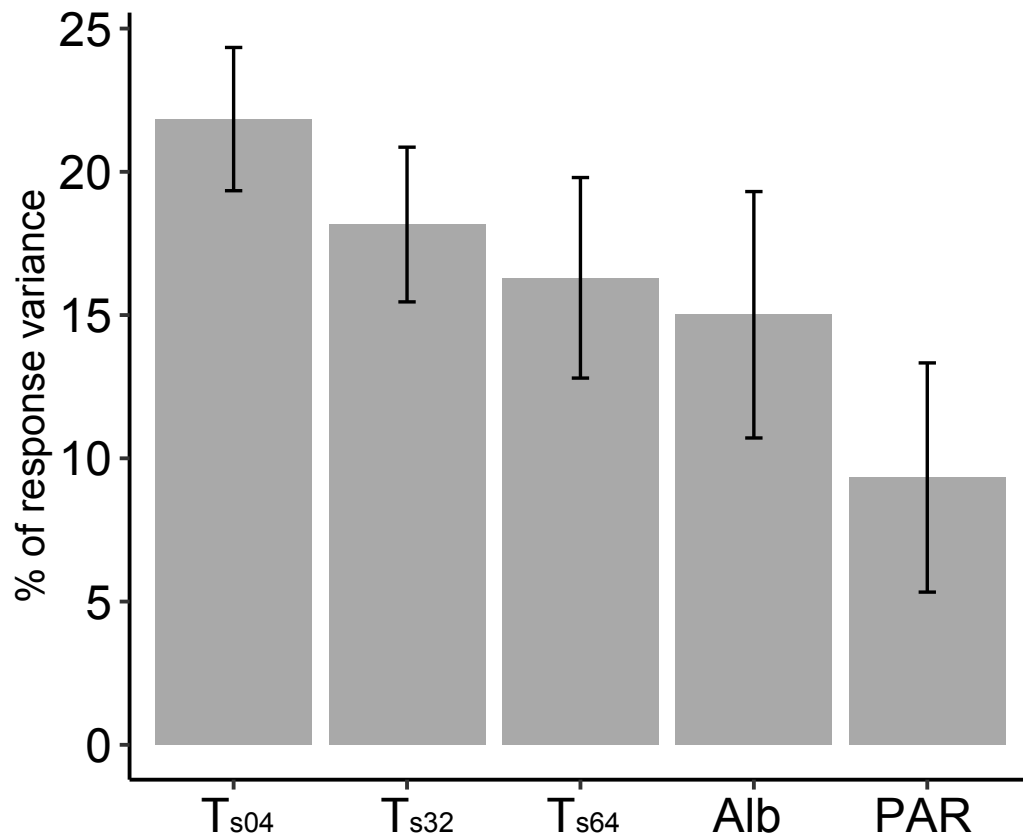


Figure 4.4 Relative importance of five abiotic variables for CO₂ flux for the Zotino bog (ZB) with the bootstrapped 95% confidence intervals. Bootstrap replicates (n) were set to 1000 and R^2 was 80.64%, which is the sum of the percentage of response variance. The variables are denoted in the order of importance: peat temperature in the depths of 0.04m (T_{s04}), 0.32m (T_{s32}), 0.64m (T_{s64}), surface albedo (Alb), photosynthetically active radiation (PAR), respectively. Total 216 daily mean values from DOY 111-155 in 2013 and DOY 99-155 during 2014-2016 were used. Peat temperatures at the depth of 0.08m and 0.16m were excluded from the analysis due to the long-term gaps (>3 months) during springtime in 2014-2015.

4.2 CO₂ fluxes and abiotic drivers during the transition period

This subsection describes the variability of time series of meteorological drivers (i.e Alb, T_s, and T_a) and CO₂ fluxes focusing on start of CO₂ uptake (SCU) and its proxies. Only the two contrasting years with the earliest and the latest start of CO₂ uptake are shown.

At ZF, change in Alb (together with PAR) was the major driver of CO₂ fluxes (Fig. 4.3). As Alb decreased close to 15%, CO₂ uptake started (Fig. 4.5). During the snowmelt period (10-20 days), the forest transitioned from a net CO₂ source to a net CO₂ sink. However CO₂ fluxes were still highly variable during this time, fluctuating between being a net CO₂ source and a net CO₂ sink. This pattern was apparent across the entire study period, resulting in a positive correlation between the start of CO₂ uptake (SCU) and the beginning of snowmelt (SCU_{Bsnow}) ($SCU = 0.88 * SCU_{Bsnow} + 13.44, R^2 = 0.99, p < 0.05$, see also Appendix Table S 4.3).

The start of CO₂ uptake occurred during periods with cold or frozen soil (Fig. 4.5). However, the magnitude of daily CO₂ uptake was lower than -1 g C m⁻² d⁻¹ until thawing of the surface soil (T_{s04} < 0 °C) or snowmelt was complete.

Variability of T_a and CO₂ flux coincided during the transition periods (Fig. 4.5a, b, Table 4.4). Once CO₂ uptake began, CO₂ uptake rates fluctuated in response to T_a (Pearson correlation coefficient, $r = -0.48, p < 0.05$ for 2016 and $r = -0.35, p < 0.05$ for 2017).

T_a in April triggers SCU through the timing of snowmelt (Appendix Table S 4.3, Fig. 4.5). For instance, Wilcoxon rank sum test confirmed that both SCU and SCU_{Bsnow} were significantly correlated with T_a in April ($Z = 2.0226, p = 0.04311$). This means that the beginning of snowmelt determined the start of CO₂ uptake. For instance, the warmest spring was observed in 2015 (Table 4.4), however the earliest SCU occurred in 2016, when snowmelt began earlier than in the other years (Fig. 4.5d, Appendix Table S 4.3).

Surface albedo at ZB showed the remarkable difference to the one at the forest because of the higher radiation absorption by forest (Fig. 4.5a, b, Fig. 4.6a, b). The CO₂ fluxes at ZB had a lower magnitude and fluctuated less compared to ZF (Fig. 4.6c, d). Similar to ZF, ZB also remained a weak net CO₂ sink (-0.5 g C m⁻² d⁻¹) before the snowmelt completed and the surface unfrozen. The transition from source to sink in NEE generally coincided with the SCU_{Ts04(0 °C)} (Fig. 4.6).

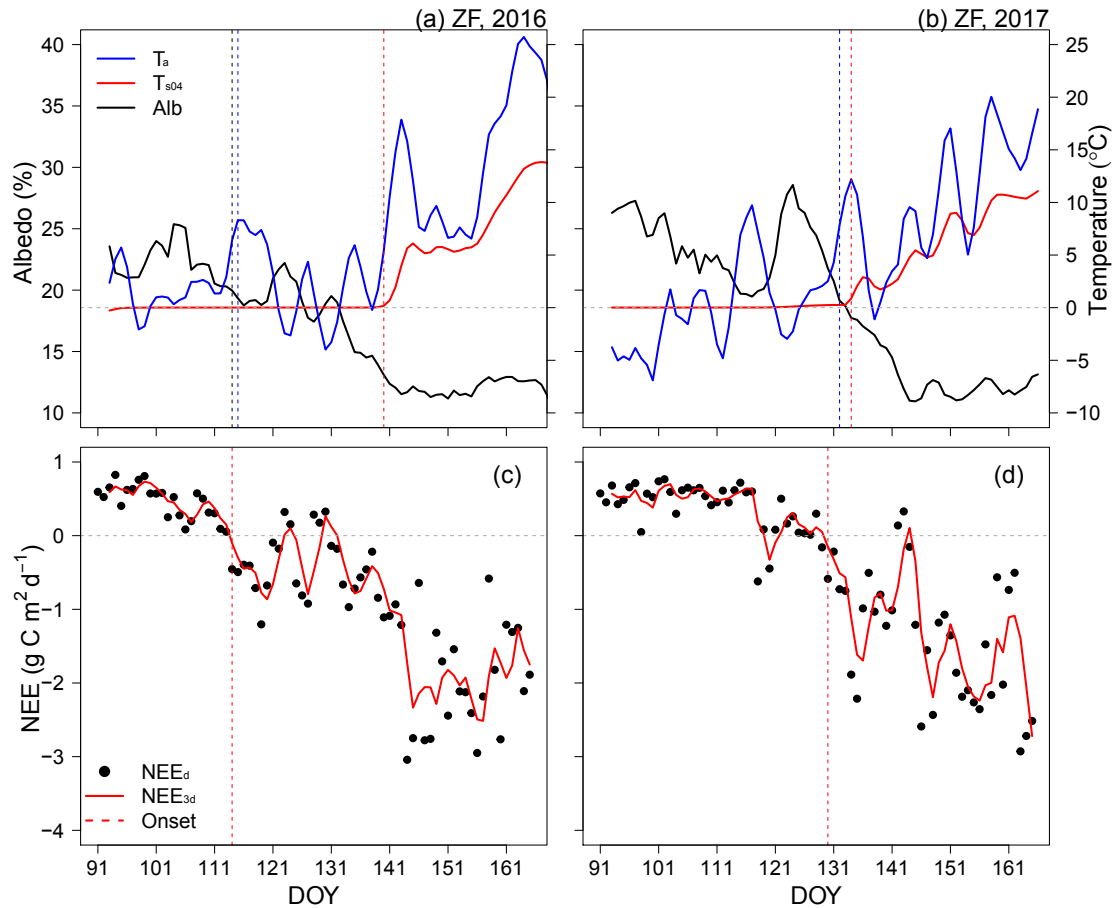


Figure 4.5 Time series of 3-day moving averaged meteorological variables and net ecosystem exchange of CO₂ (NEE) from DOY 91 to DOY 165 for the forest site (ZF) in 2016 and 2017. In (a) and (b), blue lines denote air temperature (T_a), red lines denote soil temperature at the depth of 0.04m (T_{s04}), and black lines denote surface albedo (Alb). In (c) and (d), black dots and red lines indicate daily sum of NEE (NEE_d) and moving averaged value (NEE_{3d}). The earliest and the latest start of CO₂ uptake were in 2016 and in 2017 during the study period. Vertical dotted lines in (a) and (b) indicate SCU_{Bsnow} (grey), $SCU_{T5(5\text{ }^\circ\text{C})}$ (blue), and $SCU_{Ts04(0\text{ }^\circ\text{C})}$ (red). Horizontal red dotted lines in (c) and (d) denote the start of CO₂ uptake (SCU). $SCU_{T5(5\text{ }^\circ\text{C})}$ were DOY 115 in 2016 and DOY 132 in 2017. $SCU_{Ts04(0\text{ }^\circ\text{C})}$ were DOY 140 in 2016 and DOY 134 in 2017. SCU_{Bsnow} were DOY 114 in 2016 and DOY 132 in 2017. SCU_{Fsnow} were DOY 139 in 2016 and DOY 134 in 2017. SCU were DOY 114 in 2016 and DOY 130 in 2017. Vertical dashed line in (c) and (d) corresponding to the start of CO₂ uptake (red). Negative NEE is a net CO₂ uptake, positive NEE is a net CO₂ release.

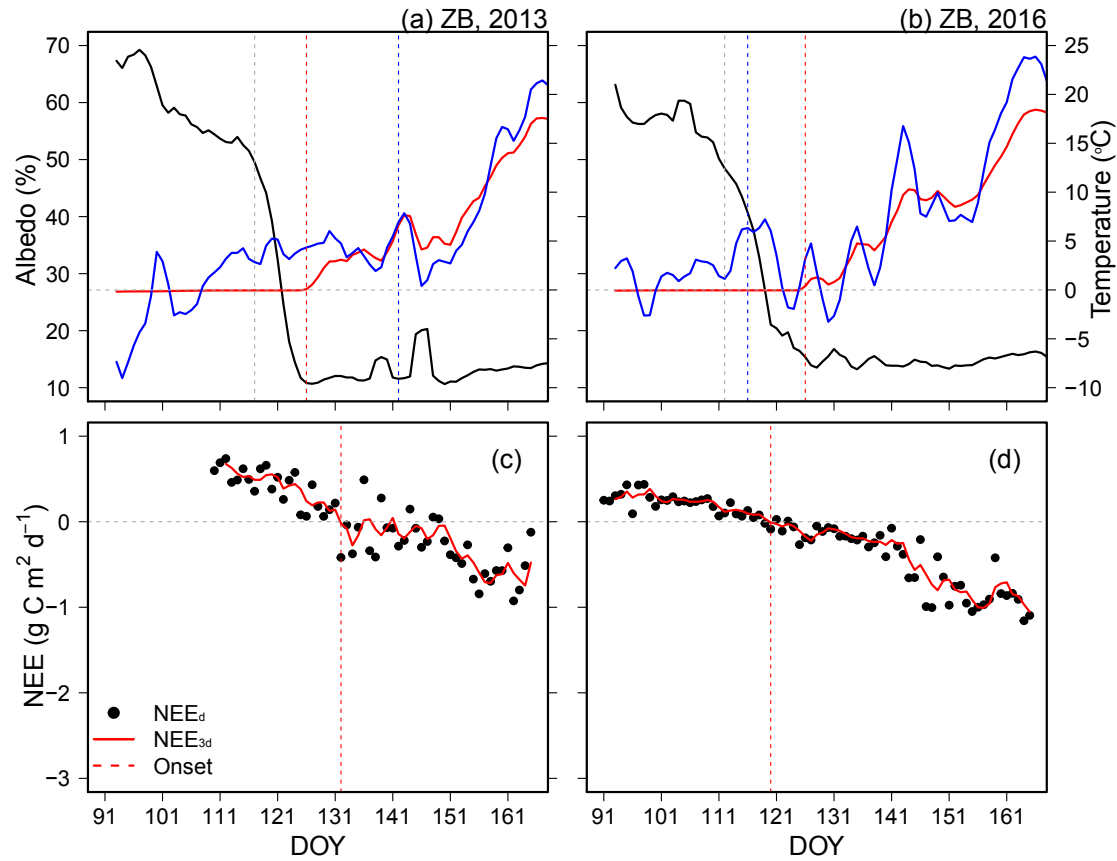


Figure 4.6 Same as Fig. 4.5 but for ZB. Horizontal red dotted lines in (c) and (d) denote the start of CO₂ uptake (SCU). SCU_{T5(5 °C)} were DOY 142 in 2013 and DOY 116 in 2016. SCU_{Ts4(0 °C)} were both DOY 126 in 2013 and 2016. SCU_{Bsnow} were DOY 117 in 2013 and DOY 112 in 2016. SCU_{Fsnow} were DOY 126 in 2013 and DOY 127 in 2016. SCU were DOY 132 in 2013 and DOY 120 in 2016.

4.3 Interannual variability in spring cumulative net ecosystem exchange of CO₂

The variability in spring NEE_{cum} was highly dependent on year and differed between the two sites (Fig. 4.7). Spring NEE_{cum} of ZF had larger magnitude and higher maximum values than ZB. The averages of spring NEE_{cum} were -22.5 g C m⁻² for ZF and -9.8 g C m⁻² for ZB.

To compare the interannual variability of NEE_{cum} and its rate of change, the mean slopes of the curve ($\frac{\partial NEE_{cum}}{\partial DOY}$) were calculated within two sub-periods at pre- and post peak of NEE_{cum} (Table 4.4). For both ecosystems, the declines of NEE_{cum} from its peak were the steepest (-1.62 for ZF and -0.92 for ZB, respectively) in the warmest year (2015). Both ecosystems were the strongest net CO₂ sinks in 2015 (Fig. 4.7 and Table 4.4). The range of NEE_{cum} varied from -8.13 (2013) to -37.15 (2015) g C m⁻² for ZF and -6.80 g C m⁻² (2016) and -14.94 g C m⁻² (2015), respectively. This result is

consistent with the largest ecosystem productivities in 2015 (Table 4.4). The net source of NEE_{cum} varied between 3.90 and 11.38 g C m⁻² at ZF, whereas it varied between 3.40 and 8.33 g C m⁻² at ZB. Particularly at ZF in 2017 between DOY 99-110, daily NEE was higher than among other years.

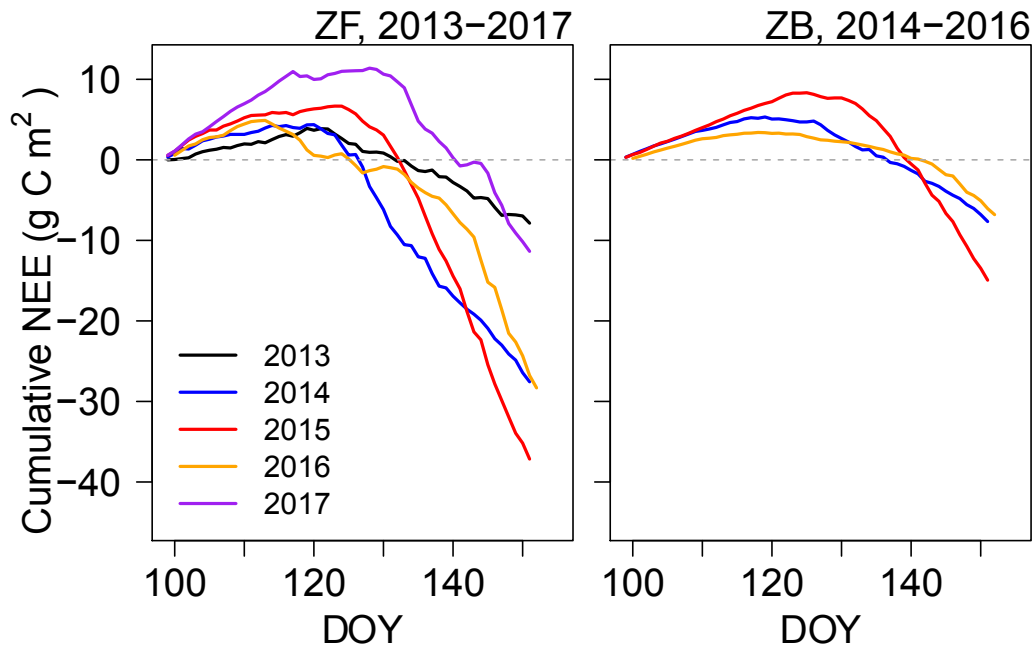


Figure 4.7 Cumulative net ecosystem exchange of CO₂ (NEE_{cum}) at the Zotino forest (ZF) and Zotino bog (ZB) from DOY 99-151 during 2013-2017. The grey dashed zero-line denotes the transition from a cumulative CO₂ source (positive) to cumulative CO₂ sink (negative). Positive values indicate a cumulative ecosystem carbon loss, and negative values indicate a cumulative ecosystem carbon uptake.

The features of the transition day from NEE_{cum} source to NEE_{cum} sink were different between the two sites (Fig. 4.7, Table 4.4). The transition day for ZF was highly variable from year-to-year during the study period, whereas it was similar among years for ZB. At least for ZF, the earliest source-sink transition in NEE_{cum} is likely caused by the highest T_a in April, 2016 and the earliest start of CO₂ uptake (Fig.4.5, Table 4.4).

Table 4.4. The day of year (DOY) of transition from NEE_{cum} source to NEE_{cum} sink, maximum NEE_{cum} ($(NEE_{cum})_{peak}$) with corresponding DOY, mean slopes ($\frac{\partial NEE_{cum}}{\partial DOY}$) before and after reaching peak of the NEE_{cum} for ZF and ZB during 2013-2017. The same data were used in Fig.4.3. Values in bold indicate the maximum, whereas values in bold and italic indicate the minimum.

Year	Source-sink transitions (DOY)		$(NEE_{cum})_{peak}$ (g C m ⁻² d ⁻¹)		DOY of $(NEE_{cum})_{peak}$		mean slope before $(NEE_{cum})_{peak}$ (g C m ⁻² d ⁻²)		mean slope after $(NEE_{cum})_{peak}$ (g C m ⁻² d ⁻²)	
	ZF	ZB	ZF	ZB	ZF	ZB	ZF	ZB	ZF	ZB
2013	132	-	3.90	-	119	-	0.20		-0.37	-
2014	127	<i>137</i>	4.37	5.32	120	119	0.19	0.25	-1.05	-0.41
2015	133	140	6.67	8.33	123	125	0.25	0.31	-1.62	-0.92
2016	<i>126</i>	142	4.90	<i>3.40</i>	<i>113</i>	<i>118</i>	0.33	0.18	-0.86	-0.31
2017	141	-	11.38	-	128	-	0.37		-1.03	-

4.4 Spring air temperature and cumulative net ecosystem exchange of CO₂

The highest ecosystem productivity for both ecosystems occurred in 2015, probably because of the very warm T_a in May 2015 (Table 4.5, Fig. 4.7). The highest T_a anomalies in May were +4.35 °C for ZF and +3.85 °C for ZB compared to the 2013-2017 mean, respectively (hereafter, anomaly values are compared with the 2013-2017 mean). Consequently, the warmest spring T_a exceeded 2 °C in 2015 (anomalies of +2.35 °C for ZF and +2.38 °C for ZB). The spring NEE_{cum} in 2015 was -37.15 g C m⁻² for ZF and -14.94 g C m⁻² for ZB. Both ecosystems showed a linear negative relationship between overall springtime NEE_{cum} and season-average T_a . While the correlation was statistically significant for the ZF site ($NEE_{cum} = -5.645 \cdot T_a + 1.558$, $R^2 = 0.5162$, $p = 0.01715$), it was not significant at the ZB site, likely due to the small sample size ($NEE_{cum} = -4.64 \cdot T_a + 15.021$, $R^2 = 0.6634$, $p = 0.1855$). However, when just May data were used, we found a positive relationship between these variables at ZF: $NEE_{cum} = 0.90 \cdot T_a + 0.73$, $R^2 = 0.99$, $p < 0.005$, but insignificant at the ZB site: $NEE_{cum} = -2.27 \cdot T_a + 0.15$, $R^2 = 0.95$, $p = 0.1398$.

The very warm April was the trigger of the earliest SCU_{Bsnow} in 2016, resulting in the earliest SCU (Fig. 4.5). Therefore, the forest ecosystem had more days

for carbon uptake because of a longer spring days in 2016 (NEE_{cum} : -32.8 g C m^{-2}) than in 2017 (NEE_{cum} : -22.0 g C m^{-2}). Similarly, at ZB longer spring days resulted in more carbon uptake in 2016 (NEE_{cum} : -9.91 g C m^{-2}) than in 2017 (NEE_{cum} : -3.94 g C m^{-2}).

Table 4.5. Mean air temperature (T_a) and cumulative net ecosystem exchange of CO_2 (NEE_{cum}) for April, May, and season-average values for the ZF and ZB flux sites, as well as year-average values during the study period (2013-2017). Both T_a and NEE_{cum} were calculated on DOY 99 (9 April) except the NEE_{cum} in 2013 for ZB, which starts on DOY 110 (20 April). Therefore, the mean value of the NEE_{cum} for ZB only presents a three-years average over the period of 2014-2016. Bold values indicate the maximum, whereas bold and italic values indicate the minimum.

		T_a ($^{\circ}C$)		NEE_{cum} ($g \text{ C m}^{-2}$)	
Year	Month	ZF	ZB	ZF	ZB
2013	April	2.57	1.93	3.57	5.93
	May	3.76	3.91	-11.70	1.38
	Spring	3.27	3.09	-8.13	7.31
2014	April	0.94	1.40	4.37	5.06
	May	4.84	5.08	-31.93	-12.72
	Spring	3.22	3.56	-27.56	-7.66
2015	April	2.47	2.42	6.33	7.22
	May	10.16	9.84	-43.48	-22.16
	Spring	6.97	6.76	-37.15	-14.94
2016	April	3.28	3.15	0.46	3.31
	May	4.89	5.15	-28.77	-10.12
	Spring	4.21	4.30	-28.31	-6.80
2017	April	1.03	1.63	9.98	-
	May	5.42	5.98	-21.34	-
	Spring	3.64	4.21	-11.36	-
Mean	April	2.06	2.11	4.94	5.20
	May	5.81	5.99	-27.44	-15.00
	Spring	4.62	4.38	-22.50	-9.80

4.5 Impact of spring frost on photosynthetic related process

Frost in April did influence the magnitude of forest CO₂ flux, changing it from a net CO₂ sink to a net CO₂ source until T_{s04} exceeded 0 °C (Fig. 4.5a, c). For example, at the ZF site, after the warm spell on DOY 150 in 2017, T_a decreased by 10 °C, resulting in a change of the CO₂ flux from negative to positive. The forest then recovered to a net CO₂ sink after T_{s04} exceeded 0 °C (Fig. 4.5b, d). Similar features were found at the ZB site as well (Fig. 4.6, Table 4.6).

Warm spring temperature reduced both the overall frequency of frost days as well as the frequency of late frost days. The very warm May and spring in 2015 had the lowest number of frost days and the lowest number of late frost days for both sites (Fig. 4.8, Appendix Table S4.4).

Frost reduced net ecosystem productivity (NEP) for both ecosystems (Fig. 9, Table 6). For example, ecosystem light response curves show that NEP₁₅₀₀ for both ecosystems decreased during the frost days and recovered after frost days. At ZF, NEP₁₅₀₀ decreased from 5.27 to 3.06 due to frost, but increased again after frost. Similar features were found at ZB.

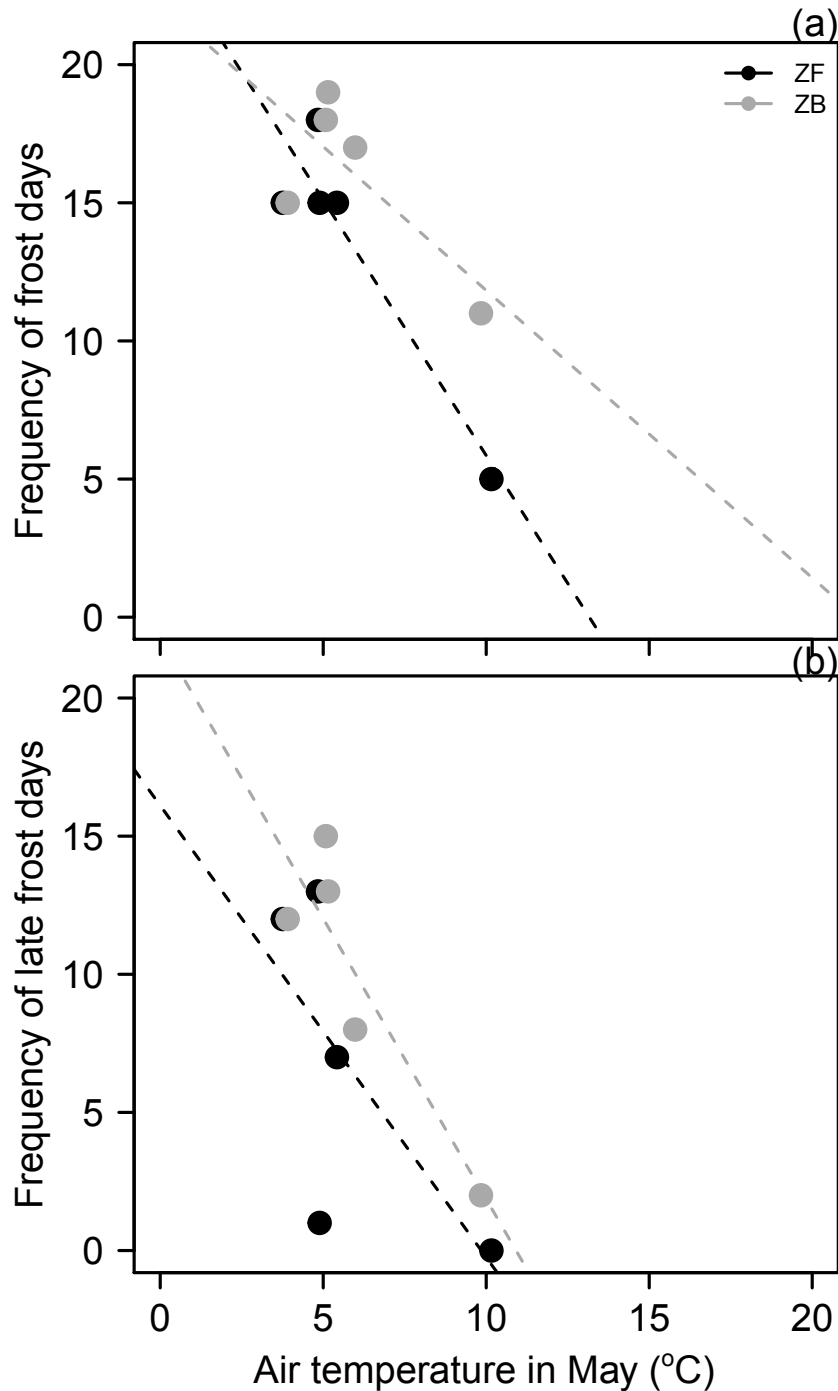


Figure 4.8 The relationships (a) between the frequency of frost days and air temperature in May and (b) between the frequency of late frost days and air temperature in May from 2013-2017 for the ZF and ZB sites. Black colours denote the ZF and the grey colours denote the ZB. Linear regressions for (a), frequency of frost days = $-1.8505 \cdot T_a$ in May + 24.3589, $R^2=0.8652$, $p=0.02191$ for ZF and $-1.0405 \cdot T_a$ in May + 22.2346, $R^2=0.5598$, $p=0.1458$ for ZB. Linear regressions for (b), Frequency of frost days = $1.635 \cdot T_a$ in May + 16.109, $R^2=0.4617$, $p=0.207$ for ZF and $-2.0312 \cdot T_a$ in May + 22.1708, $R^2=0.805$, $p=0.03894$ for ZB.

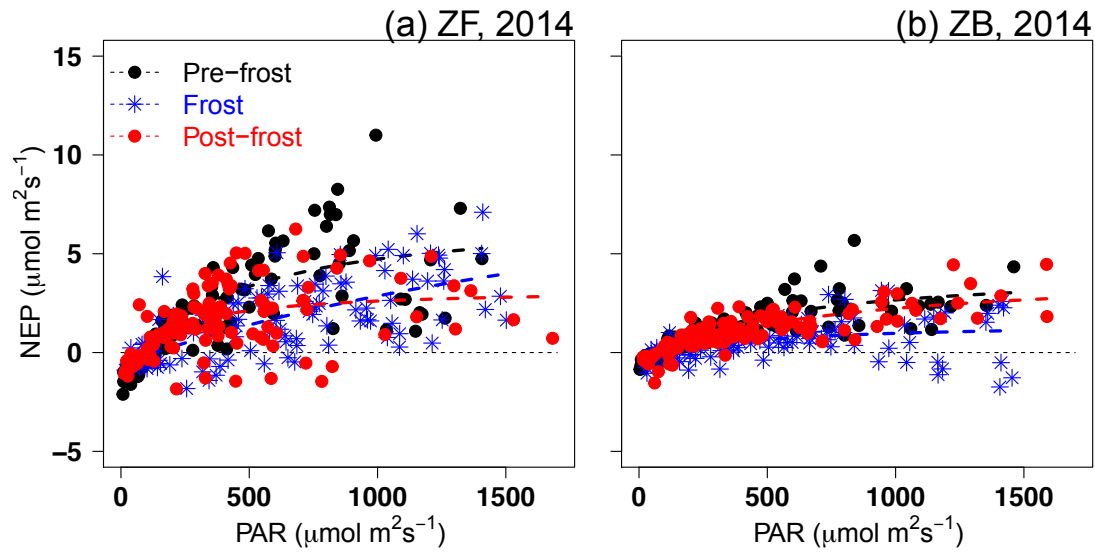


Figure 4.9 Ecosystem light response curves on pre-frost days (black dot and line), frost days (blue dot and line), and post-frost days (red dot and line) for (a) the Zotinio forest (ZF) and Zotino bog (ZB). Half-hourly days in 2014 were chosen after the snowmelt (DOY 134 for ZF and DOY 133 for ZB, respective): DOY 133-136 for the pre-frost days, DOY 137-140 for the frost days, DOY 141-144 for the post-frost days, respectively. Model parameters are listed in Table 4.6.

Table 4.6. Model parameters of the rectangular light response function for pre-frost, and post-frost days for the Zotino forest (ZF) and Zotino bog (ZB). Numbers in parentheses denote the standard errors of the mean parameters. R^2 is coefficient of determination and n is the number of half-hourly data. NEP_{1500} was computed with three parameters as saturating PAR of $1500 \mu\text{mol photon m}^{-2} \text{s}^{-1}$. The standard deviations of NEP_{1500} were computed from the mean of the maximum and minimum of each parameter.

Site	Period	A_{\max} [$\mu\text{mol m}^{-2} \text{s}^{-1}$]	NEP_{1500} [$\mu\text{mol m}^{-2} \text{s}^{-1}$]	α	R_d [$\mu\text{mol m}^{-2} \text{s}^{-1}$]	R^2	n
ZF	Pre-frost	9.02 (0.77)	5.27 (0.85)	0.025 (0.007)	-1.93 (0.44)	0.68	117
	Frost	13.18 (10.74)	3.06 (2.43)	0.005 (0.002)	-0.59 (0.40)	0.45	105
	Post-frost	4.57 (0.87)	2.05 (1.53)	0.027 (0.0235)	-1.43 (1.01)	0.20	118
ZB	Pre-frost	4.98 (0.41)	2.96 (0.39)	0.0111 (0.0023)	-0.78 (0.16)	0.78	108
	Frost	2.15 (0.47)	1.20 (0.66)	0.0067 (0.0072)	-0.65 (0.50)	0.20	83
	Post-frost	4.63 (0.58)	2.62 (0.46)	0.0065 (0.0016)	-0.47 (0.18)	0.66	123

4.4 Discussion

4.4.1 Abiotic variables regulating springtime CO₂ flux

ZF: Although the rankings of variables from the MARS model and the relative importance evaluated by the lmg method were different, the top three abiotic drivers were identical: PAR, Alb, and T_{s04} (Appendix Table S4.1 and Fig. 4.3). In a previous study we found that PAR was the most important driver of CO₂ fluxes (Park *et al.* 2018b). Despite the fact that the study used a different temporal scale (e.g. entire growing season) and different model assumptions, both models identified that PAR was one of the important drivers of CO₂ fluxes. This is strong evidence that PAR is a key driver of spring CO₂ flux in boreal forests.

The second top driver, Alb, is a function of incoming and reflected solar radiation and indicates snowmelt. In spring, snow cover decreases as temperature rises as shown in reverse patterns of Alb and T_a (Fig. 4.5). The contribution of T_a to Alb may not be as strong as Alb itself (Fig. 4.3).

Both the MARS model and “relaimp” metrics in the linear model confirmed that T_{s04} played a more important role than T_a in explaining springtime CO₂ fluxes (Fig. 4.3, Appendix Table S4.2). This may be related to the fact that CO₂ uptake rates remarkably increased after T_{s04} exceeded 1 °C. Mäkelä *et al.* (2004) addressed the importance of the idea that a delayed effect of rising air temperature was a good predictor for spring photosynthesis recovery in Finnish Scots pine forests. The importance of soil temperatures in our study may imply that soil temperature is a more integrative measure of temperature evolution than just T_a in spring.

VPD is a function of T_a, thus the absolute value of VPD became very low when T_a dropped to subfreezing temperatures. In the MARS model variable selection procedure, the model drops one variable if two variables co-vary and are of similar importance. This may be a reason that VPD was not selected as an important driver.

ZB: In contrast to ZF, PAR was not the primary control of CO₂ flux in bog. A relatively low contribution of PAR was possible in northern peatland because *Sphagnum* mosses are well adapted to low-light conditions and low light saturation levels (Moore *et al.* 2006). In previous northern peatland studies, PAR values ranged from 55 to 900 μmol m⁻² s⁻¹ and the light saturation points were between 600 - 900 μmol m⁻² s⁻¹ (Small 1972; Titus and Wagner 1984; Frolking *et al.* 1998). This

supports our finding that PAR makes only a small contribution to explaining springtime CO₂ fluxes at the bog site.

Our study focused on abiotic drivers of spring CO₂ fluxes; however, a recent study found that biotic controls (e.g. vegetation composition and phenology) in boreal peatlands were more important for determining the variability of maximum vegetation productivity (e.g. GPP_{max}) than abiotic drivers (e.g. air temperature, water table depth, radiation) (Peichl *et al.* 2018). Therefore, further investigation of the role of biotic drivers in regulating peatland CO₂ fluxes may be needed to explain the unknown underlying processes of spring vegetation productivity.

4.4.2 Triggers of the start of CO₂ uptake

At ZF, earlier start of snowmelt can be a cause of earlier SCU (Fig. 4.5, Appendix Table S4.3). In addition, T_a triggers the SCU through snowmelt. Our data supports the previous finding that the early start of snowmelt induced by warm air temperature resulted in early SCU and spring net ecosystem productivity (Dye and Tucker, 2003; Pullainen *et al.*, 2017).

T_a was not identified as an important driver for explaining springtime CO₂ flux in bog (Fig. 4.4). However, warm T_a (> 6 °C) may influence the timing of SCU. For instance, SCU in 2013 began after surface peat became unfrozen (SCU_{T_s04(0 °C)}}) at which T_a was approximately 5 °C. SCU in 2016 began before SCU_{T_s04(0 °C)}} at which T_a was approximately 8 °C (Fig. 4.6). Similar features were found in 2014-2015 as well as ZF (data not shown). Therefore, when an intermittent warm spell (T_a > 6 °C) remained for several days in spring, it contributed to an earlier start of CO₂ uptake for both ecosystems.

Coniferous forest was already a net CO₂ sink before the end of snowmelt and while part of the soil surface was still frozen (Fig. 4.5). This supports the previous finding of Thum *et al.* (2009) that the beginning of snowmelt was more strongly correlated with the start of spring photosynthesis than the end of snowmelt in boreal coniferous forests. In a broad context, our result agrees with Parazoo *et al.* (2018), who showed that spring thaw was the crucial trigger for the start of spring photosynthesis and net CO₂ uptake in boreal forests in Arctic ecosystems.

The period when T_{s04} remained near 0 °C had a ‘zero-curtain effect’ (Fig. 5a, b), which is a typical feature in high-northern latitude ecosystems in spring (Outcalt *et al.* 1990; Shibistova *et al.* 2002; Tanja *et al.* 2003; Arneeth *et al.* 2006; Moore *et al.*

2006). While subfreezing soil temperatures can inhibit spring photosynthesis recovery or slow CO₂ uptake rates in boreal forests (Bergh and Linder 1999; Ensminger *et al.* 2008), studies have shown that neither cold nor frozen soils suppress the spring photosynthesis recovery process completely (Ensminger *et al.* 2008). We also found that the start of CO₂ uptake can in fact occur during the zero-curtain period (Fig. 4.5, Appendix Table S4.3). Our finding supports the finding of Ensminger *et al.* (2008) that soil temperature is an important driver of spring CO₂ fluxes but it does not totally hinder the start of CO₂ uptake.

In our study, the start of CO₂ uptake occurred during periods with cold or frozen soil (Fig. 4.5). Consistent with the finding of Suni *et al.* (2003), we found that photosynthesis could begin even when the surface soil temperature was still fluctuating around 0 °C, although it remained at a very low rate until the air temperature remained above 0 °C. This may be evidence that Scots pine growing in high latitudes have adapted to water-limited environments during the long winters. Boreal coniferous trees use stem-stored water during the winter-to-spring transition period regardless of snowmelt termination or available soil water (Sevanto *et al.* 2006; Thum *et al.* 2009). The onset of spring photosynthetic recovery under frozen soil conditions suggests that coniferous trees are able to maintain their metabolism through efficient use of this stored water, rather than taking up water from deeper soil layers during this period.

Both ecosystems were weak in terms of net CO₂ uptake while snow is still melting (Fig. 4.5-4.6). Similar to forest, bog was a weak net CO₂ sink before the snowmelt completed and surface peat temperature remained of 0 °C (Fig. 4.6, Appendix Table S4.3). Such behaviour was also observed in other bogs located in Russia and in Canada (Arneeth *et al.* 2002; Arneeth *et al.* 2006; Moore *et al.* 2006). The start of CO₂ uptake occurred during the last phase of snowmelt, therefore *Sphagnum* mosses can absorb the surface water from the snowmelt to use for plant growth and photosynthesis. Although *Sphagnum* mosses have no roots they can photosynthesize and grow quickly when snow melts and light is available in early spring (Moore *et al.* 2002). This feature was also found in our study that rapid increases in that CO₂ uptake occurred after T_{s04} exceeded 5 °C (Fig. 4.6). The main cause of this feature is likely that peat temperatures between 0.10-0.20 m depth and leaf nitrogen and chlorophyll *a* concentrations contributed to the rapid increases in photosynthesis (Moore *et al.* 2006).

A longer springtime in 2016 may be caused by earlier snowmelt, at least for ZF (Fig. 5, Appendix Table S4.3). At a regional scale, Pulliainen *et al.* (2017) found that about an 8-day earlier start of CO₂ uptake over the last 35 years (1979-2014) was caused by an earlier snowmelt, resulting in increased spring cumulative gross primary productivity by 6.8% (15.5 g C m⁻² per decade) for Eurasian boreal forests. An earlier snowmelt was observed until the latest year in 2017 (personal communication with Jouni Pulliainen). Our study supports Pulliainen *et al.* (2017) in a broad context in that spring net CO₂ uptake in 2016 was greater than in 2017 because of a longer spring day length caused by an earlier SCU in 2016. Similar features are anticipated at ZB. Further long-term observation would improve the reliability of the result.

4.4.3 Variability of spring CO₂ fluxes after the start of CO₂ uptake

Time evolutions of CO₂ fluxes and abiotic drivers for both ecosystems show their dynamical changes during the winter-to-spring transition (Fig. 4.5-4.6). Distinct differences in surface albedo between the two ecosystems (Fig. 4.5a, b, Fig. 4.6a, b) were mentioned by previous studies. Arneth *et al.* (2006) found that albedo at Zotino forests had a small variation from pre- to post-snow melt periods and showed a relatively gradual decline compared to bogs.

At ZF, variability of T_a coincided with CO₂ fluxes during the transition periods (Fig. 4.5a, b, Table 4.4). Similar observations have been found in other boreal coniferous forests located in the Fenno-Scandinavian region and in the past at the Zotino site (Suni 2003; Tanja *et al.* 2003; Thum *et al.* 2009). This suggests that air temperature is a key driver of spring photosynthetic activity. After the start of CO₂ uptake, increases in CO₂ uptake rate and T_a and were also accompanied by rapidly rising PAR (data not shown). This implies that once CO₂ uptake begins, boreal forests respond quickly to rising air temperature to maximize vegetation productivity over the short growing season (Arneth *et al.* 2006).

The magnitude of daily CO₂ uptake was lower than -1 g C m⁻² d⁻¹ until thawing of the surface soil (T_{s04} < 0 °C) or snowmelt was complete (Fig. 4.5). Similar findings were reported by Lloyd *et al.* (2002) and Arneth *et al.* (2006), who also showed that CO₂ uptake of the Scots pine forests at Zotino remained at a low level of ~ -1 g C m⁻² d⁻¹ until the surface soil temperature exceeded 0 °C. A manipulation experiment conducted in boreal spruce forests showed that a continuous photosynthetic increase always occurred after the surface soil temperature exceeded 0

°C (Wallin *et al.* 2013). In line with these findings, we found that net CO₂ uptake increased to over -2 g C m⁻² d⁻¹ after T_{s04} exceeded 0 °C at our sites (Fig. 4.5c, d).

4.4 Variability of spring cumulative net ecosystem exchange of CO₂

The overall pattern and magnitude of spring NEE_{cum} in this study (Fig. 4.7) show a reasonable range compared with past measurements. Specifically, during DOY 100-150 1999-2001, spring NEE_{cum} at the Zotino forest was approximately -25 g C m⁻², whereas it was approximately -10 g C m⁻² at the Zotino bog (Dolman *et al.* 2012). We found -22.5 g C m⁻² for ZF and -9.8 g C m⁻² for ZB in our study.

Surface albedo representing snow cover was the strongest explanatory variable of the variability in forest CO₂ flux, whereas T_{s04} was the strongest explanatory variable in the bog CO₂ flux variability (Fig. 4.3, Fig.4.4). For both sites, T_a increased rapidly after the end of snowmelt, accompanied by NEE_d (Fig. 4.6). The beginning of snowmelt was the most likely factor to explain NEE_{cum} based on the time series of CO₂ flux during the transitional period (Fig. 4.5, 4.6). Therefore, changes in abiotic drivers likely regulate the variability in spring NEE_{cum} (Fig. 4.7). For example, Bartch *et al.* (2007) found that freeze-thaw cycles (detected via remote sensing data) were strongly correlated with the beginning of the growing season in Zotino forests.

4.4.4 Effect of spring frost on the photosynthesis-related processes

Warm spring temperatures reduced the overall frequency of frost days as well as the frequency of late frost days (Fig. 4.8). However, frost may not influence the start of CO₂ uptake at our site. Although frost days were more frequent in April than in May, there was no statistically significant relationship between the frequency of frost days and the onset of CO₂ uptake. For instance, the start of CO₂ uptake at ZF was the earliest in 2016, yet the frequency of frost days in April was not particularly lower than other years (Appendix Table S4.4).

We confirmed that warm spells influence the start of CO₂ uptake for both ecosystems (Fig. 4.5, Fig. 4.6). Highly fluctuating CO₂ fluxes during the spring frost may broadly align with previous findings that the start of CO₂ uptake was postponed by spring frost (Ensminger *et al.* 2004; Wallin *et al.* 2013). Nevertheless, our data clearly showed that spring frost reverses the magnitude of CO₂ uptake in boreal forests (Ensminger *et al.* 2004, 2008; Wallin *et al.* 2013).

We found that both ecosystems reduced NEP_{1500} on frost-days (Fig. 4.9). However, NEP_{1500} for ZF showed different behaviours than A_{max} . CO_2 fluxes at ZF are generally more highly variable than at ZB, probably containing a large uncertainty in A_{max} . NEP_{1500} is a saturated NEP at which PAR reaches at $1500 \mu\text{mol m}^{-2}\text{s}^{-1}$ where this value is realistic PAR in Zotino site, NEP_{1500} gives more realistic estimates than A_{max} .

Effects of frost on net ecosystem productivity were discernable for both ecosystems (Fig. 4.9, Table 4.8). Based on previous studies, the effect of spring frost on photosynthesis recovery seems relatively better understood in forest than in bog. For example, a seedling experiment study showed that spring photosynthetic recovery processes in coniferous forests were halted and postponed due to frost (Ensminger *et al.* 2004). Another controlled experiment showed that spring frost slowed the photosynthetic recovery process down by up to 60 days in boreal coniferous forests (Wallin *et al.* 2013). The relationship between temperature and photosynthetic uptake in boreal and alpine forests could be complex because frost can reverse spring photosynthetic recovery (Tanja *et al.* 2003; Monson *et al.* 2005).

In peatlands, the environmental conditions in the previous year and adaptation of microbial activities may play important roles in explaining the effects of frost on carbon uptake processes due to the complexity of soil microorganisms in response to frost (Sorensen *et al.* 2018). Another study suggests that the frequency and severity of soil frost may affect vegetation, phenology, and microbial structure in boreal peatlands (Küttim *et al.* 2017). They addressed that the status of soil frost changed the microbial activities and resulted in reduction of the *Sphagnum* photosynthesis and ecosystem respiration, although the long-term effects on growing season vegetation production remain uncertain.

4.5 Conclusion

Our observation confirmed that the differences in spring CO₂ fluxes between a boreal coniferous forest and a bog were distinct. The beginning of snowmelt and surface peat thaw triggered by increasing air temperature regulate springtime CO₂ flux in boreal ecosystems. We found that both ecosystems started net CO₂ uptake as snow was melted. In addition, although snowmelt is incomplete intermittent warm spells can lead to an earlier start of CO₂ uptake. Especially in the coniferous forest, this intermittent warm may stimulate the beginning of snowmelt. Continuous increases in CO₂ uptake rates occurred when snowmelt completely melted or surface soil temperatures unfrozen. Late frost influenced the maximum photosynthetic capacity for both ecosystems, but they recovered to similar levels after frost.

The very warm spring in 2015 likely resulted in the highest vegetation productivity, at least for forest. In addition, both ecosystems may not always start early net CO₂ uptake during the very warm spring. The effect of spring frost on the start of CO₂ uptake remains unclear. Probably previous winter climate conditions may also influence the net ecosystem productivity in the following year. We anticipate that further analysis including entire annual CO₂ fluxes with both abiotic and biotic drivers will improve our understanding of the effect of spring environmental changes on the seasonal to annual CO₂ uptake in boreal ecosystems.

4.6 Supplementary material

Table S 4.1 The ranking of variable importance of CO₂ flux estimated by the MARS model during spring (9 April-15 June) from 2013-2017 at the Zotino forest (ZF) site. Daily mean values of the nine variables were used as an initial data: T_a, T_{s04}, T_{s08}, T_{s16}, T_{s32}, T_{s64}, Alb, PAR, and vapour pressure deficit (VPD). Proportion of variance in daily CO₂ fluxes explained by model (R^2) was 84%.

Variables	nsubsets	GCV	RSS
T _{s4}	11	100.0	100.0
PAR	19	59.0	60.5
Alb	9	44.8	46.9
T _a	7	30.9	33.5
T _{s16}	6	25.8	28.4
T _{s64}	5	17.2	21.0

Table S 4.2 Same as Table S4.1 but for ZB. Data is used from 2013-2016. Proportion of variance in daily CO₂ fluxes explained by model (R^2) was 89%.

Variables	nsubsets	GCV	RSS
T _{s4}	12	100.0	100.0
Alb	11	46.1	48.7
T _{s64}	9	29.5	33.0
PAR	9	29.5	33.0
T _{s32}	8	26.3	29.7

Table S 4.3 The metrics for the start of CO₂ uptake using 5-day mean air temperature threshold (SCU_{T5(5°C)}), the start of surface soil or peat warming (SCU_{Ts4(0°C)}), the beginning of snowmelt (SCU_{Bsnow}), the final day of snowmelt (SCU_{Fsnow}), and the start of CO₂ uptake (SCU) at forest (ZF) and bog (ZB) during 2013-2017. Bold values indicate the maximum, whereas bold and italic values indicate the minimum.

Year	SCU _{T5(5°C)}		SCU _{Ts4(0°C)}		SCU _{Bsnow}		SCU _{Fsnow}		SCU	
	ZF	ZB	ZF	ZB	ZF	ZB	ZF	ZB	ZF	ZB
2013	142	142	132	126	123	117	130	126	122	132
2014	124	124	<i>129</i>	<i>125</i>	121	<i>110</i>	<i>128</i>	<i>125</i>	121	<i>120</i>
2015	128	128	134	132	126	124	134	133	125	127
2016	<i>115</i>	<i>116</i>	140	126	<i>114</i>	112	<i>139</i>	127	<i>114</i>	<i>120</i>
2017	132	132	134	134	132	115	134	135	130	-
mean	128	119	132	129	123	115	133	129	122	125

Table S 4.4 The frequency of frosts ($T_{\min} < 0 \text{ }^{\circ}\text{C}$) and late frosts (after snowmelt) in April and May and spring (April and May) for the ZF and ZB flux sites from 2013-2017. Bold values indicate the maximum in spring, whereas bold and italic values indicate the minimum in spring. DOY in parentheses is the last day of frost. DOY in bracket indicates the end of frost days.

		Frequency of frosts days		Frequency of late frosts days	
Year	Month	ZF	ZB	ZF	ZB
2013	April	20	23		
	May	15 (149)	15 (149)	12	12
	Spring	35	38		
2014	April	19	23		
	May	18 (148)	18 (148)	13	15
	Spring	37	41		
2015	April	21	27		
	May	5 (126)	11 (147)	0	2
	Spring	26	38		
2016	April	19	23		
	May	15 (145)	19 (151)	1	13
	Spring	34	42		
2017	April	24	24		
	May	15 (147)	17 (147)	7	8
	Spring	39	41		
Mean	April	21	24		
	May	14	16	7	10
	Spring	35	40		

4.7 References

- Alekseychik, P., Mammarella, I., Karpov, D., Dengel, S., Terentieva, I., Sabrekov, A., Glagolev, M., Lapshina, E., 2017. Net ecosystem exchange and energy fluxes in a West Siberian bog. *Atmos. Chem. Phys. Discuss.* 1–20. doi:10.5194/acp-2017-43
- Arnth, a, Arneth, a, Lloyd, J., Lloyd, J., Bird, M., Bird, M., Grigoryev, S., Grigoryev, S., Kalaschnikov, N., Kalaschnikov, N., Gleixner, G., Gleixner, G., Schulze, D., Schulze, D., 2002. Response of central Siberian Scots pine to soil water deficit and long-term trends in atmospheric CO₂ concentration 16.
- Arnth, A., Kurbatova, J., Kolle, O., Shibistova, O.B., Lloyd, J., Vygodskaya, N.N., Schulze, E.-D., 2002. Comparative ecosystem-atmosphere exchange of energy and mass in a European Russian and a central Siberian bog II. Interseasonal and interannual variability of CO₂ fluxes. *Tellus B* 54, 514–530. doi:10.1034/j.1600-0889.2002.01349.x
- Arnth, A., Lloyd, J., Shibistova, O., Sogachev, A., Kolle, O., 2006. Spring in the boreal environment : observations on pre- and post-melt energy and CO₂ fluxes in two central Siberian ecosystems. *Boreal Environ. Res.* 11, 311–328.
- Baldocchi, D., Chu, H., Reichstein, M., 2018. Inter-annual variability of net and gross ecosystem carbon fluxes: A review. *Agric. For. Meteorol.* 249, 520–533. doi:10.1016/j.agrformet.2017.05.015
- Bartsch, A., Kidd, R.A., Wagner, W., Bartalis, Z., 2007. Temporal and spatial variability of the beginning and end of daily spring freeze/thaw cycles derived from scatterometer data. *Remote Sens. Environ.* 106, 360–374. doi:10.1016/j.rse.2006.09.004
- Bubier, J.L., Crill, P.M., Moore, T.R., Savage, K., Varner, R.K., 1998. Seasonal patterns and controls on net ecosystem CO₂ exchange in a boreal peatland complex. *Global Biogeochem. Cycles* 12, 703–714. doi:10.1029/98GB02426
- Dolman, A.J., Shvidenko, A., Schepaschenko, D., Ciais, P., Tchebakova, N., Chen, T., Van Der Molen, M.K., Belelli Marchesini, L., Maximov, T.C., Maksyutov, S., Schulze, E.D., 2012. An estimate of the terrestrial carbon budget of Russia using inventory-based, eddy covariance and inversion methods. *Biogeosciences* 9, 5323–5340. doi:10.5194/bg-9-5323-2012
- Dye, D.G., Tucker, C.J., 2003. Seasonality and trends of snow-cover, vegetation

- index, and temperature in northern Eurasia. *Geophys. Res. Lett.* 30, 3–6.
doi:10.1029/2002GL016384
- Ensminger, I., Schmidt, L., Lloyd, J., 2008. Soil temperature and intermittent frost modulate the rate of recovery of photosynthesis in Scots pine under simulated spring conditions. *New Phytol.* 177, 428–442. doi:10.1111/j.1469-8137.2007.02273.x
- Ensminger, I., Sveshnikov, D., Campbell, D.A., Funk, C., Jansson, S., Lloyd, J., Shibistova, O., Öquist, G., 2004. Intermittent low temperatures constrain spring recovery of photosynthesis in boreal Scots pine forests. *Glob. Chang. Biol.* 10, 995–1008. doi:10.1111/j.1365-2486.2004.00781.x
- Gorham, E., 1991. Northern Peatlands: Role in the Carbon Cycle and Probable Responses to Climatic Warming. *Ecol. Appl.* 1, 182–195. doi:10.2307/1941811
- Korrensalo, A., Alekseychik, P., Hájek, T., Rinne, J., Vesala, T., Mehtätalo, L., Mammarella, I., Tuittila, E.S., 2017. Species-specific temporal variation in photosynthesis as a moderator of peatland carbon sequestration. *Biogeosciences* 14, 257–269. doi:10.5194/bg-14-257-2017
- Korrensalo, A., Hájek, T., Vesala, T., Mehtätalo, L., Tuittila, E.-S., 2016. Variation in photosynthetic properties among bog plants. *Botany* 94, 1127–1139. doi:10.1139/cjb-2016-0117
- Lafleur, P.M., Roulet, N.T., Bubier, J.L., Frolking, S., Moore, T.R., 2003. Interannual variability in the peatland-atmosphere carbon dioxide exchange at an ombrotrophic bog. *Global Biogeochem. Cycles* 17, n/a-n/a. doi:10.1029/2002GB001983
- Lindroth, A., Grelle, A., More, A., 1998. Long-term measurements of boreal forest carbon balance. *Glob. Chang. Biol.* 4, 443–450. doi:10.1046/j.1365-2486.1998.00165.x
- Liu, Q., Piao, S., Janssens, I.A., Fu, Y., Peng, S., Lian, X., Ciais, P., Myneni, R.B., Peñuelas, J., Wang, T., 2018. Extension of the growing season increases vegetation exposure to frost. *Nat. Commun.* 9. doi:10.1038/s41467-017-02690-y
- Lloyd, J., Shibistova, O., Zolotoukhine, D., Kolle, O., Arneth, A., Wirth, C., Styles, J.M., Tchebakova, N.M., Schulze, E.-D., 2002a. Seasonal and annual variations in the photosynthetic productivity and carbon balance of a central Siberian pine forest. *Tellus B* 54, 590–610. doi:10.1034/j.1600-0889.2002.01487.x
- Lloyd, J., Shibistova, O., Zolotoukhine, D., Kolle, O., Arneth, A., Wirth, C., Styles,

- J.M., Tchebakova, N.M., Schulze, E.D., 2002b. Seasonal and annual variations in the photosynthetic productivity and carbon balance of a central Siberian pine forest. *Tellus, Ser. B Chem. Phys. Meteorol.* 54, 590–610. doi:10.1034/j.1600-0889.2002.01487.x
- Lund, M., Lafleur, P.M., Roulet, N.T., Lindroth, A., Christensen, T.R., Aurela, M., Chojnicki, B.H., Flanagan, L.B., Humphreys, E.R., Laurila, T., Oechel, W.C., Olejnik, J., Rinne, J., Schubert, P., Nilsson, M.B., 2010. Variability in exchange of CO₂ across 12 northern peatland and tundra sites. *Glob. Chang. Biol.* 16, 2436–2448. doi:10.1111/j.1365-2486.2009.02104.x
- Mammarella, I., Peltola, O., Nordbo, A., Järvi, L., Rannik, Ü., 2016. Quantifying the uncertainty of eddy covariance fluxes due to the use of different software packages and combinations of processing steps in two contrasting ecosystems. *Atmos. Meas. Tech.* 9, 4915–4933. doi:10.5194/amt-9-4915-2016
- Moore, T.R., Lafleur, P.M., Poon, D.M.I., Heumann, B.W., Seaquist, J.W., Roulet, N.T., 2006. Spring photosynthesis in a cool temperate bog. *Glob. Chang. Biol.* 12, 2323–2335. doi:10.1111/j.1365-2486.2006.01247.x
- Myneni, R.B., Keeling, C.D., Tucker, C.J., Asrar, G., Nemani, R.R., 1997. Increased plant growth in the northern high latitudes.pdf.
- Ögren, E., 2001. Effects of climatic warming on cold hardiness of some northern woody plants assessed from simulation experiments. *Physiol. Plant.* 112, 71–77. doi:10.1034/j.1399-3054.2001.1120110.x
- Ottander, C., Campbell, D., Oquist, G., 1995. Seasonal changes in photosystem-II organization and pigment composition in *Pinus sylvestris*. *Planta* 197, 176–183.
- Parazoo, N.C., Arneth, A., Pugh, T.A.M., Smith, B., Steiner, N., Luus, K., Commane, R., Benmergui, J., Stofferahn, E., Liu, J., Rödenbeck, C., Kawa, R., Euskirchen, E., Zona, D., Arndt, K., Oechel, W., Miller, C., 2018. Spring photosynthetic onset and net CO₂ uptake in Alaska triggered by landscape thawing. *Glob. Chang. Biol.* 24, 3416–3435. doi:10.1111/gcb.14283
- Park, S., Hamm, S.Y., Jeon, H.T., Kim, J., 2017. Evaluation of logistic regression and multivariate adaptive regression spline models for groundwater potential mapping using R and GIS. *Sustain.* 9. doi:10.3390/su9071157
- Park, T., Ganguly, S., Tømmervik, H., Euskirchen, E.S., Høgda, K., Karlsen, S.R., Brovkin, V., Nemani, R.R., Myneni, R.B., 2016. Changes in growing season duration and productivity of northern vegetation inferred from long-term remote

- sensing data. *Environ. Res. Lett.* 11, 1–11. doi:10.1088/1748-9326/11/8/084001
- Pelletier, L., Strachan, I.B., Roulet, N.T., Garneau, M., 2015. Can boreal peatlands with pools be net sinks for CO₂? *Environ. Res. Lett.* 10, 035002. doi:10.1088/1748-9326/10/3/035002
- Piao, S., Friedlingstein, P., Ciais, P., Viovy, N., Demarty, J., 2007. Growing season extension and its impact on terrestrial carbon cycle in the Northern Hemisphere over the past 2 decades. *Global Biogeochem. Cycles* 21, 1–11. doi:10.1029/2006GB002888
- Piao, S., Tan, J., Chen, A., Fu, Y.H., Ciais, P., Liu, Q., Janssens, I.A., Vicca, S., Zeng, Z., Jeong, S.J., Li, Y., Myneni, R.B., Peng, S., Shen, M., Peñuelas, J., 2015. Leaf onset in the northern hemisphere triggered by daytime temperature. *Nat. Commun.* 6. doi:10.1038/ncomms7911
- Post, E., Steinman, B.A., Mann, M.E., 2018. Acceleration of phenological advance and warming with latitude over the past century. *Sci. Rep.* 8, 1–8. doi:10.1038/s41598-018-22258-0
- Pulliainen, J., Aurela, M., Laurila, T., Aalto, T., Takala, M., Salminen, M., Kulmala, M., Barr, A., Heimann, M., Lindroth, A., Laaksonen, A., Derksen, C., Mäkelä, A., Markkanen, T., Lemmetyinen, J., Susiluoto, J., Dengel, S., Mammarella, I., Tuovinen, J.-P., Vesala, T., 2017. Early snowmelt significantly enhances boreal springtime carbon uptake. *Proc. Natl. Acad. Sci.* 114, 201707889. doi:10.1073/pnas.1707889114
- Schulze, E.D., Lapshina, E., Filippov, I., Kuhlmann, I., Mollicone, D., 2015. Carbon dynamics in boreal peatlands of the Yenisey region, western Siberia. *Biogeosciences* 12, 7057–7070. doi:10.5194/bg-12-7057-2015
- Schulze, E.D., Prokuschkin, A., Arneth, A., Knorre, N., Vaganov, E.A., 2002. Net ecosystem productivity and peat accumulation in a Siberian Aapa mire. *Tellus, Ser. B Chem. Phys. Meteorol.* 54, 531–536. doi:10.1034/j.1600-0889.2002.01386.x
- Smith, L.C., 2004. Siberian Peatlands a Net Carbon Sink and Global Methane Source Since the Early Holocene. *Science (80-.)*. 303, 353–356. doi:10.1126/science.1090553
- Smith, N. V., Saatchi, S.S., Randerson, J.T., 2004. Trends in high northern latitude soil freeze and thaw cycles from 1988 to 2002. *J. Geophys. Res. D Atmos.* 109, 1–14. doi:10.1029/2003JD004472

- Suni, T., 2003. Interannual variability and timing of growing-season CO₂ exchange in a boreal forest. *J. Geophys. Res.* 108, 4265. doi:10.1029/2002JD002381
- Suni, T., Berninger, F., Vesala, T., Markkanen, T., Hari, P., Mäkelä, A., Ilvesniemi, H., Hänninen, H., Nikinmaa, E., Huttula, T., 2003. Air temperature triggers the recovery of evergreen boreal forest photosynthesis in spring. *Glob. Chang. Biol.* 9, 1410–1426.
- Stoop, M. 2010. Recovery of forest mosses after snowmelt (Master thesis). Retrieved from <http://files.webb.uu.se/uploader/858/1515-Stoop-Mark-uppsats.pdf>
- Thum, T., Aalto, T., Aurela, T.L., Hatakka, J., Lindroth, A., Vesala, T., 2009. Spring initiation and autumn cessation of boreal coniferous forest CO₂ exchange assessed by meteorological and biological variables. *Tellus, Ser. B Chem. Phys. Meteorol.* 61, 701–717. doi:10.1111/j.1600-0889.2009.00441.x
- Wallin, G., Hall, M., Slaney, M., Råntfors, M., Medhurst, J., Linder, S., 2013. Spring photosynthetic recovery of boreal Norway spruce under conditions of elevated [CO₂] and air temperature. *Tree Physiol.* 33, 1177–1191. doi:10.1093/treephys/tpt066
- Wutzler, T., Lucas-Moffat, A., Migliavacca, M., Knauer, J., Sickel, K., Šigut, L., Menzer, O., and Reichstein, M.: Basic and extensible post-processing of eddy covariance flux data with REddyProc, *Biogeosciences*, 15, 5015-5030, <https://doi.org/10.5194/bg-15-5015-2018>, 2018.

Chapter 5 Reliability of regional CO₂ flux estimates from tall tower profile measurements

5.1. Introduction

Sunrise and sunset generate diurnal cycles of temperature and humidity in the lower troposphere of the atmospheric boundary layer (ABL). Particularly, the lowest 10% of the ABL is a turbulent layer at the ground surface that can extend 200 m to 4 km above the ground surface. This layer is also called the surface boundary layer (SBL) or surface layer (SL) (Stull, 1988). Carbon, water, energy, and momentum exchanges occur between the atmosphere and these land surface layers.

These fluxes can be directly measured by the eddy covariance (EC) method, a widely used micrometeorological approach. The typical spatial scale for flux measurements represent a few square kilometres where measurement height is less than 60 m (Baldocchi et al., 2001; Rannik et al. 2012), while flux measurements by the EC method at taller towers can quantify larger scale source-sink and flux distributions (Davis et al., 2003; Desai et al., 2015; Haszpra et al., 2005). The typical spatial scale for these flux estimates is representative for an order of 100 km x 100 km.

However, if a measurement station is established for monitoring atmospheric GHG concentrations, fast-response sensors for flux measurements (e.g. infrared gas analysers and ultrasonic anemometers) are not always necessary. In such cases, alternative micrometeorological methods to estimate turbulent flux of trace gases can be used. For instance, the modified Bowen Ratio method (MBR) can estimate turbulent flux or eddy flux using gradients of concentration and temperature measurements based on the similarity theory (Businger, 1986). The MBR was used to estimate ecosystem CO₂ fluxes (net ecosystem exchange or NEE) using profile temperature and mixing ratios measurements at regional scale (Winderlich et al., 2014).

This research is an extension of the study of Winderlich et al. (2014) with the most available recent measurements at the Zotino Tall Tower Observatory (ZOTTO). The purpose of this study is to obtain regional CO₂ flux estimates during the growing

season (June-September) from years 2012-2015. The main focus of this study is to evaluate the performance of tall-tower based CO₂ fluxes by utilizing EC flux measurements. Throughout this paper, we refer to this tall-tower based CO₂ flux estimate as “regional NEE”.

5.2 Material and methods

5.2.1 Measurements system

The ZOTTO was established to monitor long-term biogeochemical cycles in central Siberia over the last 10 years (Heimann et al., 2014). The station is located in a relatively horizontally homogeneous landscape near the western Yenisei River. The tall tower measurement system consists of two parts: a GHG measurement system (i.e., CO₂, CH₄, and CO) and a meteorological measurement system (Chi et al., 2013; Winderlich et al., 2010). The GHG measurement system consists of quasi-continuous high accuracy atmospheric CO₂ and CH₄ mixing ratio measurements at six heights (302 m, 227 m, 157 m, 92 m, 52 m, and 4 m above the ground surface) using a EnviroSense 3000i analyser (CFDS-17, Picarro Inc., Santa Clara, USA). The measurement sensor is based on the cavity-ring down spectroscopy (CRDS) technique widely used by GHG observatories which provides fast, highly precise, and accurate measurements of mixing ratios of atmospheric gases (Rella et al., 2013). The meteorological measurement system includes instruments for measuring wind speed, air temperature, relative humidity, and atmospheric pressure at a height 1 m higher than the inlets of the GHG measurement system (Table 5.1). Atmospheric pressure transmitters were installed at three heights (4 m, 92 m, and 301 m), thus observations at 52 m and 158 m were interpolated between 4 m and 92 m & 92 and 301 m heights, respectively. Detailed descriptions of the data logging system and calibration procedure are described in Winderlich et al. (2010). The CO₂ fluxes measured from the two EC flux towers were used to calculate the up-scaled CO₂ flux (described in Ch. 3.3 and Ch. 4.2).

Table 5.1 Set up for meteorological measurements at the Zotino tall tower.

Variable	Instrument type (manufacture)	Measurement heights (m)
Wind velocities (u, v, and w) and wind direction	R3 (Gill Instruments Ltd., Lymington, UK)	5, 52, 93, 159, 228, 302 m
Air temperature and relative humidity	KPK 1/6-ME-H38 (MELA Sensortechnik GmbH, Bondorf, Germany)	5, 52, 93, 159, 228, 302 m
Atmospheric pressure	61302 V (R.M. Young company, Traverse city, USA)	5, 93, 302 m

5.2.2 Data processing

All the summertime data (June to September) from 2012-2015 were averaged to a half-hourly time scale. The data processing scheme, including water correction of CO₂ mixing ratio (to derive a dry air mole fraction from wet air measurements) was adopted from Winderlich et al. (2010).

Ambient air temperature (T_a) is a critical parameter for calculating both storage and eddy fluxes as shown in Eq. (5.2) and Eq. (5.3). However, at the ZOTTO site the air temperature and humidity sensor at located at 228 m frequently malfunctioned during the summertime: thus long-term gaps were inevitable. Therefore, the gradient of potential temperature between 302 m and 228 m could not be calculated. To overcome the loss of T_a data, sonic anemometer temperature (T_s) was used as a surrogate of T_a . The measurement frequency of T_s is higher and the accuracy lower than that of T_a , and the absolute measurement values are instrument dependent. However, the gradient of two temperatures is more important than the absolute temperature to calculate fluxes in the MBR method. Therefore, T_s measurements are potentially still potentially useful for computing flux terms. Prior to using T_s directly, T_s at heights of 301 m and 227 m were corrected using T_a measured at the same heights when T_s was available. Correction factors were obtained using

linear relationship between the two temperature observations measured in August 2012 (slope= 0.87, intercept = -0.21 for 301 m and slope= 0.97, intercept = +0.04 for 227 m, respectively, and $R^2 > 0.95$ for both). Overall patterns and variability of T_a and corrected T_s were in agreement. Therefore, the same correction factors were applied to the entire study period.

Analysis of potential temperature (T_{pot}) is useful to assess atmospheric stability within the part of the ABL observed by the tall tower. T_{pot} is the temperature of an air parcel that is lifted adiabatically to the pressure p_0 of 1013 hPa at sea level:

$$T_{pot} = T \cdot \left(\frac{p_0}{p}\right)^{\frac{R_d}{c_p}} \quad \text{Eq. (5.1)}$$

where T [K] is the temperature at pressure p [hPa], R_d is the specific gas constant of dry air ($R_d = R/M_d$) as $287.058 \text{ J kg}^{-1}\text{K}^{-1}$. We used an $\frac{R_d}{c_p}$ value of 0.286 for dry air.

The gradient of T_{pot} is larger than 0 under stable conditions, whereas lower T_{pot} with height indicates unstable conditions. Vertical wind velocity, direction, and potential temperature provide a measure of the atmospheric stability. A change in potential temperature with height is typically accompanied by a change in wind speed and wind direction. Thus, T_{pot} is a measure of both the atmospheric stability condition and of the vertical distribution of emissions from the surface.

Note that the procedures for post-processing and quality control of EC CO_2 fluxes are described in Chapter 3.2 and Chapter 4.2.

5.2.3 Flux calculation

The net ecosystem exchange of CO_2 (NEE) is the sum of storage flux (F_{stor}), eddy flux (F_{Eddy}), and advection (F_{Adv}) terms.

$$NEE = F_{stor} + F_{Eddy} + F_{Adv} \quad \text{Eq. (5.1)}$$

The storage term (F_{stor}) is the amount of carbon accumulated over time below the highest measurement height. It is calculated by the change in half-hourly concentration measurements and air density for every time step, following Eq. (5.2). To derive contributions to F_{stor} below the lowermost measurement height (4 m), it is assumed that the CO_2 concentration below this height is constant (Fig. 5.1). In cases where T_a data were missing for more than one levels, F_{str} could be not calculated.

However, when T_a was missing for a single level between the two neighbouring heights, it was interpolated from temperatures measured at neighbouring levels.

$$\begin{aligned}
F_{stor}(t_i, z_h) &= \int_{z_{h+1}}^{z_h} \frac{1}{V_m} \cdot \frac{\partial \bar{c}(t_i)}{\partial t} dz \\
&= \int_{z_{h+1}}^{z_h} \frac{\rho_{Air}(z)}{M_{Air}} \cdot \frac{\partial \bar{c}(t_i)}{\partial t} dz \\
&\cong \sum_{h=1}^5 \frac{\frac{1}{2}(\rho_h + \rho_{h+1})}{28.9644 \text{ gmol}^{-1}} \cdot \frac{\frac{1}{2}((c_h(t_{i+1}) - c_h(t_i)) + (c_{h+1}(t_{i+1}) - c_{h+1}(t_i)))}{t_{i+1} - t_i}} \cdot (z_h - z_{h+1})
\end{aligned}$$

Eq. (5.2)

To estimate F_{Eddy} , we can use the MBR method. This method requires the gradients of concentration and temperature between two adjacent tower heights at five intermediate levels (28, 72, 125, 193 and 264 m) following the equation:

$$F_{Eddy} = \frac{H}{c_p M_{air}} \frac{\partial c / \partial z}{\partial T_{pot} / \partial z} \quad \text{Eq. (5.3)}$$

where H is the measured sensible heat flux (W m^{-2}), C_p is the specific heat of air ($1.006 \text{ kJ kg K}^{-1}$), M_{air} is the molecular weight of air mass of dry air, $\partial c / \partial z$ is the gradient of the CO_2 mixing ratio, and $\frac{dT_{pot}}{dz}$ is the vertical potential temperature gradient (K). ρ_{air} (kg m^{-3}) is the air density of dry air as a function of pressure and temperature, and K_T is the eddy diffusivity ($\text{m}^2 \text{ s}^{-1}$) as a parameter for defining an effective diffusion coefficient of turbulence. In this study, advection term (F_{Adv}) is ignored. Details in theoretical background and procedure for calculating NEE terms are described in Winderlich et al. (2014).

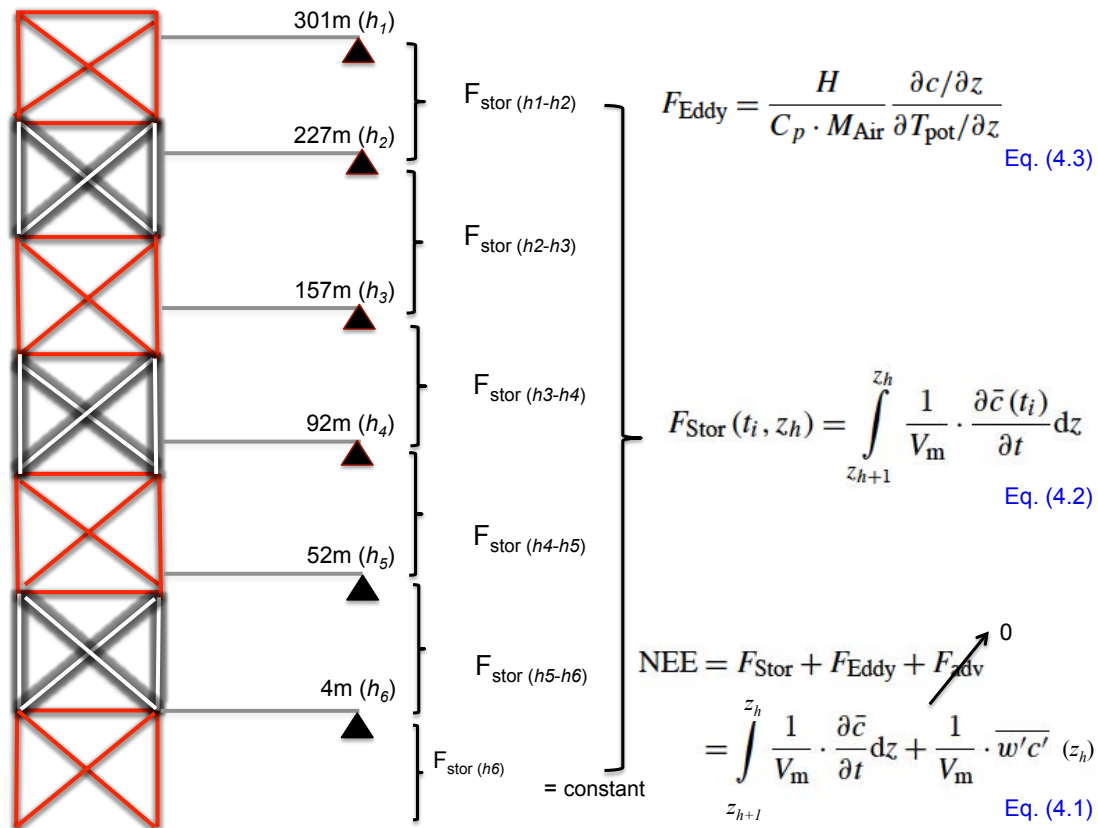


Figure 5.1 Diagram of flux calculations using profile measurements. The six measurement heights are shown in Table 5.1. Regional net ecosystem exchange (NEE) of CO₂ is the sum of storage flux (F_{stor}), turbulent flux (F_{Eddy}), and advection flux (F_{Adv}) terms. Note that F_{Adv} term is ignored in this study.

5.3. Results and discussion

5.3.1 The PBL structure from the tall tower profile data

The diurnal cycle of CO₂ concentration show four distinct stages of the atmospheric boundary layer structure (Fig. 5.2). The potential temperatures mirror the vertical patterns of CO₂ concentrations (Fig. 5.4). The four development stages of the ABL were classified by Reid and Steyn (1997):

(1) *Stage 1*: The CO₂ concentrations showed a distinct early morning peak between 05:00 and 07:00 LST due to the night-time inversion and the existence of a stable boundary layer. In this stage, weak wind velocities allowed for the development of a shallow mixed layer. The data showed higher variability closer to the ground surface: CO₂ concentration at a height of 4 m varied in the range of 385 - 415 ppm with a high

amplitude, whereas the observation at the top (301 m) varied only from 390 - 395 ppm with a low amplitude.

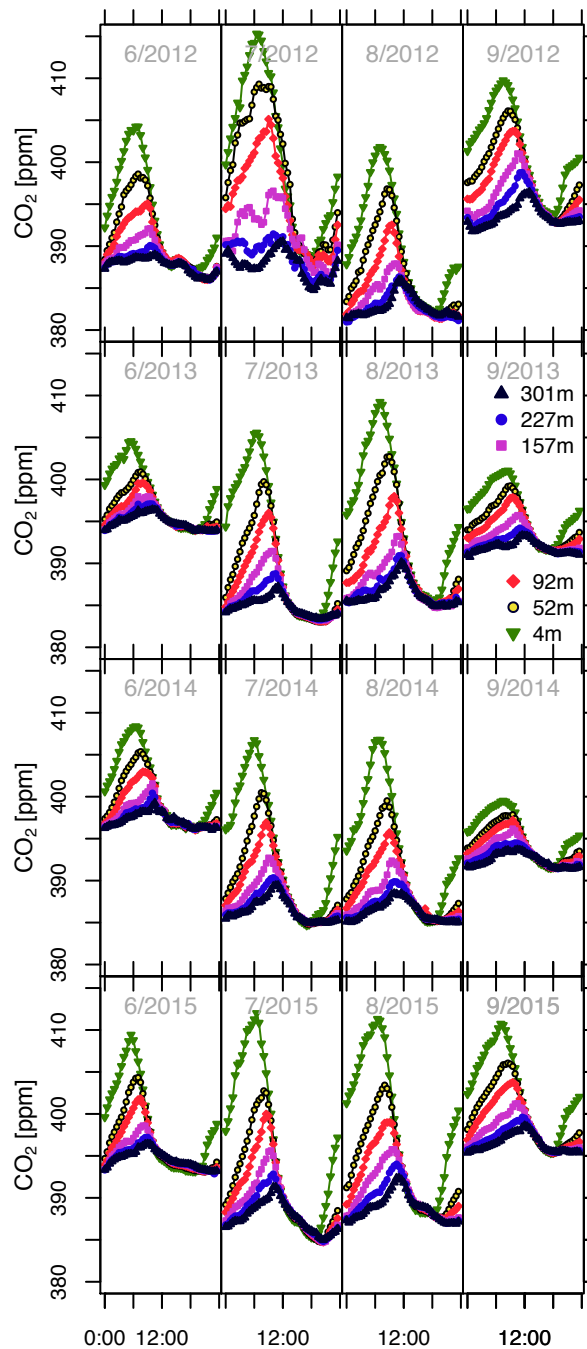


Figure 5.2 Diurnal cycle of half-hourly averaged CO₂ concentrations [ppm] measured at six levels (301 m, 227 m, 157 m, 92 m, 52 m, and 4 m) for individual months and years (2012-2015).

(2) *Stage 2*: The high CO₂ concentration peak in the shallow mixed layer decreased after sunrise as incoming solar radiation and wind speed increase. Overall, the

features showed the drawdown of CO₂ concentrations from morning peak to afternoon minima. This suggests that vertical mixing enhanced the decrease in CO₂ concentrations.

(3) *Stage 3*: During daytime, a strong turbulent mixing resulted in the afternoon minima of CO₂ concentrations, potential temperature, and humidity. Therefore, daytime measurements were observed to have the lowest variability with height.

(4) *Stage 4*: After sunset (18:30-21:30 LST between June to September), radiative cooling of the surface began and low wind velocity generated a shallow nocturnal boundary layer (NBL). Weak vertical mixing combined with efflux of CO₂ from the terrestrial biosphere (due to the lack of photosynthesis) resulted in an increase of CO₂ concentrations starting at the lowermost levels.

Mixing ratios of CO₂ at 301 m showed a smaller variability than at 4 m, but shows an increase during the early morning (Fig. 5.2). If the measurement tower is high enough to capture any upward flux beyond the NBL height, F_{stor} alone can be representative of night-time CO₂ fluxes (Winderlich et al., 2014). If there are many days of stable nights (or stable NBL), CO₂ fluxes are less likely to reach beyond the top of the tower, such that F_{Eddy} is not needed, meaning that night-time CO₂ fluxes have small uncertainties. For instance, during unstable nights CO₂ gases were well-mixed, indicated by weak gradients of concentration (ΔCO_2) and potential temperature (ΔT_{pot}) of 0.07 K and 0.05 ppm between at 302 m and 247 m, respectively (Fig. 5.3, black). In contrast, gradients were larger (ΔT_{pot} of 1.37 K and ΔCO_2 of 0.29 ppm) (Fig. 5.3, grey) during stable nights. Results showed that about 95% of night-time CO₂ flux estimates were captured under the stable NBL that does not exceed 301 m. The percentage of night-time data where the top of the stable layer exceeds the 302 m level or an unstable layer was present, was only 5%. This suggests that night-time CO₂ flux estimates are generally reliable without measuring direct turbulent flux as in the EC method.

The concentration at the height of 301 m showed a smaller variability than one at 4m, however it shows an increment during the early morning (Fig. 5.2). If the measurement tower is high enough to capture any upward flux beyond the nocturnal boundary layer height, estimated CO₂ storage fluxes can be representative for night-time CO₂ fluxes, and the more uncertain F_{Eddy} component can be neglected during

night-time (Winderlich et al., 2014). If there are many stable nights, CO₂ fluxes are less likely reach beyond the top of the tower, and we can assume that the CO₂ storage flux estimates are representative for NEE values. For instance, during unstable nights, CO₂ gases were well-mixed, indicated by weak gradients between at 302 m and 247 m of the concentration (ΔCO_2) and potential temperature (ΔT_{pot}) of 0.07 K and 0.05 ppm, respectively (Fig. 5.3, black). In contrast, at stable night the gradients were larger than the unstable condition: 1.37 K for ΔT_{pot} and 0.29 ppm for ΔCO_2 (Fig. 5.3, grey). Results showed that about 95 % of nighttime CO₂ fluxes during the summertime occur under the stable nocturnal boundary layer. The fraction of unstable night-time data was only 5 %. Therefore, the regional CO₂ fluxes estimated by tall tower measurements can be assumed representative for regional night-time NEE.

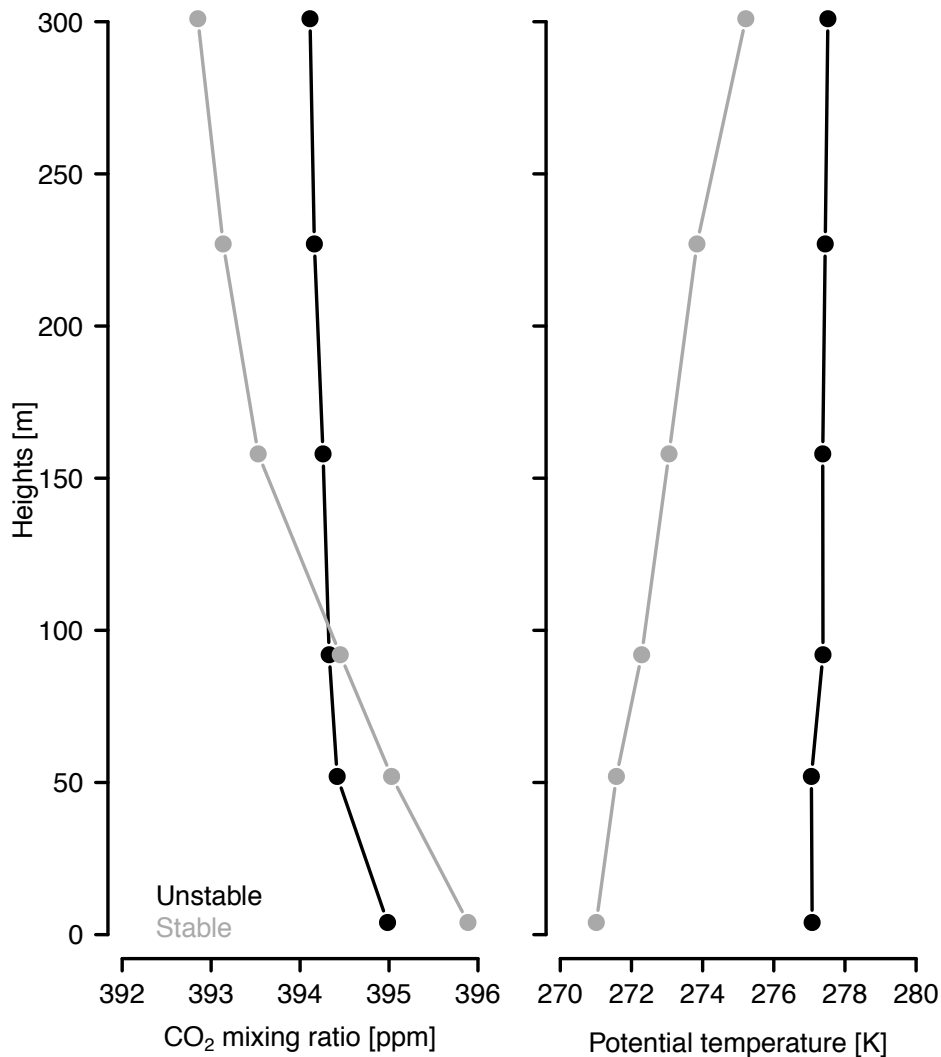


Figure 5.3 Two contrasting nights, showing unstable or well-mixed (black) and stable (dark grey) boundary layers. Profiles of half-hourly CO₂ mixing ratios and potential

temperatures on 2014-09-20 at 02:30:00 were chosen for the unstable night and on 2014-09-25 at 23:00:00 for the stable night, respectively. The time is given for the Krasnoyarsk time zone (KRAT=UTC+7h).

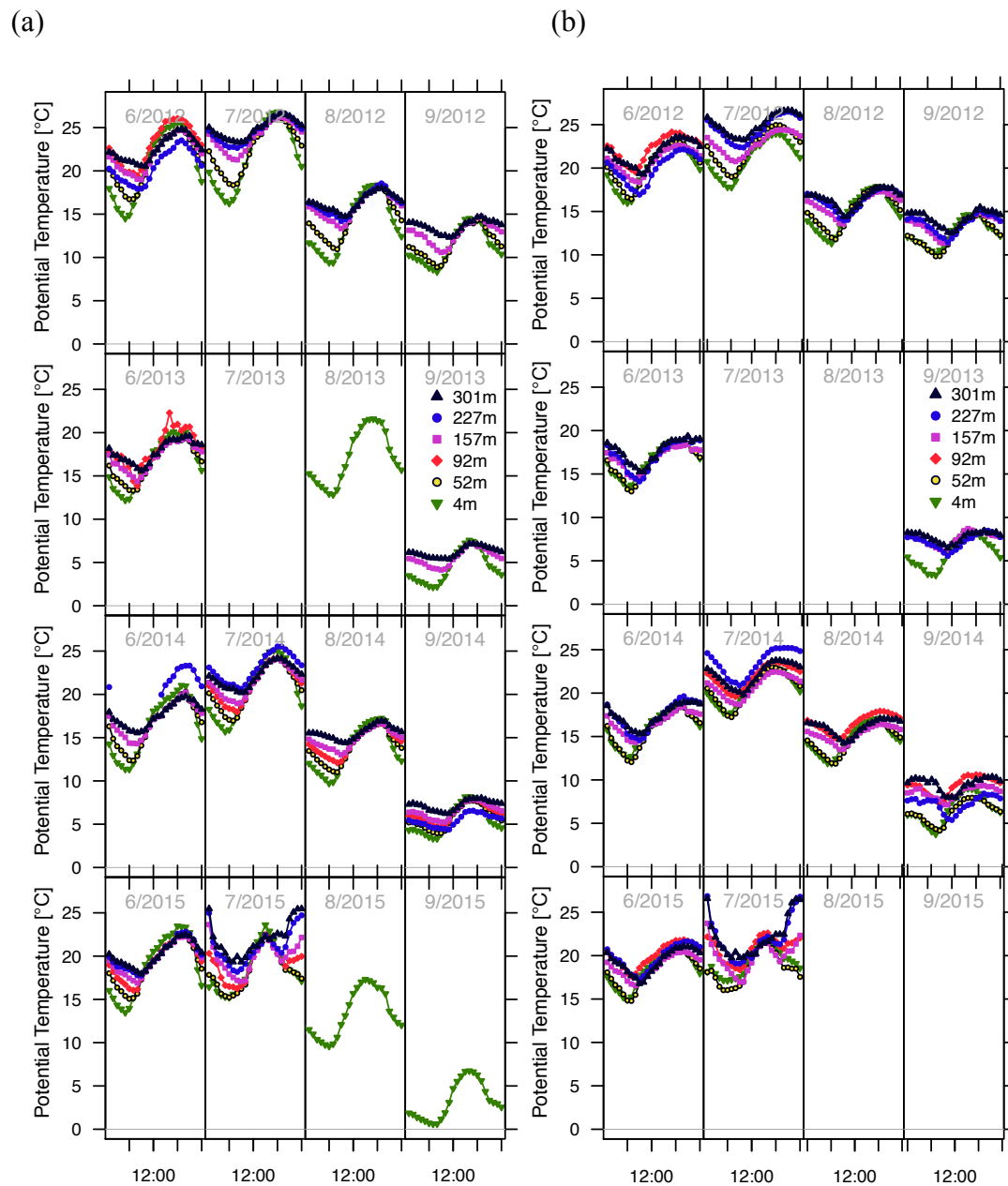


Figure 5.4 Diurnal cycle of the half-hourly averaged potential temperature for all height levels (301 m, 227 m, 157 m, 92 m, 52 m, and 4 m) for individual months from 2012-2015. (a) potential temperature using ambient air temperature (T_a), (b) corrected sonic air temperature (T_s).

Table 5.2 Availability of half-hourly net ecosystem exchange (NEE) of CO₂ and storage flux (F_{stor}) using the best temperature measurements during summertime (June-September) 2012-2015. The last row of each month indicates the temperature data used for flux calculations. T_a denotes the ambient air temperature measurement and T_s denotes the sonic air temperature measurements. “-“ denotes that none of temperature measurements were available to calculate NEE.

	6/2012		7/2012		8/2012		9/2012	
Flux term	NEE	F _{stor}	NEE	F _{stor}	NEE	F _{stor}	NEE	F _{stor}
Data availability (%)	38.3	85.2	78.2	78.8	81.3	83.9	94.8	95.8
Best temperature	T _a		T _a		T _s		T _s	
	6/2013		7/2013		8/2013		9/2013	
Flux term	NEE	F _{stor}	NEE	F _{stor}	NEE	F _{stor}	F _{NEE}	F _{stor}
Data availability (%)	33.9	35.0	0	0	0	0	0	0
Best temperature	T _s		-		-		-	
	6/2014		7/2014		8/2014		9/2014	
Flux term	NEE	F _{stor}	NEE	F _{stor}	NEE	F _{stor}	NEE	F _{stor}
Data availability (%)	15.8	15.8	71.0	71.0	0	0	45.2	56.9
Best temperature	T _s		T _s		-		T _a	
	6/2015		7/2015		8/2015		9/2015	
Flux term	NEE	F _{stor}	NEE	F _{stor}	NEE	F _{stor}	NEE	F _{stor}
Data availability (%)	94.9	97.6	5.0	5.0	0	0	0	0
Best temperature	T _a		T _a		-		-	

5.3.2 Evaluation of regional NEE estimates

Regional NEE using the best temperature products captured generally reasonable patterns of diurnal cycle of NEE comparable with NEE measured at the two flux sites (Fig. 5.5). In addition to flux measurements made at the Zotino Forest (ZF) and the Zotino Bog (ZB), up-scaled NEE utilizing respective land cover fraction for forest and bog are shown in this figure. Good agreements between regional NEE and EC NEE were for night-time and daytime CO₂ fluxes during August 2012, July 2014, and September 2014. During those months, errors in regional NEE were relatively small. Average diurnal cycles of F_{str} and NEE showed strong fluctuations in June and July of 2012 (Fig. 5.5). During this time, strong wildfires occurred in the tall tower footprint region, contributing to weaker daytime net CO₂ uptake or strong night-time net CO₂ release. In addition, carbon monoxide (CO) concentrations at the tower showed significant plume events with enhancement of several hundred part per billion (ppb) (not shown). Strong fluctuations in the average diurnal cycles of NEE result from sporadic events, where wind advected air masses containing smoke plumes from the area of wildfires.

During the months not affected by fires or low data coverage, regional NEE during the daytime, specifically during late afternoon, was substantially lower as compared to EC NEE (Fig. 5.5). A reason for this underestimation in regional NEE may be related to shortcomings in the MBR method used to calculate turbulent flux (Winderlich et al., 2014). Strong turbulent mixing during daytime results in marginal potential temperature gradients in Eq. (5.3), producing large uncertainties in flux terms. In addition, uncertainties in sensible heat flux measurements also influence F_{eddy} . Under strong wind speed conditions, temperature responses of each sonic anemometer can substantially differ, and errors in temperature fluctuations and sensible heat fluxes can be as high as 20-40% (Burns et al., 2012; Richiardone et al., 2012).

Large fluctuations in regional NEE can also be due to low data coverage, such as during June 2014 and July 2015 (Fig. 5.5, Table 5.2). Generally, night-time CO₂ fluxes at ZOTTO were more reliable than daytime CO₂ fluxes, as also found by Winderlich et al. (2014). Nights with midnight sun in northern Eurasia between June and July may influence some of night-time net CO₂ uptake, however it is unclear to which degree this can be seen in the regional NEE estimates.

For data in June 2012, the meteorological measurement system malfunctioned during more than 50% of months from the beginning of June, therefore only approximately 40% regional NEE was available (Table 5.2). Data coverage of regional NEE was over 70% for August 2012 and July 2014, whereas for September 2014 it was less than 45%.

Different temperature data sources (T_a or T_s) were used for regional NEE resulted in different estimates (Fig. 5.6). For instance, net CO_2 uptake on August 2012 based on T_s was larger than when using T_a . During some hours, the differences between T_a and T_s during daytime became large, contributing to uncertainties in turbulent flux calculations. In general, differences between the flux estimates using different temperatures are rather small, with the exception of in daytime at around noon, where small gradients in temperatures dominate the uncertainty.

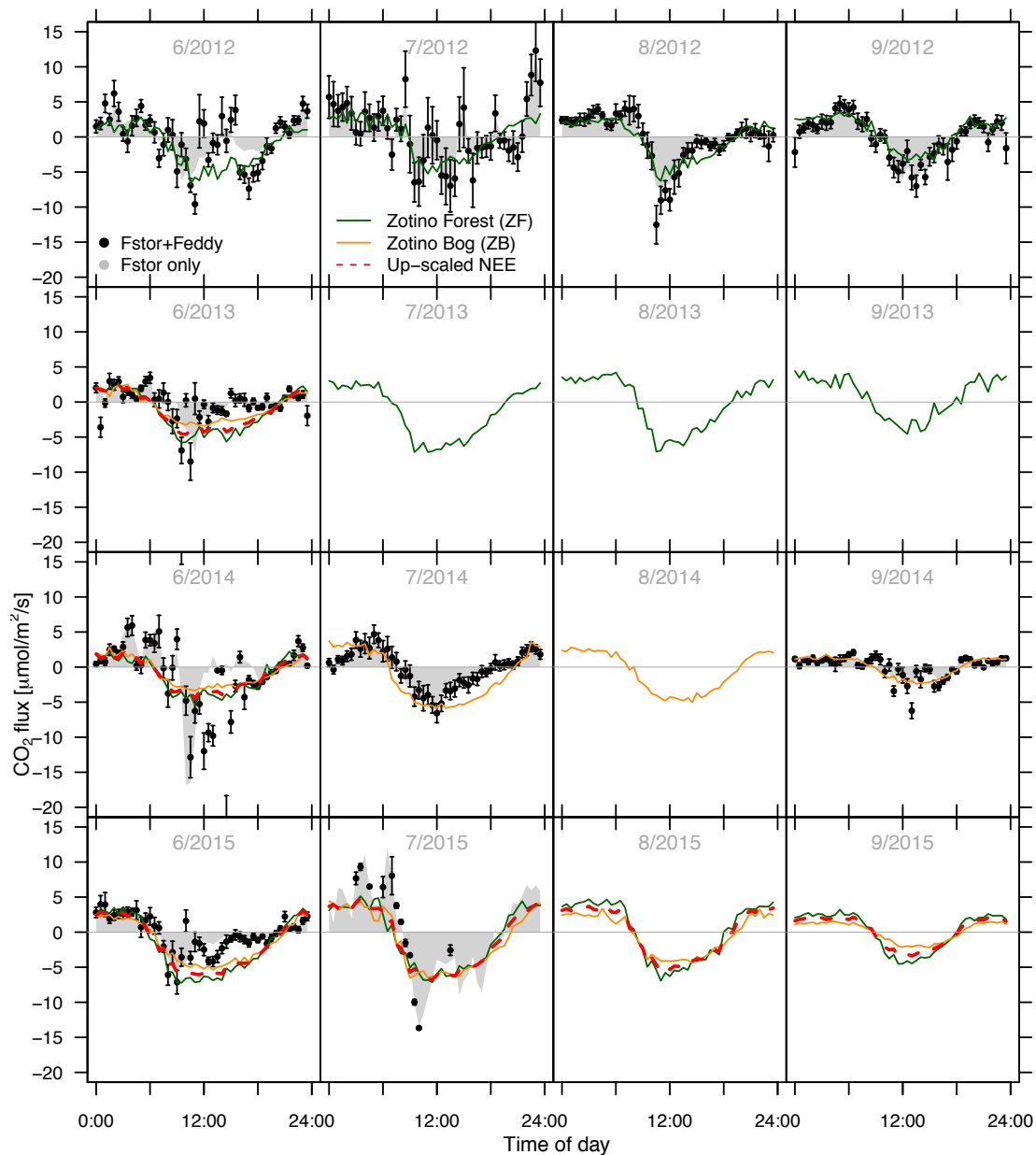


Figure 5.5 Diurnal cycles of regional NEE (black dots with error bar and grey shaded area) using the best temperature data during summertime from 2012-2015. Error bar denotes errors of mean of half-hourly data. Overlaying dark green and orange line denote CO₂ fluxes measured at the Zotino Forest (ZF) and the Zotino Bog (ZB) flux towers, respectively. Red dashed line is up-scaled CO₂ fluxes using the weighted average of fractions of forests (60%) and bogs (40%) in the ZOTTO footprint (Timokhina et al. 2016).

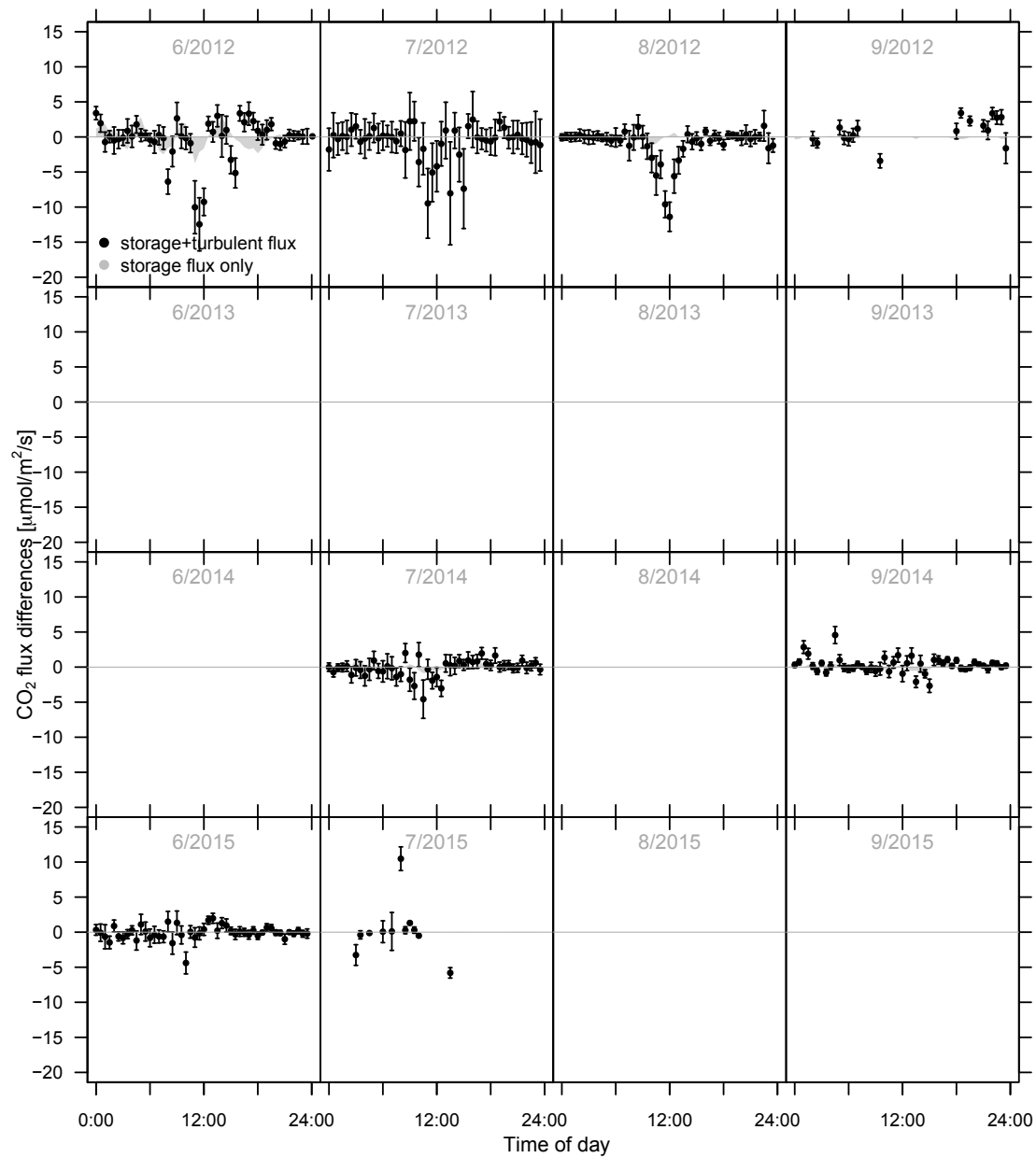


Figure 5.6 Diurnal cycle of differences in half-hourly regional NEE using sonic air temperature (T_s) and ambient air temperature (T_a) with standard error of the mean for individual months and years from 2012-2015. Shaded area indicates the storage flux (F_{stor}). Error bar denotes errors of mean of half-hourly data.

5.4 Conclusion

Tall tower profiles of CO₂ mixing ratios and meteorological measurements at ZOTTO help to understand the structure of the surface boundary layer. Since the top of the nocturnal stable boundary layer was usually below 304 m, night-time CO₂ flux estimates are based mostly on storage fluxes and thus have small uncertainties. Regional NEE using the best temperature dataset showed generally reasonable patterns and magnitudes of diurnal cycles in comparison to the flux tower measurements. In addition, up-scaled NEE estimated using fractional of forest and bog area surrounding ZOTTO provide a reference for regional NEE.

Ultimately, regional NEE estimates obtained from this study can be compared with CO₂ flux estimates from inverse modeling, in which fluxes are estimated based on CO₂ mixing ratio measurements and other observation sites in combination with transport models. However, this is currently only possible for timescales of a day or longer, as inversions do not yet provide reliable information on the diurnal cycle of fluxes. Therefore, careful interpretation of local- to regional- scale CO₂ fluxes is required because local flux measurements, regional flux estimates, and inverse modelling products all represent information on different spatial and temporal scales.

5.5 References

- Baldocchi, D., Falge, E., Gu, L., Olson, R., Hollinger, D., Running, S., Anthony, P., Bernhofer, C., Davis, K., Evans, R., Fuentes, J., Goldstein, A., Katul, G., Law, B., Lee, X., Malhi, Y., Meyers, T., Munger, W., Oechel, W., Paw, K.T.U., Pilegaard, K., Schmid, H.P., Valentini, R., 2001. FLUXNET : A New Tool to Study the Temporal and Spatial Variability of Ecosystem-Scale Carbon Dioxide , Water Vapor , and Energy Flux Densities 2415–2434.
- Burns, S.P., Horst, T.W., Jacobsen, L., Blanken, P.D., Monson, R.K., 2012. Using sonic anemometer temperature to measure sensible heat flux in strong winds. *Atmos. Meas. Tech.* 5, 2095–2111. doi:10.5194/amt-5-2095-2012
- Businger, J. A.: Evaluation of the Accuracy with Which Dry Deposition Can Be Measured with Current Micrometeorological Techniques, *J. Clim. Appl. Meteorol.*, 25, 1100–1124, doi:10.1175/1520-0450(1986)025<1100:EOTAWW>2.0.CO;2,1986.
- Chi, X., Winderlich, J., Mayer, J.C., Panov, A. V., Heimann, M., Birmili, W., Heintzenberg, J., Cheng, Y., Andreae, M.O., 2013. Long-term measurements of aerosol and carbon monoxide at the ZOTTO tall tower to characterize polluted and pristine air in the Siberian taiga. *Atmos. Chem. Phys.* 13, 12271–12298. doi:10.5194/acp-13-12271-2013
- Davis, K.J., Bakwin, P.S., Yi, C., Berger, B.W., Zhao, C., Teclaw, R.M., G., I.J., 2003. The annual cycles of CO₂ and H₂O exchange over a northern mixed forest as observed from a very tall tower 2, 1278–1293.
- Desai, A.R., Xu, K., Tian, H., Weishampel, P., Thom, J., Baumann, D., Andrews, A.E., Cook, B.D., King, J.Y., Kolka, R., 2015. Landscape-level terrestrial methane flux observed from a very tall tower. *Agric. For. Meteorol.* 201, 61–75. doi:10.1016/j.agrformet.2014.10.017
- Haszpra, L., Barcza, Z., Bakwin, P.S., Berger, B.W., Davis, K.J., Weidinger, T., 2001. Measuring system for the long-term monitoring of biosphere/atmosphere exchange of carbon dioxide. *J. Geophys. Res. Atmos.* 106, 3057–3069. doi:10.1029/2000JD900600
- Haszpra, L., Barcza, Z., Davis, K.J., Tarczay, K., 2005. Long-term tall tower carbon dioxide flux monitoring over an area of mixed vegetation. *Agric. For. Meteorol.*

- 132, 58–77. doi:10.1016/j.agrformet.2005.07.002
- Heimann, M., Schulze, E.-D., Winderlich, J., Andreae, M.O., Chi, X., Gerbig, C., Kolle, O., Kuebler, K., Lavrič, J. V., Mikhailov, E., Panov, A., Park, S., Rödenbeck, C., Skorochood, A., 2014. The Zotino Tall Tower Observatory (ZOTTO): Quantifying large scale biogeochemical changes in Central Siberia. *Nov. Acta Leopoldina* 117, 51–64.
- Rannik, Ü, Sogachev, A., Foken T., Goekede M., Kljun N., Leclerc M.Y., and Vesala T. 2012, Footprint analysis. in M Aubinet, T Vesala & D Papale (eds), *Eddy Covariance. A Practical Guide to Measurement and Data Analysis*. Springer, pp. 211-261. https://doi.org/10.1007/978-94-007-2351-1_8
- Reid, K.H., Steyn, D.G., 1997. Diurnal variations of boundary-layer carbon dioxide in a coastal city - Observations and comparison with model results. *Atmos. Environ.* 31, 3101–3114. doi:10.1016/S1352-2310(97)00050-2
- Rella, C.W., Chen, H., Andrews, A.E., Filges, A., Gerbig, C., Hatakka, J., Karion, A., Miles, N.L., Richardson, S.J., Steinbacher, M., Sweeney, C., Wastine, B., Zellweger, C., 2013. High accuracy measurements of dry mole fractions of carbon dioxide and methane in humid air. *Atmos. Meas. Tech.* 6, 837–860. doi:10.5194/amt-6-837-2013
- Richiardone, R., Manfrin, M., Ferrarese, S., Francone, C., Fernicola, V., Gaviolo, R.M., Mortarini, L., 2012. Influence of the Sonic Anemometer Temperature Calibration on Turbulent Heat-Flux Measurements. *Boundary-Layer Meteorol.* 142, 425–442. doi:10.1007/s10546-011-9688-z
- Saeki, T., Maksyutov, S., Sasakawa, M., Machida, T., Arshinov, M., Tans, P., Conway, T.J., Saito, M., Valsala, V., Oda, T., Andres, R.J., Belikov, D., 2013. Carbon flux estimation for Siberia by inverse modeling constrained by aircraft and tower CO₂ measurements 118, 1100–1122. doi:10.1002/jgrd.50127
- Sasakawa, M., Machida, T., Tsuda, N., Arshinov, M., Davydov, D., 2013. Aircraft and tower measurements of CO₂ concentration in the planetary boundary layer and the lower free troposphere over southern taiga in West Siberia : Long-term records from 2002 to. doi:10.1002/jgrd.50755
- Stull, R.B., 1998. An introduction to boundary layer meteorology. 1997th ed. Dordrecht: Kluwer Academic Publishers. 670 pp.
- Winderlich, J., Chen, H., Höfer, A., Gerbig, C., Panov, A., 2010. Continuous CO₂ / CH₄ measurement at Zotino Tall Tower Observatory (ZOTTO) in Central

Siberia 12, 4931.

Winderlich, J., Gerbig, C., Kolle, O., Heimann, M., 2014. Inferences from CO₂ and CH₄ concentration profiles at the Zotino Tall Tower Observatory (ZOTTO) on regional summertime ecosystem fluxes. *Biogeosciences* 11, 2055–2068.

doi:10.5194/bg-11-2055-2014

Zhang, X., Lee, X., Griffis, T.J., Baker, J.M., Xiao, W., 2014. Estimating regional greenhouse gas fluxes: An uncertainty analysis of planetary boundary layer techniques and bottom-up inventories. *Atmos. Chem. Phys.* 14, 10705–10719.

doi:10.5194/acp-14-10705-2014

Tans, P. P.: An observational strategy for assessing the role of terrestrial ecosystems in the global carbon cycle: scaling down to regional levels, *Scaling down to regional levels, Scaling Processes Between Leaf and Landscape Levels*, Academic, San Diego, CA, USA, 1991.

Chapter 6 Synopsis

Boreal forests and peatlands are the major types of vegetation in northern Eurasia. These ecosystems store large amount of C in their vegetation and soil, thus are essential ecosystems to understand the global C cycle. Compared to the North America and Scandinavian regions, tower-based CO₂ measurements in the Eurasian boreal ecosystems of central Siberia are very sparse. The objective of my thesis is to investigate temporal variability of CO₂ fluxes and their driving factors using tower-based measurements located at a coniferous forest and a bog in Zotino, near the ZOTTO in Krasnoyarsk, Russia.

Wildfires and snowmelt influence the dynamics of CO₂ fluxes in central Siberia. Therefore, understanding the variability in CO₂ fluxes in response to abiotic drivers during these periods is essential. To do so, I present CO₂ fluxes measured during wildfire periods from 2012 to 2013 and during spring snowmelt from 2013 to 2017. CO₂ fluxes were measured using the EC method. Statistical analyses were performed to identify and quantify the importance of environmental drivers. In addition, summertime regional CO₂ fluxes were inferred from the MBR method using mixing ratios of CO₂ and meteorological measurements at the tall tower. The site-level CO₂ fluxes measured at the two EC flux sites were used as reference data for investigating the reliability of regional CO₂ flux estimates. The summary of my main findings, overall discussion, outlook for future research, and conclusions is as follows:

6.1 Net ecosystem productivity reduction by clouds and fire aerosols at a sparse boreal coniferous forest

Solar radiation is the main energy source for vegetation photosynthesis. Clouds and aerosols change the amount and the proportion of diffuse and direct solar radiation on the Earth's surface. In turn, plant photosynthesis related processes are influenced by these changes in radiation and associated meteorological conditions.

Generally, the impact of diffuse light, or DRF effect, induced by clouds and aerosols increase photosynthesis and net CO₂ uptake. However, these effects on vegetation can differ due to ecosystem properties such as canopy structure and plant functional types.

Chapter 3 investigates the potential DRF effect based on tower-based measurements during the Siberian wildfire period from 2012-2013. In order to identify abiotic environmental drivers of forest NEP, the data-driven model (ANNs) was trained by CO₂ fluxes and meteorological measurements. Approximately 54-58% of variability in forest NEP during the growing season was controlled by PAR, VPD, and f_{dif} . Forest NEP showed a strong negative sensitivity to VPD, and a small positive response to f_{dif} . In addition, the impacts of clouds and smoke aerosols on radiation components and forest NEP were investigated. Incoming PAR decreased significantly at very high levels of f_{dif} and high aerosol loading. Substantial reduction in NEP occurred under high aerosol loadings (i.e. AOD > 2) and high level of f_{dif} values due to the strong reduction of incoming radiation. Results showed that forest NEP increased by diffuse radiation enhancements from clouds and smoke aerosols. However, the overall potential DRF effect at Zotino forest was weak (<10%) mainly due to sparse canopy structure. These findings support the previous study of Alton (2008) that an increase in forest productivity due to diffuse radiation was smaller for sparse forests compared to that in denser forests. Diffuse radiation enhancement caused by clouds and smoke plumes or smoke aerosols increased forest productivity, but the effect was less substantial than what has been observed in tropical forests due to the different canopy structure, LAI, and maximum radiation regime (Cirino et al., 2014; Park et al., 2018). The findings of Chapter 3 suggests that careful implementation and interpretation is required to quantify the DRF effect at regional scales or to model aerosol-climate feedbacks in boreal forests.

Boreal forests contain various types of trees. Deciduous, coniferous, and mixed forests have different canopy structures and LAIs. Generally, mixed forests have a more complex canopy structure and higher LAI than other types of forest. The recent study of Ezhova et al. (2018) supports this idea that the relationship between forest productivity (i.e. GPP) and diffuse fraction have different features depending on canopy structure based on the measurements from Eurasian boreal and hemi-boreal forests (Ezhova et al., 2018). A parabolic feature of the relationship between GPP and diffuse fraction was more pronounced in mixed forests than coniferous forests because of the dense canopy structure. Mixed forests are widely distributed on the

eastern side of Yenisey River, where presumably the DRF effect would be greater than Zotino.

In this study, the effect of aerosols from clouds on radiation was not clearly separated. However, Ezhova et al. (2018) present the direct effect of aerosols on solar radiation and forest photosynthesis using a radiative transfer model and ground-based measurements in Eurasian boreal and hemi-boreal forests. The direct effect of aerosol loading can increase GPP by 6-14%; both mixed forests and dense coniferous forests showed the largest increase in GPP when compared to sparse coniferous forests. In addition, GPP increases due to clouds were greater in mixed forests than coniferous forests, particularly with an open canopy: 32-33% enhancement for mixed forests and 21-26% for sparse coniferous forests. Although Park et al. (2018) and Ezhova et al. (2018) used different approaches to quantify aerosol effect on vegetation productivity, results suggest that the diffuse radiation enhancement by intermittent cloud cover and low aerosol loading increased forest productivity.

Wildfires produce not only CO₂ and CH₄ but also emit tropospheric ozone (O₃), carbon monoxide (CO), and massive amount of biogenic volatile organic compounds (BVOC) (Wentworth et al., 2018). These atmospheric chemical compounds and aerosols have a contrasting effect on photosynthesis. For instance, high O₃ concentrations from fire emissions damage the stomata of plants and decrease GPP, whereas aerosols increase GPP because of an increase in diffuse fraction (Yue and Unger, 2018). The net effect of fire emissions on GPP was negative because GPP reduction by O₃ was greater than an increase of GPP by aerosols. Pollutant aerosols can also influence precipitation process by changing aerosol and cloud properties (Lohmann and Feichter, 2005). Quantifying the amount of aerosols and other trace gases emitted from fires and fire-induced biogeochemical process are essential for understanding biosphere-atmosphere interactions under both present and future climatic changes (Kulmala et al., 2012; Yue and Unger, 2018). Hence, the Zotino measurement system would best provide in-depth knowledge in aerosol-radiation-vegetation-climate feedbacks when ecosystem flux measurements, aerosols and other chemical composition measurements are utilized altogether.

6.2 The impact of spring snowmelt on variability in CO₂ fluxes in boreal forest and bog

Chapter 4 presents the inter-annual variability of CO₂ fluxes at coniferous forest and bog sites in Zotino. Temperature warming in high-northern latitude zones significantly shift the timing of spring photosynthesis recovery. Still, the number of published studies investigating this are limited, mainly due to unavailability of long-term CO₂ flux measurements in central Siberia. The aims of this study are to report net ecosystem exchange of CO₂ and investigate the role of abiotic drivers (e.g. light, temperature, and snowmelt) on this exchange. The two ecosystems showed clear differences in the variability of CO₂ flux and the timing of CO₂ uptake due to different surface reflectance and snowmelt. Major findings are: 1) Surface albedo and radiation were the key drivers of CO₂ fluxes in coniferous forest. Surface peat temperature was the primary driver of bog CO₂ fluxes. 2) Both ecosystems became net CO₂ sinks before snowmelt concluded and while surface soils were still frozen. 3) Intermittent warm spells may play a role in determining the start of CO₂ uptake for both ecosystems. 4) Spring frost reduced the net ecosystem productivity in both ecosystems; however, vegetation productivity increased again after frost. This study suggests that transitions from net CO₂ sources to net CO₂ sinks and net ecosystem productivity during springtime are regulated by the mixed effects of air temperature, snowmelt, and frost.

Total snow period at the Zotino site is about 7 months. However, flux stations are often inaccessible during the wintertime when air temperature is very low (< -30 °C) and early springtime (e.g., May) when floods occur. The closest weather station is 30 km from ZOTTO; therefore, the absolute amount of snow and timing of start and end of snow are likely not similar as those which are directly measured at the station. For instance, the Zotino station likely has more snowfall (> 100 cm) than the weather station (< 100 cm). Therefore, the exact date of the completion of snowmelt and the amount of snow depth are different depending on the location. To improve the current knowledge of when ground vegetation emerges from snow cover and when snowmelt concludes, continuous site-level snow measurements are required. Ultimately, these data will provide useful information for determining season and characterizing dynamics of carbon and energy fluxes.

In addition, installing automated cameras (i.e., “PhenoCam”) at the flux tower would improve the understanding of an annual carbon budget in combination with other remote sensing data (e.g., Landsat, MODIS, VIIRS) (Liu et al., 2017; Richardson et al., 2010; Westergaard-Nielsen et al., 2017). Timing of the start and end of snowmelt influence the phenological development stage that regulates the seasonal dynamics of carbon and water fluxes. Measurements of these variables at a site-level should be taken into account for future research.

6.3 Understanding of the reliability of regional CO₂ flux estimates

Chapter 5 presents the variability of summertime CO₂ fluxes below the surface boundary layer at the Zotino tall tower. Generally, the representative area of site-level CO₂ flux measurements is approximately 1-3 km². Flux estimates from a tall tower directly provide CO₂ fluxes at a larger scale. However, the measurement system at Zotino tall tower does not fulfil the specific requirements for the EC method due to the low measurement frequency of the gas analyser, the flow distortion from the long tubing length, and long air sample mixing time inside of buffers. In this case, the MBR method is a practical approach to estimate turbulent flux (Winderlich et al. 2014).

Analysis of diurnal cycles of CO₂ mixing ratios and meteorological variables measured at the six heights showed that profile measurements are useful to understand the structure of the boundary layer near the surface. In addition, night-time mixing mostly did not extend beyond the top of the tall tower (304 m), and so CO₂ fluxes can be derived directly from changes in the CO₂ concentrations along the profile. This suggests that night-time CO₂ flux estimates can be reliable without direct EC flux measurement. The tower-based EC CO₂ fluxes at the forest and bog sites were used as reference CO₂ fluxes for characterizing regional CO₂ flux estimates. Despite underestimates in daytime regional CO₂ fluxes, diurnal cycles of regional CO₂ fluxes were comparable with the flux tower measurements.

Analysis in this study was restricted to comparing the patterns of mean diurnal cycles. In order to provide compatible CO₂ fluxes from the three towers, measurement data should cover the same time period. In addition, flux footprint analysis is required

to understand source-sink distributions at the forest and bog sites. Then, CO₂ fluxes from the three different towers can be utilized as a complementary dataset.

Overall, this thesis investigates seasonal variability of CO₂ fluxes. However, CH₄ is the second most critical greenhouse gas, with a greenhouse warming potential (GWP) 28-36 times stronger than CO₂ over 100 years (IPCC, 2013). Wetlands are generally considered sinks of atmospheric CO₂ and natural sources of methane (CH₄) emissions. Unlike Arctic permafrost or other boreal regions, methane flux measurements in Eurasian wetlands are rare, especially in central Siberia (Peltola et al., 2019). In Russia, especially in western Siberian lowlands, methane flux measurements using a static chamber method are popular (Glagolev et al., 2011). This suggests that central Siberia, including Zotino, is a critical zone in which to measure methane flux.

Operating year-round CH₄ flux measurements using the EC technique in remote high-northern latitudes station is challenging. At Zotino bog, more than three years of effort beginning in June 2012, to measure CH₄ flux using a Picarro G2301-f were unsuccessful due to structural defects of the device and communication and logistical problems transporting the instrument for repairs from the remote site. Unlike the other version of Picarro CH₄ flux gas analyzers (Peltola et al. 2013, 2014), G2301-f may not a suitable device at a remote station like ZOTTO. However, long-term monitoring of CH₄ fluxes with the same device have been successfully operated in temperate and tropical rice paddy fields in Japan and Thailand (Komiya, 2016). In more harsh Arctic tundra ecosystems, successful examples of methane flux measurements by using EC technique are reported in recent years (Goodrich et al., 2016; Kittler et al., 2017). Frequent maintenance is critical to uphold stable operation of such instruments at remote stations. Therefore, DLT-100 (Los Gatos Res.) or LI-7700 (LI-COR) devices are likely suitable for remote sites such as Zotino bog because these devices are generally known as being robust and relatively easy to maintain (Peltola et al., 2014, 2013). Methane flux measurements will be valuable to understand the spatiotemporal patterns, variability, and their driving factors, such as water table depth (Rinne et al., 2018). Furthermore, CH₄ flux measurements at bog sites like Zotino can be used as reference data to evaluate regional CH₄ flux estimates from tall tower profile measurements (Winderlich et al., 2014).

6.4 Conclusion

This thesis investigates the temporal variability of CO₂ fluxes from local to regional scale based on tower-based measurements in central Siberian from 2012-2017. An overview of findings in this study is addressed graphically as in Fig. 6.1.

Chapter 3 highlights the abiotic controlling factors of forest net ecosystem productivity and the potential diffuse radiation fertilization effect due to clouds and aerosols measured at a sparse coniferous forest during wildfire periods.

The following questions were answered;

- 1) What are the major environmental factors controlling the variability of forest NEP? *During the growing season, approximately 54-58% of variability in forest NEP was controlled by PAR, VPD, and f_{dif} .*
- 2) How does forest NEP respond to diffuse radiation caused by smoke particles during wildfires? *Diffuse radiation increases from smoke particles only were not able to be separated from the contributions of clouds. However, the partial derivative of forest NEP with f_{dif} , including both clouds and smoke particle effects, increased over the full range of f_{dif} values.*
- 3) How strong is the diffuse radiation fertilization effect on NEP? *The diffuse radiation fertilization effect has a weakly positive effect on NEP mainly due to the sparse canopy structure and low leaf area index.*

Chapter 4 investigates the abiotic controls of CO₂ fluxes during winter-spring transition period at a coniferous forest and bog.

The following questions were answered;

- 4) What are the factors controlling the variability of CO₂ at a coniferous forest and bog in spring? *Surface albedo was a statistically significant driver for CO₂ flux variability in the forest, whereas surface peat temperature was the primary driver of CO₂ flux variability in the bog.*
- 5) How do coniferous forest and bog ecosystems differ in their responses to environmental variables during spring? *Coniferous forest became net CO₂ uptake approximately a week earlier than bog. Both ecosystems start net CO₂ uptake during snowmelt while surface soil was still frozen. The net CO₂ uptake rates continuously increased after the start of snow melt once surface soil*

temperature exceeded 1°C. Spring frost reduced the net ecosystem productivity in both ecosystems, however ecosystem productivity recovered to similar levels after frost.

- 6) What influence does the very warm spring in 2015 have on the timing of snowmelt, frequency of frost days, and the strengths of net CO₂ sinks? *The earliest snowmelt across all years studied did not occur during the 2015 spring. During the very warm spring, both ecosystems had the least frequent frost and showed the highest cumulative NEE, however results were statistically insignificant.*

Chapter 5 investigates the summertime CO₂ fluxes on a regional scale.

The following questions were answered;

- 7) How reliable are regional CO₂ flux estimates from profile measurements? *Night-time CO₂ fluxes showed smaller uncertainties than daytime CO₂ fluxes. Despite underestimation of daytime CO₂ fluxes, magnitudes and patterns of diurnal cycle of CO₂ fluxes generally followed the EC CO₂ fluxes.*

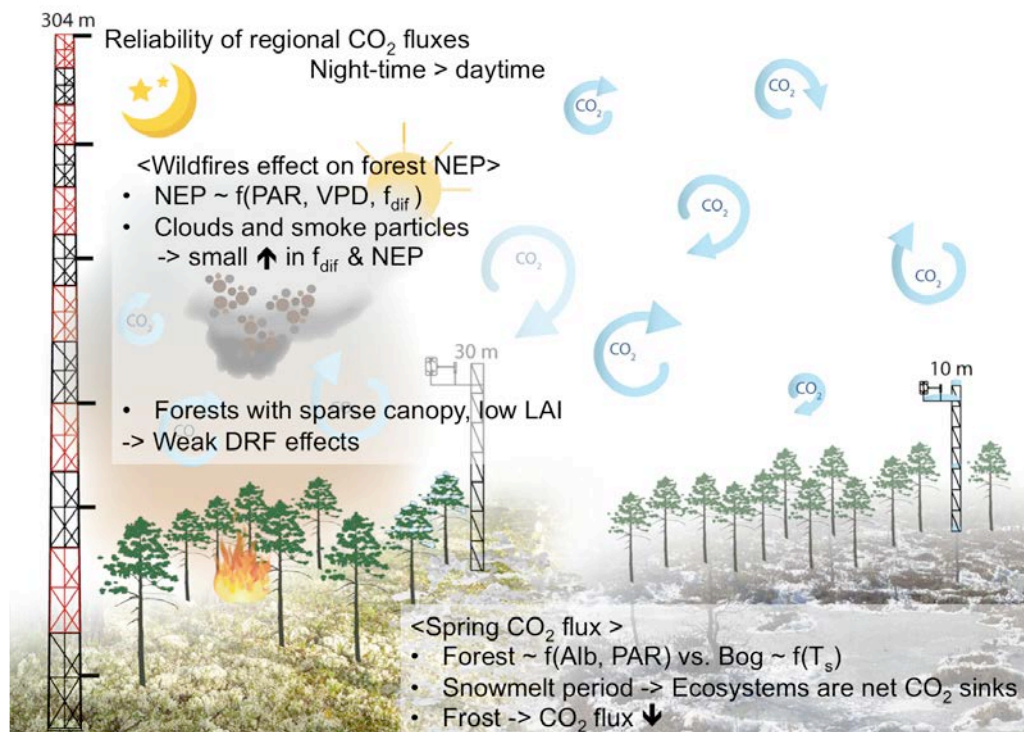


Figure 6.1 A graphical abstract, presenting main findings in this thesis.

This thesis mainly focuses on abiotic parameters influencing seasonal vegetation CO₂ uptakes. Results were based on CO₂ measurements in central Siberia where tower-based CO₂ measurements are very sparse. Overall, results show that boreal ecosystems' responses to changing environmental conditions are non-linear and complex. The results would be useful to evaluate CO₂ fluxes from both process-based biosphere models and inverse models. However, there are unknown or unmeasured abiotic or biotic parameters not covered in this study. Therefore, further efforts, such as CH₄ flux, water table, and phenology measurements at bog, flux footprint analysis, and uncertainty estimation in flux partitioning of NEE would be necessary to characterize long-term annual carbon budget or seasonal CO₂ fluxes at Zotino.

6.5 References

- Cirino G.G., Souza R.A.F., Adams D.K. & Artaxo P. 2014. The effect of atmospheric aerosol particles and clouds on net ecosystem exchange in the Amazon. *Atmospheric Chemistry and Physics* 14: 6523–6543.
- Ezhova E., Ylivinkka I., Kuusk J., Komsaare K., Vana M., Krasnova A., Noe S., Arshinov M., Belan B., Park S.-B., Lavrič J.V., Heimann M., Petäjä T., Vesala T., Mammarella I., Kolari P., Bäck J., Rannik Ü., Kerminen V.-M. & Kulmala M. 2018. Direct effect of aerosols on solar radiation and gross primary production in boreal and hemiboreal forests. *Atmospheric Chemistry and Physics* 18: 17863–17881.
- Glagolev M., Kleptsova I., Filippov I., Maksyutov S. & MacHida T. 2011. Regional methane emission from West Siberia mire landscapes. *Environmental Research Letters* 6.
- Goodrich J.P., Oechel W.C., Gioli B., Moreaux V., Murphy P.C., Burba G. & Zona D. 2016. Impact of different eddy covariance sensors, site set-up, and maintenance on the annual balance of CO₂ and CH₄ in the harsh Arctic environment. *Agricultural and Forest Meteorology* 228–229: 239–251.
- Kittler F., Heimann M., Kolle O., Zimov N., Zimov S. & Göckede M. 2017. Long-Term Drainage Reduces CO₂ Uptake and CH₄ Emissions in a Siberian Permafrost Ecosystem. *Global Biogeochemical Cycles* 31: 1704–1717.
- Kulmala M., Guenther A., Boy M., Makkonen R., Arneth A., Kerminen V.-M. & Asmi A. 2012. BVOC-aerosol-climate interactions in the global aerosol-climate model ECHAM5.5-HAM2. *Atmospheric Chemistry and Physics* 12: 10077–10096.
- Liu Y., Hill M.J., Zhang X., Wang Z., Richardson A.D., Hufkens K., Filippa G., Baldocchi D.D., Ma S., Verfaillie J. & Schaaf C.B. 2017. Using data from Landsat, MODIS, VIIRS and PhenoCams to monitor the phenology of California oak/grass savanna and open grassland across spatial scales. *Agricultural and Forest Meteorology* 237–238: 311–325.
- Lohmann U. & Feichter J. 2005. Global indirect aerosol effects: a review. *Atmospheric Chemistry and Physics Discussions*: 715–737.
- Park S.-B., Knohl A., Lucas-Moffat A.M., Migliavacca M., Gerbig C., Vesala T., Peltola O., Mammarella I., Kolle O., Lavrič J.V., Prokushkin A. & Heimann M. 2018. Strong radiative effect induced by clouds and smoke on forest net

- ecosystem productivity in central Siberia. *Agricultural and Forest Meteorology* 250–251: 376–387.
- Peltola O., Hensen A., Helfter C., Belelli Marchesini L., Bosveld F.C., Bulk W.C.M. Van Den, Elbers J.A., Haapanala S., Holst J., Laurila T., Lindroth A., Nemitz E., Röckmann T., Vermeulen A.T. & Mammarella I. 2014. Evaluating the performance of commonly used gas analysers for methane eddy covariance flux measurements: the InGOS inter-comparison field experiment. *Biogeosciences* 11: 3163–3186.
- Peltola O., Mammarella I., Haapanala S., Burba G. & Vesala T. 2013. Field intercomparison of four methane gas analyzers suitable for eddy covariance flux measurements. *Biogeosciences* 10: 3749–3765.
- Peltola O., Vesala T., Gao Y., Rätty O., Alekseychik P., Aurela M., Chojnicki B., Desai A., Dolman H., Euskirchen E., Friborg T., Göckede M., Helbig M., Humphreys E., Jackson R., Jocher G., Joos F., Klatt J., Knox S., Kutzbach L., Lienert S., Lohila A., Mammarella I., Nadeau D., Nilsson M., Oechel W., Peichl M., Pypker T., Quinton W., Rinne J., Sachs T., Samson M., Schmid H.P., Sonntag O., Wille C., Zona D. & Aalto T. 2019. *Dataset for ‘Monthly Gridded Data Product of Northern Wetland Methane Emissions Based on Upscaling Eddy Covariance Observations’*.
- Richardson A.D., Andy Black T., Ciais P., Delbart N., Friedl M.A., Gobron N., Hollinger D.Y., Kutsch W.L., Longdoz B., Luysaert S., Migliavacca M., Montagnani L., William Munger J., Moors E., Piao S., Rebmann C., Reichstein M., Saigusa N., Tomelleri E., Vargas R. & Varlagin A. 2010. Influence of spring and autumn phenological transitions on forest ecosystem productivity. *Philosophical Transactions of the Royal Society B: Biological Sciences* 365: 3227–3246.
- Rinne J., Tuittila E.-S., Peltola O., Li X., Raivonen M., Alekseychik P., Haapanala S., Pihlatie M., Aurela M., Mammarella I. & Vesala T. 2018. Temporal Variation of Ecosystem Scale Methane Emission From a Boreal Fen in Relation to Temperature, Water Table Position, and Carbon Dioxide Fluxes. *Global Biogeochemical Cycles* 32: 1087–1106.
- Wentworth G.R., Aklilu Y., Landis M.S. & Hsu Y. 2018. Impacts of a large boreal wild fire on ground level atmospheric concentrations of PAHs, VOCs and ozone. *GRAPHICAL ABSTRACT. Atmospheric Environment* 178: 19–

30.

- Westergaard-Nielsen A., Lund M., Pedersen S.H., Schmidt N.M., Klosterman S., Abermann J. & Hansen B.U. 2017. Transitions in high-Arctic vegetation growth patterns and ecosystem productivity tracked with automated cameras from 2000 to 2013. *Ambio* 46: 39–52.
- Winderlich J., Gerbig C., Kolle O. & Heimann M. 2014. Inferences from CO₂ and CH₄ concentration profiles at the Zotino Tall Tower Observatory (ZOTTO) on regional summertime ecosystem fluxes. *Biogeosciences* 11: 2055–2068.
- Yue, X., Unger, N., 2018. Fire air pollution reduces global terrestrial productivity. *Nat. Commun.* 9. doi:10.1038/s41467-018-07921-4